Faculty of Medicine and Health Sciences

Laboratory of Experimental Hematology (LEH)

Development, characterization and application of luminescent human iPSC-derived neurospheroids in ischemic stroke research

Ontwikkeling, karakterisering en toepassing van luminescente humane iPSC-afgeleide neurosferoïden in onderzoek naar ischemische beroerte

PhD thesis submitted for the degree of Doctor of Medical Sciences at the University of Antwerp to be defended by:

Elise Van Breedam

Supervisor

Prof. Dr. Peter Ponsaerts

Antwerp, 2022

Doctoral committee

Supervisor

Prof. Dr. Peter Ponsaerts

Laboratory of Experimental Hematology, University of Antwerp

Internal jury members

Prof. Dr. Samir Kumar-Singh

Molecular Pathology group, Laboratory of Cell Biology & Histology, University of Antwerp

Prof. Dr. Benedicte De Winter

Laboratory of Experimental Medicine and Pediatrics, University of Antwerp

External jury members

Prof. Dr. Tarja Malm

A.I. Virtanen Institute for Molecular Sciences, University of Eastern Finland

Prof. Dr. Ira Espuny Camacho

Département des sciences biomédicales et preécliniques, GIGA Stem Cells – Molecular Regulation of Neurogenesis, University of Liège

Table of content

List of abbreviations

2D	Two-dimensional
3D	Three-dimensional
AF488	Alexa fluor 488
AMP	Adenosine monophosphate
AMPA	Alpha-amino-3-hydroxy-5-methyl-4-isoxazole propionate
AMPK	AMP-activated protein kinase
ATP	Adenosine triphosphate
BBB	Blood-brain barrier
BDNF	Brain-derived neurotrophic factor
BEC	Brain endothelial cell
Ca^{2+}	Calcium
CCL2	C-C Motif chemokine ligand 2
CCL3	C-C Motif chemokine ligand 3
CD200	Cluster of differentiation 200
CD200R	CD200 receptor
CD45	Cluster of differentiation 45
CI	Confidence interval
Cl. casp-3	Cleaved caspase-3
CMVie	Immediate early CMV promoter
cNEM	Complete neural expansion medium
CNS	Central nervous system
CNV	Copy number variation
CO_2	Carbon dioxide
CRISPR/Cas9	Clustered Regularly Interspaced Short Palindromic Repeats/CRISPR associated genes 9
CSF-1	Colony stimulating factor 1
CX3CL1	C-X3-C Motif chemokine ligand 1
CX3CR1	C-X3-C Motif chemokine receptor 1
CXCL10	C-X-C Motif chemokine ligand 10
CXCL12	C-X-C Motif chemokine ligand 12
Cy3	Cyanine 3
DAMPs	Damage-associated molecular patterns
DAPI	4’,6-diamidino-2-phenylindole dihydrochloride
DCX	Doublecortin

DIV-BBB	Dynamic *in vitro* model of the BBB
DMSO	Dimethylsulfoxide
DNA	Deoxyribonucleic acid
EB	Embryoid body
ECM	Extracellular matrix
EFS	Elongation factor 1α short promoter
eGFP	Enhanced green fluorescent protein
ELISA	Enzyme-linked immunosorbent assay
ESC	Embryonic stem cell
FBS	Fetal bovine serum
FGF-2	Fibroblast growth factor-2
FITC	Fluorescein isothiocyanate
GDNF	Glial-derived neurotrophic factor
GFAP	Glial fibrillary acidic protein
GOX/CAT	Glucose oxidase and catalase
hCS	Human cortical spheroids
HE	Hematoxylin and eosin
HFF	Human foreskin fibroblast
hiPSC	Human induced pluripotent stem cell
hiPSC-NSC	hiPSC-derived NSC
Hop	Homeodomain-only protein
HRP	Horseradish peroxidase
Iba-1	Ionized calcium-binding adaptor molecule 1
ICAM	Intercellular adhesion molecule
ICC	Immunocytochemistry
IF	Immunofluorescence
IL-1β	Interleukin-1β
IL-34	Interleukin 34
iPSC	Induced pluripotent stem cell
K^+	Potassium
LDH	Lactate dehydrogenase
Luc	Luciferase
MAPK	Mitogen-activated protein kinase
MBP	Myelin basic protein
MCAO	Middle cerebral artery occlusion
M-CSF	Macrophage colony-stimulating factor

MEA	Multi-electrode array
MFI	Mean fluorescent intensity
MMP	Matrix metalloproteinase
mRNA	Messenger RNA
MTT	3-(4,5-dimethylthiazol-2-yl)-2,5-diphenyl-2H-tetrazolium bromide
N_2	Nitrogen
Na^+	Sodium
NeuN	Neuronal nuclear protein
NMDA	N-methyl-D-aspartate
NO	Nitric oxide
NSC	Neural stem cell
NVU	Neurovascular unit
O_2	Oxygen
Oct3/4	Octamer binding transcription factor 3/4
OGD	Oxygen-glucose deprivation
ORF	Open reading frame
P2RY12	Purinergic receptor P2Y12
PAX6	Paired box protein 6
PBS	Phosphate-buffered saline
PDMS	Polydimethylsiloxane
PFA	Paraformaldehyde
PKM2	Pyruvate kinase isoform M2
PPAR	Peroxisome proliferator-activated receptor
PS	Penicillin-streptomycin
PSC	Pluripotent stem cell
qRT-PCR	Quantitative reverse transcription polymerase chain reaction
rhEGF	Human recombinant epidermal growth factor
rhFGF-2	Human recombinant fibroblast growth factor
RLU	Relative light units
RNA	Ribonucleic acid
ROCK-inhibitor	Rho-associated protein kinase inhibitor
ROI	Region of interest
RT	Room temperature
S100B	S100 calcium binding protein B
SOX1	SRY-Box transcription factor 1

SOX2	SRY-Box transcription factor 2
STS	Staurosporine
TBR1	T-box brain transcription factor 1
TBR2	T-box brain transcription factor 2
TBS	Tris-buffered saline
TEER	Transendothelial electrical resistance
TMEM119	Transmembrane protein 119
tPA	Tissue plasminogen activator
TRA-1-60	T cell receptor alpha locus 1-60
TRA-1-81	T cell receptor alpha locus 1-81
Tuj1	Class III beta-tubulin
ULA	Ultra-low attachment
Z-VAD-FMK	Carbobenzoxy-valyl-alanyl-aspartyl-[O-methyl]-fluoromethylketone

Summary

Stroke is one the leading causes of death and disability worldwide. In the majority of cases, stroke is caused by occlusion of an arterial vessel by an embolus or thrombus, referred to as ischemic stroke. Despite the impact of ischemic stroke on the patient's quality of life and on society, the current treatment is limited to the administration of the thrombolytic agent tissue plasminogen activator or to mechanical clot retrieval by thrombectomy. However, only a small proportion of all acute ischemic stroke patients are eligible for last-mentioned treatments mainly due to the very narrow therapeutic time window after stroke onset. Moreover, even though effective in some patients, these approaches do not act on the brain tissue to provide neuroprotection. In an urgent need to find new therapies, decades of research resulted in over a thousand of candidate neuroprotective drugs of which none have led to an effective therapy to date. Although considered promising in rodent and *in vitro* models for ischemic stroke, many neuroprotective agents failed when translated to the clinic. Multiple reasons may account for this lack of success, such as deficiencies in animal studies or clinical trial design, but it is equally clear that the predictive power of the systems currently used to model human ischemic stroke *in vitro* should be questioned. Especially regarding the latter, the field of ischemic stroke research would greatly benefit from the implementation of more complex *in vitro* models with improved physiological relevance to model human-specific ischemic responses and to predict clinical outcomes with greater accuracy. The development and application of human iPSC-derived 3D neurospheroid models represent an appropriate approach to fulfill this need.

In a first part of this doctoral thesis, a highly reproducible luminescent human iPSC-derived neurospheroid model enabling the real-time read-out of neural viability after ischemia-like conditions was developed and characterized. By depriving 1- and 4-week-old neurospheroids from oxygen and glucose, the ability of the applied bioluminescent system to detect neurotoxicity was demonstrated. Moreover, differences in behaviour after oxygen-glucose deprivation between the different ages of neurospheroids were observed, whereby 1-week-old but not 4-week-old neurospheroids displayed spontaneous recovery. This underscores the need for more mature neurospheroids in *in vitro* stroke research that more faithfully recapitulate the *in vivo* adult situation. Furthermore, evaluation of the pan-caspase inhibitor Z-VAD-FMK in the established model demonstrated its inability to increase overall neural survival in neurospheroids in contrast to a 2D culture of the same hiPSC-derived neural stem cells, where neuroprotection was observed. This exemplifies how the increased complexity of

spheroid models can result in a different outcome when testing neuroprotective compounds, further stressing the importance of introducing human-based 3D models in the preclinical stage of drug discovery and development, complementing 2D *in vitro* models and preclinical *in vivo* models.

In the second part of this doctoral thesis, the foundation was laid to further increase the complexity and predictivity of the developed human neurospheroid model by generating more mature, multicellular neurospheroids. Glial cells, including astrocytes and microglia, have been ascribed important roles in the exacerbation as well as the recovery following ischemia-induced brain damage. Hence, introduction of these cell types would enable to mimic human ischemic responses even more closely. In a first set of explorative experiments, culture conditions were optimized in order to obtain neurospheroids with increased maturity and the presence of astrocytes. Hereby, increasing the culture time of the neurospheroids markedly increased neuronal maturity as well as the spontaneous development of astrocytes. It was also noted that culture of neurospheroids in selected differentiation media did not give rise to astrocytes for the evaluated time points despite their ability to display faster differentiation and maturation. In a second set of explorative experiments, the integration of hematopoietic progenitors cells into neurospheroids was explored for the future creation of an immune-competent, microglia-enriched neurospheroid model for ischemic stroke. Comparison of different time points for the addition of hematopoietic progenitor cells to neurospheroids, showed higher integration efficiency when added to pre-established neurospheroids and suggest a role for cytokine CSF-1 herein.

In conclusion, the human iPSC-derived neurospheroid model developed here, together with the advances in increasing the maturity and multicellularity, would enable to provide a new model better recapitulating human ischemic responses than current *in vitro* and *in vivo* models. Therefore, their introduction in preclinical research, next to traditional 2D cultures and animal models, may more accurately predict clinical outcomes, providing more insight into the efficacy of candidate interventions in the human brain eventually aiding the development of urgently needed novel neuroprotective therapies for ischemic stroke.

Samenvatting

Beroerte is wereldwijd een van de belangrijkste oorzaken van overlijden en invaliditeit. In de meeste gevallen wordt een beroerte veroorzaakt door afsluiting van een slagader door een embolie of trombus, ook wel ischemische beroerte genoemd. Ondanks de impact van ischemische beroerte op de kwaliteit van leven van de patiënt en op de samenleving, is de huidige behandeling beperkt tot de toediening van het trombolytische middel weefselplasminogeenactivator of tot het mechanisch verwijderen van stolsels door trombectomie. Slechts een klein deel van alle patiënten met een acute ischemische beroerte komt echter in aanmerking voor laatstgenoemde behandelingen, voornamelijk vanwege het zeer smalle therapeutische tijdvenster na aanvang van de beroerte. Bovendien, hoewel effectief bij sommige patiënten, werken deze therapeutische interventies niet in op het hersenweefsel om neuroprotectie te bieden. In een dringende noodzaak om nieuwe therapieën te vinden, heeft tientallen jaren onderzoek geresulteerd in meer dan duizend kandidaat-neuroprotectieve geneesmiddelen, waarvan er tot op heden nog geen enkele tot een effectieve therapie heeft geleid. Hoewel ze als veelbelovend worden beschouwd in knaagdier- en *in vitro*-modellen voor ischemische beroerte, faalden veel neuroprotectieve middelen wanneer ze naar de kliniek werden vertaald. Meerdere redenen kunnen dit gebrek aan succes verklaren, zoals tekortkomingen in dierenproeven of in de opzet van klinische proeven, maar het is evenzeer duidelijk dat het predictief vermogen van de systemen die momenteel worden gebruikt om humane ischemische beroerte *in vitro* te modelleren, in twijfel moet worden getrokken. Vooral wat dit laatste betreft, zou het onderzoek naar ischemische beroertes enorm gebaat zijn bij de implementatie van complexere *in vitro* modellen met verbeterde fysiologische relevantie om mens-specifieke ischemische responsen te modelleren en om klinische uitkomsten te voorspellen met grotere nauwkeurigheid. De ontwikkeling en toepassing van humane iPSC-afgeleide 3D neurosferoïd-modellen is een geschikte benadering om aan deze behoefte te voldoen.

In een eerste deel van dit doctoraatsproefschrift werd een zeer reproduceerbaar, luminescent, humaan iPSC-afgeleid neurosferoïde model ontwikkeld en gekarakteriseerd dat de real-time uitlezing van neurale viabiliteit na ischemie-achtige condities mogelijk maakt. Door 1 en 4 weken oude neurosferoïden zuurstof en glucose te ontnemen, werd het vermogen van het toegepaste bioluminescente systeem om neurotoxiciteit te detecteren aangetoond. Bovendien werden verschillen in gedrag na zuurstof-glucose deprivatie waargenomen tussen de verschillende leeftijden van neurosferoïden, waarbij neurosferoïden van 1 week oud, maar niet 4 weken oud,

spontaan herstel vertoonden. Dit benadrukt de behoefte aan meer mature neurosferoïden in *in vitro* beroerte-onderzoek die de *in vivo* volwassen situatie getrouwer recapituleren. Verder toonde de evaluatie van de pan-caspase inhibitor Z-VAD-FMK in het gevestigde model zijn onvermogen aan om de algehele neurale overleving in neurosferoïden te verhogen in tegenstelling tot een 2D-cultuur van dezelfde hiPSC-afgeleide neurale stamcellen, waar neuroprotectie wel werd waargenomen. Dit illustreert hoe de toegenomen complexiteit van sferoïde modellen kan resulteren in een ander resultaat bij het testen van neuroprotectieve middelen, wat verder het belang benadrukt van de invoering van mens-gebaseerde 3D-modellen in de preklinische fase van de ontdekking en ontwikkeling van geneesmiddelen, als aanvulling op 2D *in vitro*-modellen en preklinische *in vivo* modellen.

In het tweede deel van deze doctoraatsthesis werd de basis gelegd om de complexiteit en de voorspelbaarheid van het ontwikkelde humane neurosferoïd model verder te verhogen door meer mature, multicellulaire neurosferoïden te genereren. Gliacellen, waaronder astrocyten en microglia, spelen een belangrijke rol in zowel de verergering als het herstel na ischemie-geïnduceerde hersenschade. De introductie van deze celtypes zou het dan ook mogelijk maken de humane ischemische reacties nog beter na te bootsen. In een eerste reeks verkennende experimenten werden de kweekcondities geoptimaliseerd om neurosferoïden te verkrijgen met een verhoogde maturiteit en de aanwezigheid van astrocyten. Hierbij verhoogde de kweektijd van de neurosferoïden aanzienlijk de neuronale maturiteit evenals de spontane ontwikkeling van astrocyten. Er werd ook opgemerkt dat het kweken van neurosferoïden in geselecteerde differentiatiemedia geen aanleiding gaf tot astrocyten voor de geëvalueerde tijdstippen, ondanks hun vermogen om snellere differentiatie en maturatie te vertonen. In een tweede reeks verkennende experimenten werd de integratie van hematopoëtische voorlopercellen in neurosferoïden onderzocht met het oog op de toekomstige creatie van een immuuncompetent, met microglia verrijkt neurosferoïd model voor ischemische beroerte. Vergelijking van verschillende tijdstippen voor de toevoeging van hematopoëtische voorlopercellen aan neurosferoïden, toonde een hogere integratie-efficiëntie bij toevoeging aan vooraf gevormde neurosferoïden en suggereert een rol voor cytokine CSF-1 hierin.

Concluderend kan worden gesteld dat het hier ontwikkelde humane iPSC-afgeleide neurosferoïd-model, samen met de vooruitgang in het verhogen van de maturiteit en multicellulariteit, een nieuw model zou kunnen opleveren dat de humane ischemische reacties beter recapituleert dan de huidige *in vitro* en *in vivo* modellen. Daarom zou

hun invoering in preklinisch onderzoek, naast de traditionele 2D culturen en diermodellen, mogelijks klinische resultaten nauwkeuriger kunnen voorspellen waardoor meer inzicht verkregen kan worden in de werkzaamheid van kandidaat-interventies in de menselijke hersenen, wat uiteindelijk bijdraagt tot de ontwikkeling van dringend noodzakelijke nieuwe neuroprotectieve therapieën voor ischemische beroerten.

CHAPTER 1

General introduction, aim and thesis outline

1.1 Stroke statistics

With 6.5 million people dying from stroke annually, stroke is one of leading causes of death worldwide. The people that do survive stroke are often disabled, contributing to a huge fraction of the global disability. Besides the enormous impact of stroke on the quality of life of the patient and on society, stroke is also associated with a huge financial burden, with an estimated worldwide cost of 1.451 billion dollars only in 2017. Each year there are globally 12.2 million new stroke cases. The majority of these cases (~62%) is the result of blood vessel blockage, referred to as ischemic stroke and account for nearly 3.3 million deaths per year [1].

1.2 Ischemic stroke

1.2.1 The ischemic cascade

Cerebral ischemia occurs when the blood flow to the brain tissue becomes impaired, usually due to an embolus or thrombus. The brain's high energy demand and dependence on glucose as its main source of energy, makes this organ extremely sensitive to ischemia. Even brief periods of restricted oxygen and glucose supply can lead to energy failure and the activation of a complex cascade of events eventually resulting in brain damage (Fig. 1) [2-5].

Under physiological conditions, energy, in the form of adenosine triphosphate (ATP), is used to operate the sodium/potassium ion pumps of neuronal membranes, maintaining the ionic gradients needed for proper functioning of synaptic electrical signaling. The lack of ATP generation due to cerebral ischemia leads to dysfunction of this ion pump, resulting in membrane depolarization. Consequently, voltage-gated calcium channels become activated and lead to the influx of calcium (Ca^{2+}) into the cell, further affecting tissue damage by triggering multiple downstream mechanisms. Firstly, it causes the release of glutamate, an excitatory neurotransmitter, into the extracellular space that on its turn can further induce depolarization and glutamate release, ultimately accomplishing excitotoxicity. Together with the activation of specific glutamate receptors, the intracellular concentration of Na^{+}, Cl^{-} and Ca^{2+} ions increases causing water shifts to the intracellular space via osmosis, effectuating cell swelling and oedema, which is an important risk factor for post-stroke mortality. Furthermore, Ca^{2+}

activates different enzymes, including proteases, kinases, lipases and endonucleases, inducing among others the degradation of cytoskeletal proteins as well as extracellular matrix proteins and the generation of free radical species. These free radicals further damage DNA and cytoplasmic and mitochondrial membranes, ultimately resulting in cell death [2-5]. Moreover, together with damage-associated molecular patterns (DAMPs) released from damaged and dying cells, free radicals elicit an inflammatory response through the release of inflammatory mediators inducing the activation of microglia and astrocytes, leading to the production of cytokines and chemokines and the infiltration of leukocytes through a disrupted blood-brain barrier [2-6].

While represented here in a more simplified way, the pathophysiology of ischemic stroke is heterogenous and complex with the different events interconnected at different levels. These events can result in ischemic necrosis within minutes for the brain tissue exposed to the most drastic blood flow reduction. This irreversibly damaged brain tissue is known as the ischemic core and is surrounded by the less severely affected ischemic penumbra. The ischemic penumbra is a region between the lethal core and healthy brain tissue where the constrained blood flow partially preserves energy metabolism without supporting the tissue's function. Without reperfusion, the evolving cellular energy failure and secondary injury mechanisms including ongoing excitotoxicity, inflammation and apoptosis that develop in hours to days post-stroke may expand the infarct into the ischemic penumbra [2-5]. Interestingly, more recently, other programmed cell death mechanisms, such as necroptosis and ferroptosis, have been suggested to be implicated in the pathophysiology of ischemic stroke [7].

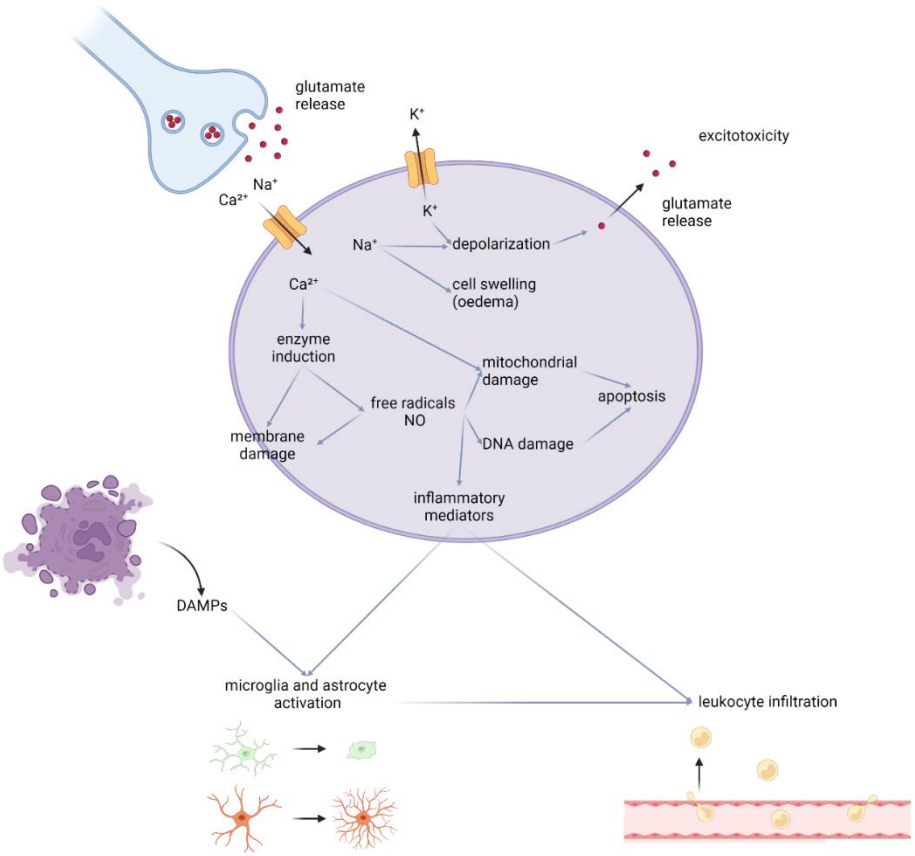

Figure 1 - Simplified overview of pathophysiological mechanisms of ischemic stroke. Ischemia-induced energy failure leads to the depolarization of neurons. Activation of specific glutamate receptors results in an increase of intracellular Ca^{2+} and Na^{+} levels, while K^{+} is released into the extracellular space. Water shifts to the intracellular space via osmosis, causing cell swelling (oedema). Intracellular Ca^{2+} activates different enzymes, including proteases, kinases, lipases and endonucleases. Free radicals damage membranes, mitochondria and DNA, in turn triggering cell death and induce – together with DAMPs - the formation of inflammatory mediators. The latter leads to the activation of glial cells and the infiltration of leukocytes via upregulation of endothelial adhesion molecules. (DAMPs, damage-associated molecular patterns; NO, nitric oxide)

1.2.2 Current treatment of ischemic stroke

Current treatment of acute ischemic stroke is based on early restoration of the blood flow through the administration of the thrombolytic agent tissue plasminogen activator

(tPA) (within 4.5h from symptoms onset) or mechanical clot removal by thrombectomy (within 6h from onset). However, the utility of these procedures is strongly limited by the narrow therapeutic time window and the multiple thrombolytic contraindications. Together with a relative high percentage of failures and the occurrence of complications, the actual number of ischemic stroke patients that can benefit from these revascularization procedures is very low. Moreover, these approaches do not affect the cascade of events leading to brain damage, neither do they target any process enhancing neuronal survival [3-5, 7, 8]. These limitations prompted researchers to investigate therapeutic strategies providing neuroprotection.

1.2.3 Neuroprotection as treatment strategy

Neuroprotection aims to protect the brain tissue from ongoing injury induced by cerebral ischemia and reperfusion. The target tissue of this therapeutic strategy is the ischemic penumbra, where brain damage evolves over the course of hours to days after the ischemic insult as a result of a cascade of events. The rather slow evolution of brain damage in the penumbra as compared to the ischemic core, extends the window of opportunity for therapeutic intervention [2, 3, 9]. The increased understanding of the cellular and molecular mechanisms in the pathophysiology of ischemic stroke, has led to the revelation of different targets for potential neuroprotective therapies. In what follows, the main strategies to induce neuroprotection are described, together with examples of compounds that have been evaluated in preclinical as well as clinical setting.

A first category of neuroprotectants are the glutamate receptor antagonists that interfere with the activation of glutamate receptors, which is responsible for excitotoxic-mediated cell death [4, 7, 10-12]. The main neuronal receptors activated by glutamate are N-methyl-D-aspartate (NMDA) and alpha-amino-3-hydroxy-5-methyl-4-isoxazole propionate (AMPA) receptors. Therefore, multiple NMDA and AMPA receptor antagonists have been tested in numerous preclinical and clinical studies [12]. MK-801 and dextromorphan - noncompetitive NMDA receptor antagonists – have been demonstrated to reduce infarct volume in experimental models of ischemic stroke. However, ensuing clinical trials were terminated due to psychotic side effects and lack of efficacy [13, 14]. Similarly, after promising results obtained in experimental stroke models, phase III clinical trials of other noncompetitive (aptiganel) and competitive (selfotel, eliprodil) NMDA receptor antagonists were discontinued owing to a lack of efficacy (as measured by the modified Rankin scale or Barthel index at 90 days after

stroke) or a trend to higher mortality in the treatment arms [12-16]. Additionally, the AMPA receptor antagonist, ZK200775, transiently worsened the neurological condition of patients with acute ischemic stroke in clinical trials [17, 18], despite the observed neuroprotection in a transient middle cerebral artery occlusion model of ischemic stroke [19]. In summary, besides the intolerable central nervous system adverse effects, glutamate receptor antagonists failed to show neuroprotective efficacy in human clinical trials. Importantly to recognize is that studies in animal models demonstrated that benefit only occurred when administered within the first 1-3 hours after ischemia, while most clinical trials have used a 6-hour window or longer [14].

Next, calcium-stabilizing agents, including glutamate receptor antagonists and voltage-gated calcium channel blockers (e.g. nimodipine and flunarazine), aim to enhance neuronal survival by inhibiting the detrimental excessive Ca^{2+} influx [4, 7, 10-12]. While nimodipine was able to decrease the infarct volume by 50% in a rat model of focal ischemia [20], results of this compound in at least 14 clinical trials were inconsistent. Whereas four trials found a positive outcome in terms of mortality, memory and neurological outcome (as assessed by Mathew scale of neurologic deficit) [21-24], this could not be confirmed by the majority of other clinical trials [13]. Moreover, flunarazine also failed to reduce mortality or to improve the functional outcome (as determined by the modified Rankin scale at 24 weeks) in acute ischemic stroke patients [25].

Another group of neuroprotectants are the antioxidants that target the damaging oxidative stress accompanying ischemic stroke [4, 7, 10-12]. A well-studied example is the free radical trapping compound, NXY-059. Profound preclinical evaluation of NXY-059 in various rodent models of cerebral ischemia and even in non-human primates showed reduced infarct size and functional improvement when given 4-5h after permanent and transient cerebral ischemia [26-29]. Based on these promising data, a first clinical trial (SAINT I) was conducted where administration of NXY-059 within 6h after the onset of acute ischemic stroke reduced disability in patients at 90 days (as measured by the modified Rankin scale) [30]. However, a larger follow-up trial (SAINT II) was not able to reproduce this result [31]. Different hypotheses are postulated to explain this inconsistency, including the statistical methods used to detect the first positive clinical outcome. Critical reanalysis of the preclinical datasets revealed that the efficacy of NXY-059 may have been overstated at this stage, as a result of bias in the conduct of animal studies and/or the negligence of potential co-morbidities (e.g. hypertension) often present in ischemic stroke patients [32]. Interestingly, a recent *in*

vitro study also showed no neuroprotective activity of NXY-059 when added to human embryonic stem cell-derived neurons deprived from oxygen and glucose, supporting the outcome of the large clinical trial [32].

Furthermore, anti-apoptotic agents, such as caspase inhibitors including Z-VAD-FMK and z-DEVD-FMK, are another category of neuroprotectants [4, 7, 10-12]. Though, showing neuroprotection in rodent models of ischemic stroke [33-35], no clinical trials with these compounds have been performed so far. In this doctoral thesis, the effect of administration of Z-VAD-FMK to the here developed luminescent neurospheroid cultures during OGD was assessed (Chapter 3).

Finally, antagonizing post-ischemic inflammation is another approach to induce neuroprotection. These neuroprotective agents can roughly be subdivided in (i) those that prevent the entrance of peripheral immune cells into the infarcted tissue (e.g. antibodies against intercellular adhesion molecules (ICAMs), selectins and integrins and matrix metalloproteinases (MMP) inhibitors) and (ii) those that inhibit the production or function of cytokines and chemokines (e.g. MAPK inhibitor) [4, 10-12]. Enlimomab – a murine monoclonal anti-ICAM-1 antibody – is an example of an anti-inflammatory agent evaluated in both preclinical as well as clinical studies. By inhibiting the endothelial-inflammatory cell interactions, administration of an anti-ICAM-1 antibody has shown to decrease the infarct size after transient focal ischemia in rats [36, 37]. However, a clinical trial using enlimomab demonstrated adverse effects and a worse neurological outcome, as determined by the modified Rankin scale at day 90, in treated ischemic stroke patients as compared to the control group [38]. It is suggested that the detrimental effects associated with enlimomab were due to an immune response towards the foreign mouse protein [39]. So far, anti-inflammatory agents targeting a single inflammatory mechanism have not yielded the expected clinical benefit. Moreover, the increasing evidence of the dual role (detrimental and protective) of immune cells after the ischemic insult has recently encouraged researchers to consider immunomodulation as a promising alternative to protect the brain tissue from progressing injury [3, 6, 40].

Since therapeutic agents targeting a single event of the ischemic cascade did not result in successful neuroprotection in clinical setting, more recently, compounds with pleiotropic effects, targeting the ischemic cascade at multiple levels, are being evaluated in experimental models and clinical trials. For instance, statins have been shown to possess anti-inflammatory and antioxidant properties, additionally able to reduce blood-brain barrier dysfunction and enhance cerebral blood flow [4, 9]. They

have proven to be effective in animal models of ischemic stroke, reducing the infarct volume and improving neurological outcome [41]. Moreover, clinical trials of statins have yielded promising results so far, improving the survival and alleviating physical disability in ischemic stroke patients at 90 days, as measured by the modified Rankin scale. Interestingly, delayed statin therapy (7 days following stroke) was as efficient as statin treatment initiated during the early phase of ischemic stroke (within 24h) [42-44]. Another promising pleiotropic approach being investigated in the acute ischemic stroke setting is therapeutic hypothermia. This strategy has previously been proven beneficial to patients after cardiac arrest [45]. While demonstrating reduced infarct size by approximately 40% and improved functional outcome in animal models of ischemic stroke [46], multiple clinical trials also showed improved functional outcome in acute ischemic stroke patients. However, a recent meta-analysis taking multiple hypothermia clinical trials into consideration, did not show a significant difference in functional independence, as measured by the modified Rankin scale, between control and therapeutic hypothermia group [47]. Interestingly, improved outcome was observed in patients undergoing selective therapeutic hypothermia (i.e. where the core body temperature is maintained), as compared to systemic therapeutic hypothermia, suggesting a role for hypothermia induction method in the efficacy of treatment [47, 48]. Further clinical trials will be needed to confirm the therapeutic benefit of cooling.

Although novel multi-target approaches hold promise and warrant optimism on the development of future neuroprotective therapies for ischemic stroke patients, it is clear that decades of research on neuroprotection have been largely disappointing. The efficacy of neuroprotective treatments, as observed in animal models for ischemic stroke, could overall not be translated to humans in clinical trials [2, 3, 9, 11, 12], resulting in not a single approved neuroprotective therapy for ischemic stroke patients able to complement current recanalization approaches.

1.2.4 Why neuroprotective agents fail in the clinic

While the majority of approaches mentioned earlier have demonstrated effective neuroprotection in the preclinical setting, they overall failed to show improvements in ischemic stroke patients. The discrepancy between bench and bedside studies may be due to several factors.

The first explanation can be allocated to the animal models themselves. The use of animal models in the evaluation of neuroprotective compounds is standard practice.

The laboratory animals used in most experimental studies are young and healthy. However, stroke patients are typically old and suffer from multiple chronic diseases such as arteriosclerosis, hypertension, diabetes, hyperlipidemia and/or a prior stroke, that can affect their functional outcome after stroke. Moreover, while the ischemic infarct of animal models in the same experiment is controlled in time and space, patients in clinical trials represent a heterogenous group with ischemic infarcts varying in terms of etiology, severity and location [2, 12]. Recently, it is recommended to include assessment of the candidate neuroprotective agent in experimental models of stroke with co-morbidities and advanced age in both sexes before moving to clinical trials [9].

A second explanation may reside in the different outcome measures used for evaluating the efficacy of the neuroprotective compound in laboratory animals versus humans. While in experimental studies typically the infarct sizes were measured until seven days after the ischemic insult, the efficacy assessment in humans mainly relies on the neurological outcome obtained by functional scores (e.g. the modified Rankin scale) three or six months post-stroke. Although markers of infarct volume or histopathology used in animal studies may be more sensitive, they poorly correlate with functional outcome because small lesions in critical locations can produce major functional deficits and vice versa. Therefore, nowadays, researchers performing studies using animal models are strongly encouraged to additionally conduct functional assessment. However, functional tests developed for animal studies may not reflect those in clinical trials [2, 12].

Furthermore, the distinct timing of treatment in relation to the therapeutic windows between animal models and humans may pose another reason. In many animal studies, the compounds were given before or immediately after the onset of ischemia resulting in successful neuroprotection. In clinical studies, drugs are often administered much later (≥ 6 hours after stroke onset), with administration times possibly falling outside the temporal window of efficacy. This explanation is especially plausible for treatments targeting injury mechanisms occurring early after stroke, e.g. excitotoxicity, that are often associated with narrow therapeutic time windows. Noteworthy is that the onset of cerebral ischemia in patients is often difficult to determine accurately, as symptoms might occur or be recognized with a delay from the onset. This entails that the time point of treatment may be inconsistent and even later than anticipated, further complicating the determination of the time window in which a certain drug might be effective in ischemic stroke patients [2, 12].

Last but not least, species-specific differences existing between humans and laboratory animals may account for the unsuccessful translation of neuroprotective strategies. The most common used species in preclinical stroke research are rodents. While the basic biology of cerebral ischemia is similar across all mammals, structural and functional differences between the human and rodent brain exist potentially translating into differences in pathophysiological stroke mechanisms or available targets between species [2, 12]. These differences are discussed in more detail in chapter 2. A potential strategy to tackle this issue is to verify the neuroprotective compounds in a model that more accurately replicates human ischemic stroke. At current, the use of human-based models in preclinical ischemic stroke research is rare because of the ignorance of species-specific differences, the difficult access of primary brain tissue and the lack of physiological relevance of easy accessible transformed cell lines. Especially in view of the latter, the introduction of complex brain tissue mimicking human-based *in vitro* models, next to animal-based models in the preclinical phase, would allow to verify the presence of targets of the neuroprotective compounds and to determine preliminary efficacy before entering the clinic, reducing the attrition rate in costly clinical trials.

1.3 Aim

The overall aim of this doctoral thesis is to develop a complex *in vitro* model with improved physiological relevance for the study of human ischemic responses and the evaluation of candidate neuroprotective compounds.

1.4 Thesis outline

In **chapter 2**, a comprehensive overview of current *in vitro* models used in ischemic stroke research is given. Furthermore, this overview is continued by a description of how more physiologically relevant *in vitro* models can look like by delineating the main factors determining the predictive value of *in vitro* models for modelling human ischemic stroke. These factors include the origin of cells or tissue, the presence of other central nervous system (CNS) cell types in co-culture models, the dimensionality of culture and the use of advanced technologies, such as microfluidics.

Putting these factors into practice, in this doctoral dissertation, I propose a human induced pluripotent stem cell (iPSC)-derived three-dimensional (3D) neurospheroid model for ischemic stroke research (Fig. 2).

In **chapter 3**, the development and characterization of luminescent human iPSC-derived neurospheroids is described. By means of the incorporated bioluminescent reporter, the viability of 1-week-old and 4-week-old neurospheroids after subjection to an ischemia-mimicking stimulus was monitored. Additionally, Z-VAD-FMK, a pan-caspase inhibitor and a candidate neuroprotective compound was evaluated in the established model.

With the aim of further increasing the complexity and predictivity of the human-based model system of chapter 3, in **chapter 4**, various explorative experiments performed to generate more mature, multicellular neurospheroids for ischemic stroke research are discussed.

Finally, **chapter 5** provides a critical discussion on the obtained results and their implications to the field of ischemic stroke research. Furthermore, future follow-up research opportunities building on the results and knowledge acquired in this doctoral thesis are proposed.

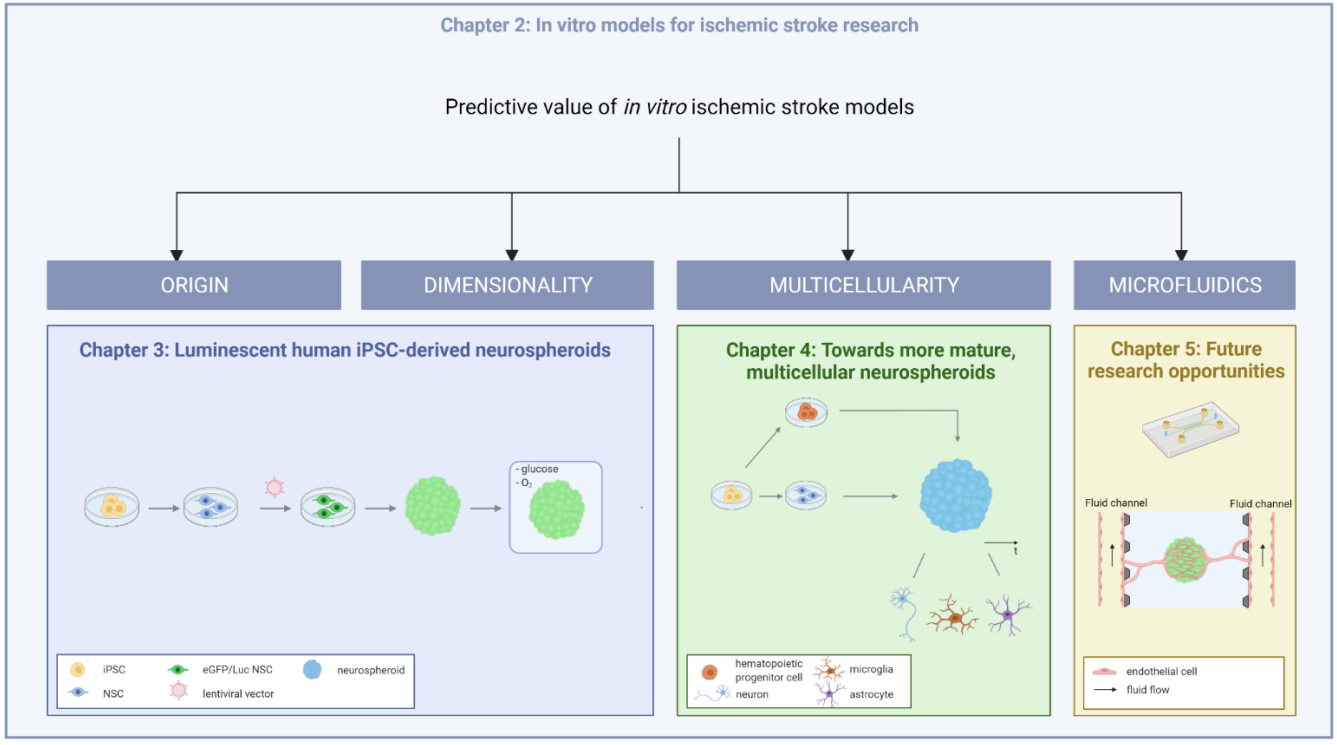

Figure 2 – Overview of the thesis outline. Putting the different factors that may improve the predictive value of in vitro models, described in chapter 2, into practice, this thesis describes the development of human iPSC-derived three-dimensional (3D) neurospheroid model for ischemic stroke research. To this end, chapter 3 covers the development and characterization of luminescent neurospheroids generated by the spontaneous self-assembling capacity of genetically engineered luciferase (Luc) positive human iPSC-derived neural stem cells. These neurospheroids are subsequently deprived from oxygen and glucose to model an ischemic stroke. Chapter 4 describes explorative experiments aimed at generating more mature, multicellular neurospheroids, including optimization of culture conditions and addition of hematopoietic progenitor cells to the neurospheroid. Chapter 5 describes future research opportunities, where microfluidics technology takes center stage. (iPSC, induced pluripotent stem cell; NSC, neural stem cell)

CHAPTER 2

In vitro models of ischemic stroke

This chapter has been published as:

Van Breedam E, Ponsaerts P. Promising strategies for the development of advanced *in vitro* models with high predictive power in ischemic stroke research. International Journal of Molecular Sciences. 2022.

2.1 Abstract

Although stroke is one of the world's leading causes of death and disability, and more than a thousand candidate neuroprotective drugs have been proposed based on extensive *in vitro* and animal-based research, an effective neuroprotective/restorative therapy for ischemic stroke patients is still missing. Especially the high attrition rate of neuroprotective compounds in clinical studies should make us question the ability of *in vitro* stroke models currently used for ischemic stroke research to recapitulate human ischemic responses with sufficient fidelity. The ischemic stroke field would greatly benefit from the implementation of more complex *in vitro* models with improved physiological relevance, next to traditional *in vitro* and *in vivo* models in preclinical studies, to more accurately predict clinical outcomes. In this review, we discuss current *in vitro* models used in ischemic stroke research and describe how more physiologically relevant *in vitro* models can look like by delineating the main factors determining the predictive value of *in vitro* models for modelling human ischemic stroke.

2.2 Introduction

Stroke is one of the leading causes of death and disability worldwide [49]. In the majority of cases (~62%), stroke is caused by occlusion of an arterial vessel by an embolus or thrombus, referred to as ischemic stroke [1]. The interruption of blood supply to the brain depletes the brain tissue from oxygen and other nutrients, causing energy failure and triggers the activation of a cascade of events eventually leading to brain damage [10]. Processes of this ischemic cascade include excitotoxicity, oxidative stress, blood-brain barrier (BBB) dysfunction, inflammation and cell death of neurons, glia and endothelial cells [5, 50].

Notwithstanding the impact of stroke on the patient's quality of life and on society, the current treatment of ischemic stroke patients is limited to the administration of the thrombolytic agent tissue plasminogen activator or to mechanical clot retrieval by thrombectomy. However, only a small proportion of all acute ischemic stroke patients are eligible for last-mentioned treatments mainly due to the very narrow therapeutic time window after stroke onset [51]. Tremendous efforts have been made to find new therapies targeting the ischemic cascade to prevent injured or vulnerable neurons from dying or even to stimulate regenerative processes. Over a thousand of candidate neuroprotective drugs have been proposed, showing promising results in animal models. Unfortunately, none of those led to an effective therapy to date as many of the neuroprotective agents failed when translated to the clinic. Multiple reasons may account for this lack of success, such as deficiencies in animal studies or clinical trial design [52, 53], but it is equally clear that the predictive power of the systems currently used to model ischemic stroke *in vitro* and as such to validate candidate compounds should be questioned.

In this review, we first describe the general experimental set-up to model ischemic stroke *in vitro*, including current main cellular platforms. Next, we describe the main factors affecting the predictive power of *in vitro* models, thereby shedding light on *in vitro* ischemic stroke research of the future.

2.3 Modelling ischemic stroke *in vitro*

Most of the knowledge on the pathophysiological mechanisms of ischemic stroke are derived from animal-based *in vitro* and *in vivo* models. Over the past decades, different animal models of stroke have been developed, induced by emboli, intraluminal suture,

photothrombosis or endothelin-1, typically in rodents [4, 10, 54]. The rat is the most commonly used species in stroke research, among other reasons, due to the similarity of the cerebral vasculature and physiology with that of human. Also mice are often used, since they are helpful in unravelling the function of certain genes in the pathophysiology of stroke by means of the creation of transgenic mice [4, 10, 54]. Animal stroke models have been an indispensable tool as they can model different aspects of the complex pathophysiology of ischemic stroke that cannot be modelled (yet) in simple *in vitro* models lacking intact blood vessels and blood flow [10, 55]. However, simplified, highly controlled *in vitro* systems are required and preferred when investigating specific basic mechanisms and cell type-specific responses under ischemia-like conditions [4, 55]. Besides, in the context of testing potential neuroprotective compounds, working *in vitro* allows high-throughput screenings, even on a human-based background [55].

2.3.1 Inducing ischemia-like conditions *in vitro*

To study ischemic stroke *in vitro*, ischemia-like conditions can be achieved by different approaches. The most common and most physiologically relevant way to induce ischemia-like conditions is by so-called 'oxygen-glucose deprivation' or OGD. In this approach cell or tissue cultures are placed in a hypoxic or anaerobic chamber, containing a N_2/CO_2 atmosphere, where the O_2/CO_2 equilibrated medium becomes replaced by glucose-free N_2/CO_2 equilibrated medium at the start of incubation [56-62]. The cultures are maintained for a duration of 30 minutes up to 24 hours in the chamber, depending on the specific cell type used and the desired degree of ischemic damage. Typically, a longer duration of oxygen and glucose deprivation is needed to cause cell injury or death *in vitro* than *in vivo*. Compared to ischemia *in vivo*, adenosine triphosphate (ATP) depletion is less severe and the release of glutamate is delayed [4]. OGD is often terminated by glucose addition and reoxygenation and is cultured under 'normal' conditions for up to 24 hours prior to downstream analyses. This allows modelling of *in vivo* reperfusion, known to further aggravate ischemic injury [63].

Besides OGD, hypoxia can be induced through either chemical or enzymatic inhibition of cellular metabolism. The chemical method relies on inhibition of the mitochondrial electron transport chain and has been regularly applied to cell cultures to study ischemic stroke. For instance, sodium azide and antimycin are commonly used chemical-hypoxia inducers in these studies [64-67]. Less common is the enzymatic induction of hypoxia, which relies on manipulating the glucose oxidase and catalase

(GOX/CAT) system [68-70]. Though less physiologically relevant, these chemical and enzymatic approaches can result in hypoxic/ischemic injury in a shorter time frame than conventional OGD [71].

Due to implementation of novel technologies in *in vitro* stroke model development, recently, researchers were able to recapitulate another factor besides oxygen and glucose depletion, namely the interrupted blood flow, by employing microfluidic systems [66, 72]. This appears to be another factor affecting the downstream ischemic cascade by reducing the integrity of the BBB and thereby allows to mimic *in vivo* stroke even more closely.

Also, specific aspects of the ischemic cascade can be modelled. For example, excitotoxicity models have been developed by exposing cultures to glutamate or glutamate receptor agonists such as N-methyl-D-aspartate (NMDA) [73]. The increase in the levels of intracellular free calcium is also an important effector of secondary injury subsequent to an ischemic insult and has been simulated in *in vitro* models by thapsigargin treatment [74].

2.3.2 Most common cellular platforms in *in vitro* stroke research

The main cellular platform used for *in vitro* stroke research consists of monocultures of rat primary neurons. In general, the use of monocultures is preferred when studying cell-specific responses to OGD and/or to evaluate the action of neuroprotective compounds on specific cell types. Among a lot of other applications, primary rat neurons have been used to evaluate the protective effect of basic fibroblast growth factor [75], intermittent hypothermia [76] and oxytocin against damage induced by an ischemic insult [61], as well as to elucidate the mechanisms underlying neuronal autophagy in ischemic stroke [77]. Moreover, rat primary neurons have been used to study the effect of hypoxia on the neuronal activity, by plating them on multi-electrode arrays during exposure of the culture to different durations of hypoxia [78].

Another widely used platform to model ischemia-like damage are organotypic brain slice cultures, typically from rodent origin. In these cultures, brain slices are obtained from young animals (postnatal day P3 to P10) and allowed to further develop and mature *in vitro* [79, 80]. The advantage of this culture type is that it largely preserves tissue structure maintaining neuronal activities and synapse circuitry [81]. Moreover, since multiple cell types are present, this model additionally allows to study cell-cell interactions [81]. Due to these unique features, this system is closer to an animal model

than is cell culture. Organotypic brain slice cultures have been valuable in the study of pathogenic mechanisms leading to ischemia-induced neuronal cell death, with in particular the excitotoxic mechanism. For instance, the involvement of glutamate – accumulating extracellularly after an ischemic insult – and glutamate receptors and transporters in the excitotoxic-induced damage have been extensively studied using the brain slice model [82, 83], reviewed in detail by Noraberg et al. [84]. Related or not to this glutamate-induced damaging mechanism, brain slice models have been applied to study calcium overload, mitochondrial dysfunction and oxidative stress, as well as to evaluate neuroprotective drugs [84]. Furthermore, in contrast to nearly all other *in vitro* systems where OGD media is applied over the entire culture, brain slice cultures could also be used as a platform to mimic focal ischemia. A protocol by Richard et al. describes a focal ischemia model by focally applying OGD medium to a small portion of the brain slice while bathing the remainder of the slice with normal oxygenated media [85].

Together with animal models, monocultures of primary rodent-derived neurons and rodent organotypic brain slices have shaped stroke research until present. These platforms have increased our understanding of the ischemic cascade and unveiled a myriad of potential targets for neuroprotective therapies. However, the high attrition rate of potential neuroprotective compounds in clinical studies should make us aware of the limitations of current models to model human ischemic stroke with sufficient fidelity. As such, the ischemic stroke field would greatly benefit from the implementation of novel, more complex *in vitro* models with improved physiological relevance next to traditional *in vitro* and *in vivo* models in preclinical studies, to more accurately predict clinical outcomes. In what follows, we will elaborate on the main factors that define the predictive value of *in vitro* stroke models, including the origin or source of cells or tissue, the presence of other central nervous system (CNS) cell types in co-culture models, the dimensionality of culture and the use of advanced technologies, such as microfluidics (Fig. 1).

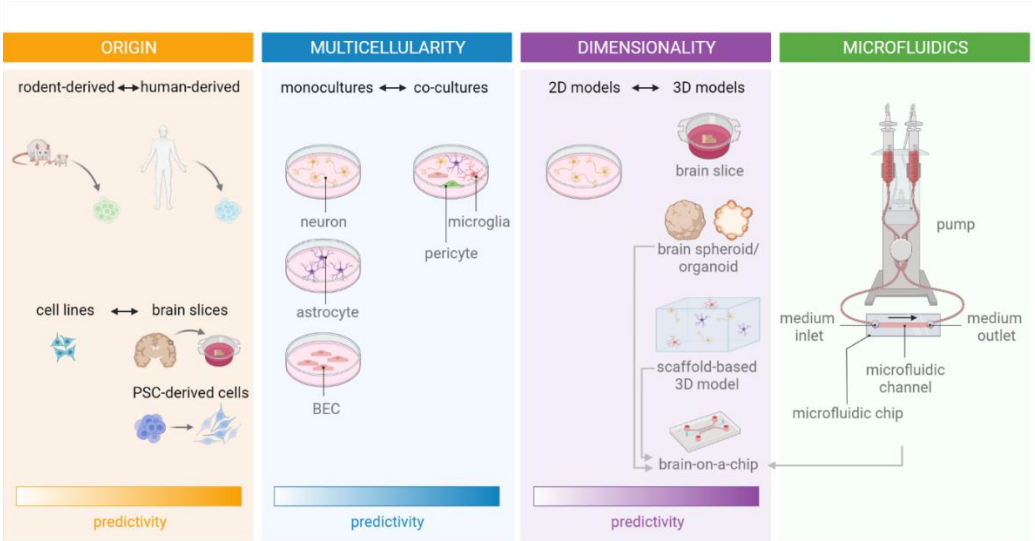

Figure 1 – Factors defining the predictive value of in vitro ischemic stroke models. Note that not all microfluidic devices are connected to a pump-system. (PSC, pluripotent stem cell; BEC, brain endothelial cell)

2.4 Factors defining the predictive value of *in vitro* ischemic stroke models

2.4.1 Origin of cells or tissue used for *in vitro* models of ischemic stroke

As described above, *in vivo* and *in vitro* rodent-based models are standard used in stroke research. Their use has led to our increased understanding of the ischemic cascade of human stroke as the main aspects of stroke hold true across all mammals. However, as rodents and humans are separated by 80 million years of evolution [53], species-specific anatomical, cellular and molecular differences exist between humans and rodents potentially affecting the outcome of neuroprotective strategies.

At the anatomical level, differences between human and rodents are evident, with humans having large gyrencephalic brains with a high proportion of white matter, whereas rodents have small smooth brains with relatively little white matter [53]. Associated to this difference in brain anatomy, the number of outer radial glia cells in rodent brains is small, while in primates this cell type is more abundant and possesses a higher self-renewal capacity [86, 87]. Furthermore, species-specific differences have

been reported on the expression levels and function of several BBB-transporters [88, 89]. Likewise, comparison of the distributions of predominant glial glutamate transporters revealed significant differences between species [90]. This variation may translate into differences in pathophysiological stroke mechanisms or available targets between species. Specifically related to stroke, it has been shown that the duration of excitotoxity after the ischemic insult differs between mice and humans, with longer duration for humans [91]. Also at the immunological level important differences exist between rodents and humans. A pioneering study of Seok et al. compared genomic responses to different acute inflammatory stresses (including endotoxemia, burns and trauma) between humans and mice, and found that the responses elicited in humans are not reproduced in the mouse models [92]. Moreover, there is increasing evidence that there are important differences between human and murine microglia [93]. Also in the context of ischemic stroke, dissimilarities are becoming apparent [94]. A study by Du et al. demonstrated that the baseline expression of cytokines/chemokines and response after OGD and reoxygenation in primary neurons, astrocytes and microglia differed significantly between rodents and humans [95]. For instance, while human primary neurons showed a downregulation in many of the determined chemokines (CX3CL1, CXCL12, CCL2, CCL3, and CXCL10) after OGD and reoxygenation, mouse neurons showed a mixed response with up- and downregulation of the same chemokines. These findings exemplify the importance of using human-based *in vitro* models in fundamental as well as translational stroke research, next to traditional *in vivo* models. The introduction of human-based *in vitro* models in the preclinical phase of drug discovery and development, would allow target identification and proof-of-principle demonstration that attacking these targets elicits appropriate cellular responses in a human context before entering the clinic, increasing chances of success for the agents to be effective in clinical setting [53]. Nevertheless, the use of human-based *in vitro* systems is rare in the field of ischemic stroke. The few human-based systems that have been used to date consist mainly of transformed cell lines and primary human brain slice preparations, each associated with their own limitations.

Most of the human-based studies were performed with immortalized neuroblastoma cell lines, such as SH-SY5Y cells [96-98]. Though interesting when considering future high-throughput screening applications, cell lines do not always accurately replicate the physiology of primary cells. Also in ischemic stroke research, their limited physiological relevance is reflected by their reduced susceptibility to hypoxic stimuli and their constant proliferation when compared to primary neurons [53]. Similar for *in vitro* stroke models of the BBB or neurovascular unit (NVU), brain endothelial cell lines, such

as HCMEC/D3, show lower protein expression of tight junctional proteins, adhesion molecules and transporters compared to their *in vivo* counterpart, possibly affecting the outcome of studies [71].

In contrast to cell lines, primary human brain slice preparations are highly physiologically relevant. The few studies employing human brain slices were focused on the excitotoxic component of the ischemic cascade [99-101]. The major issue to use these models is the extremely limited availability to human brain tissue. Moreover, caution should be given to the interpretation of results since the brain tissue is often derived from neurosurgery of young epileptic patients and preparation of the slices can introduce trauma possibly confounding results [52]. Considering similar limitations, retrospective studies using post-mortem brain tissue of human ischemic stroke patients are extremely limited but highly valuable. The few publications existing using human post-mortem stroke tissue all belong to the same research group and report on the ischemia-induced alterations in gene expression [102-104].

For decades, the limited availability and physiological relevance of human *in vitro* systems and the lack of technological advancements have favoured the use of rodent-based systems over human-based systems. Fortunately, human pluripotent stem cells have provided another cell source for generating human-based *in vitro* models with the ability to overcome aforementioned limitations. A recent publication of Liu et al. [105] describes human embryonic stem cell (ESC)-derived neurons as an alternative model for ischemic stroke research. Besides human ESCs, the advent of induced pluripotent stem cell (iPSC)-technology enabled pluripotent stem cells to be made out of terminally differentiated adult somatic cells, such as dermal fibroblasts and peripheral blood mononuclear cells [106, 107]. Since its discovery, protocols to generate different neural cells, such as neurons, astrocytes, oligodendrocytes and microglia, but also endothelial cells have been developed [108-121]. More recently, this technology has found its way in the ischemic stroke research. A first study using human iPSC-derived neurons was performed in 2020 by Juntunen et al., where the effect of OGD and potential protection by adipose stem cells was investigated [122]. Furthermore, human iPSC-derived cells are also increasingly being employed in the context of BBB/NVU models [123, 124] [66, 125]. It should be noted that, though iPSC-derived *in vitro* platforms have boosted research in many fields and hold great promise for the future, there are still challenges associated with the use of iPSCs. Residual epigenetic memory, genetic background and incomplete reprogramming could possibly influence the iPSC phenotype and differentiation potential, resulting in a great diversity among human iPSC-derived cell

lines [126]. The reproducibility may partially be increased by the improvement and standardization of differentiation protocols with the identification of environmental cues involved in neural development in the field of developmental biology.

2.4.2 Multicellular co-culture models for *in vitro* ischemic stroke research

As mentioned earlier, the majority of *in vitro* stroke research is conducted using monocultures of neurons. Apart from neurons, a monoculture of rodent primary astrocytes has been used to determine the protective roles of pinin and stem-cell derived exosomes after ischemic stroke [127, 128]. Furthermore, when focusing on the BBB-disruption facet under ischemic conditions, the use of pure cultures of brain endothelial cells has been regularly reported [129-135]. Monoculture systems are particularly useful to investigate mechanisms restricted to specific cell types or to determine the contribution of specific cell types to different pathophysiological mechanisms. However, several reasons substantiate the use of co-culture models to obtain models better resembling the human brain. First, the human brain consists of an intricate cellular network, including neurons, astrocytes, oligodendrocytes, microglia, pericytes and endothelial cells. Therefore, every cell type added to the *in vitro* system increases the complexity, approaching more the *in vivo* complexity of the human brain. Second, co-cultures enable cellular interactions that occur *in vivo* and as such the presence of different cell types and interactions can influence RNA transcription, protein production and functionality of certain cell types.

The importance of cell-cell interactions occurring under physiological conditions become evident from different publications. For example, astrocytes provide metabolic substrates to neurons (i.e. energy supply to neurons) and are actively involved in the formation and refinement of neuronal networks. Indeed, they are shown to integrate and modulate neuronal excitability and synaptic transmission [136-138]. These functions of astrocytes could also be observed in *in vitro* astrocyte-neuron co-culture models. Astrocytes, from rodent and human origin, co-cultured with human PSC-derived neurons improves the functional maturation of those neurons, as demonstrated by an increased percentage of active neurons, bursting frequency and synchronization of neuronal calcium oscillations when compared to the neuronal monocultures [139-142]. Also, mutual interactions between microglia and neurons in healthy brain exist, where neurons (e.g. through CX3CR1-CX3CL1 or CD200-CD200R interactions), or neural environment in general, keep microglia in a non-activated state, thereby favoring their homeostatic functions maintaining neuronal health and

regulating proper function of neuronal networks [113, 143-145]. Furthermore, co-cultures of brain endothelial cells with other CNS cells, such as astrocytes and pericytes, contribute to BBB integrity and function among others by stimulating tight junction formation and expression of polarized transporters in endothelial cells [71, 126, 146-149].

Also under pathological ischemic conditions, cellular interactions are important in regulating cell behavior and contribute to the mechanisms leading to brain injury or recovery. For example, co-cultures of microglia/macrophages with neurons or brain slices have been developed and employed in the field of stroke research to investigate the inflammatory response secondary to an ischemic insult. After an ischemic insult, brain-resident microglia and blood-derived macrophages can acquire a pro-inflammatory neurotoxic phenotype further exacerbating brain damage. To study the cross-talk between hypoxic neurons and macrophages, Desestret et al. subjected an organotypic hippocampal slice to OGD for 30 minutes and subsequently added macrophages for 2 days [150]. Other studies used co-cultures of rat primary microglia with primary neurons or a combination of primary neurons and astrocytes to elucidate the effect of neuronal ischemia on microglia polarization and, conversely, the effect of microglia phenotype on the fate of healthy or ischemic neurons [56, 151, 152]. These studies confirmed that pro-inflammatory activation of microglia by damage-associated molecular patterns released from damaged neurons after OGD, further exacerbates neuronal death. Likewise, a neutrophil-neuronal co-culture was recently developed to investigate mechanisms of neutrophil-dependent neurotoxicity [153]. Last-mentioned study found that cell-cell contact was required for the process of neutrophil-induced neuronal injury. Next to neuro-immune interactions, neurovascular and gliovascular interactions occurring during cerebral ischemia have also been identified. From a study comparing brain endothelial cells in monoculture versus co-cultures of brain endothelial cells with neurons or astrocytes, it became apparent that neurons and astrocytes, exposed to either OGD, aglycemia or hypoxia, affect different endothelial properties, including its barrier and lymphocyte adhesion properties, endothelial cell adhesion molecule expression and *in vitro* angiogenic potential [154]. For instance, the interaction of brain endothelial cells with neurons or astrocytes under OGD and subsequent reoxygenation, results in attenuation of BBB permeability and in recovery of the barrier. This compensatory mechanism of astrocytes for maintaining BBB function after ischemic stroke has been confirmed in another study, identifying a role for astrocyte-derived pentraxin 3 [155]. However, the excessive production of cytokines, chemokines and proteases in the ischemic infarct might undermine the

adaptive nature of the BBB, leading to increased permeability [154]. Identification of these interactions is important as changes in BBB permeability can affect cerebral edema, post ischemic brain angiogenesis (associated with survival of stroke patients) and leukocyte interactions that aggravate ischemia reperfused stroke brain damage [154].

All these examples represent only a small part of all existing (un)identified interactions occurring under ischemic stroke-pathological conditions that can affect the progression of ischemia-associated brain damage or recovery. Therefore, it is of importance to include different cell types to more faithfully recapitulate the ischemic responses occurring *in vivo*. Besides the aforementioned co-cultures of microglia, macrophages or neutrophils with neurons, other co-cultures consisting of neurons and astrocytes have been used in ischemic stroke research [59, 156]. Recently emerging three-dimensional (3D) models of the brain also consist of multiple cell types, which will be further discussed in next section 'Dimensionality'. In addition, BBB/NVU models of ischemic stroke, often combine different cell types, which will be further discussed under the 'BBB/NVU models' section.

2.4.3 Dimensionality of cell culture models for *in vitro* ischemic stroke research

Most of the knowledge derived from *in vitro* stroke studies is based on neural cells grown as monolayers. This traditional simplified culture system has been of undisputable significance for biomedical research, including stroke, especially considering their relatively low cost and reproducibility when compared to animal models [157]. Moreover, decades of research using these monolayer cultures has led to the optimization and standardization of many downstream applications tailored for 2D cultures, including the easy visualization by means of microscopic imaging. Nevertheless, 2D cultures are unable to mimic the complicated microenvironment cells experience in tissue. Unlike cells cultured in 2D, in the *in vivo* brain, cells are able to generate 3D projections and establish multiple interactions with other cells and cell types and extracellular matrix (ECM) [157, 158], eventually affecting their morphology, survival, proliferation, differentiation, gene expression and even function (e.g. electrophysiological network properties) [74, 157]. Therefore, 3D models of the brain are considered more realistic models of the human brain than conventional 2D models, better mimicking its complexity and possibly ischemia-induced responses [157].

A first model that allows ischemic stroke studies to be conducted in a more relevant 3D microenvironment, is posed by *ex vivo* acute and organotypic brain slices. As described earlier, this model is able to retain largely the tissue structures, where multiple cell types retain most of cells' *in vivo* properties and spatial organization and intricate network organization and function. However, next to different considerations, such as the limited culture time or maturation of acute and organotypic brain slices, respectively [79, 80], the scarcity of human-derived brain slices restrict research to the use rodent-based (organotypic) brain slices less faithfully predicting human pathophysiological mechanisms.

Second, the advent of iPSC-technology has boosted the development of 3D models of the brain, such as brain spheroids or organoids [159]. Neural organoids are self-assembled PSC-derived 3D *in vitro* cultures that recapitulate the developmental processes and cytoarchitecture of the developing human brain [159-161]. Different neural organoids and spheroids have been developed ranging from brain organoids containing multiple different brain regions, termed 'cerebral organoids', to brain region-specific organoids, including forebrain, midbrain, cerebellar and hippocampal and hypothalamic organoids, through the use of patterning factors [162-170]. Protocols to generate these brain spheroids/organoids differ in several aspects, such as the use of ECM, patterning factors or the initial cells used, which are either PSCs or neural stem/progenitor cells derived from PSCs. These differences can have implications on the complexity of the model making them more or less suitable for certain specific applications. The use of these organoids has proven extremely useful for the study of neurodevelopment and associated pathologies, such as microcephaly, ZIKA virus infection and autism spectrum disorders [164, 169, 171-173]. Other applications include neurodegenerative disease modelling and neurotoxicity testing [166, 174-176] [177]. Though current brain spheroids and organoids are already useful tools gaining popularity in different biomedical fields, they are subject to continuous research aimed at improving their resemblance to the human brain. One of the major limitations of current organoid and spheroid models is the lack of vascularization, causing the development of a hypoxic, necrotic core further hampering the growth and maturation of neural organoids and spheroids [157, 160, 161, 178, 179]. Researchers are therefore trying to develop vascularized brain organoids [180-182] or implement microfluidic technologies (further described in section 'microfluidic technologies'). Besides vasculature, organoids generally lack microglia [157, 160, 161, 178, 179], which have important roles in immune defense and maintenance of CNS homeostasis [183]. Recently developed differentiation protocols of iPSC-derived microglia [112-116] are

paving the way to develop state-of-the-art immune-competent brain organoids and spheroids [184-186], more closely mimicking the human brain. Ischemic stroke research would also greatly benefit from the generation of brain organoids containing vasculature (preferably with specialized BBB properties), and microglia, since it is a cerebrovascular disease with neuroinflammation being an important aspect of secondary injury after stroke. Finally, the heterogeneity of organoids, especially the cerebral organoids, in terms of size, shape and composition pose another major limitation [179, 187, 188]. Lower heterogeneity and enhanced reproducibility are crucial for controlled experiments and future potential screening approaches [187]. Several ways to reduce variability have been proposed, such as the use of bioreactors, avoidance of natural hydrogels (e.g. Matrigel) containing undefined factors, the use of patterning factors and starting from iPSC-derived neural stem/progenitor cells instead of iPSC to exclusively obtain cells of neuroectodermal lineage [157, 169, 187].

Only a few articles have been published so far in which brain organoids or spheroids were subjected to hypoxic stimuli. To date, most studies that exposed neural organoids to low oxygen tension envisaged to study the effect of hypoxia on neurodevelopment and corticogenesis. For instance, Pasça et al. subjected brain region-specific organoids called human cortical spheroids (hCS) to hypoxia to determine the effect of oxygen deprivation on corticogenesis, to model injury in the developing brain. They found that intermediate progenitors, a specific population of cortical progenitors that are thought to contribute to the expansion of the primate cerebral cortex, were reduced following hypoxia and subsequent reoxygenation. Also Kim et al. studied the effect of hypoxia on neurodevelopment [189]. They used human neural organoids, derived from neural stem cells (NSCs), and found that after hypoxia, reoxygenation was able to restore neuronal proliferation but no neuronal maturation, as shown by the retained decrease of TBR1+ cells. Similarly, Daviaud et al. subjected human cerebral organoids with dorsal forebrain specification to transient hypoxia, as a model for prenatal hypoxic injury, and demonstrated the distinct vulnerability and resilience of different neuroprogenitor subtypes [190]. They show that outer radial glia (FMA107+) and differentiating neuroblasts/immature neurons (TBR2+ and DCX+) are highly vulnerable to hypoxic injury, whereas NSCs displayed relative resilience to hypoxic injury and even provide a mechanism to replenish the stem cell pool, by shifting the cleavage plane angle favoring symmetric division. The results of last-mentioned study were also replicated by our own studies. With the aim of developing a human neurospheroid model for ischemic stroke, we equipped iPSC-derived neurospheroids with intrinsic bioluminescence to enable real-time monitoring of viability of neurospheroids subjected to OGD and were

able to model OGD-mediated neurotoxicity [191]. By comparing 1-week-old with 4-week-old neurospheroids, containing a high proportion of undifferentiated NSCs and intermediate progenitors/immature neurons, respectively, it was demonstrated that 1-week-old neurospheroids were able to completely and spontaneously recover from the initial OGD-induced damage over the course of one week, unlike 4-week-old neurospheroids. These dynamics of OGD-mediated neurotoxicity of different ages of neurospheroids underscore the need for older, more mature neurospheroids for *in vitro* stroke research.

Furthermore, cerebral organoids have also been employed to further unravel the mechanisms underlying ischemic injury. Iwasa et al. subjected cerebral organoids to OGD and reoxygenation and identified peroxisome proliferator-activated receptor (PPAR) signaling and pyruvate kinase isoform M2 (PKM2) as key markers of neuronal cells in response to OGD and reoxygenation [192]. In addition, Ko et al. described 3D cortical spheroids derived from primary rat cortical cells treated with OGD and reoxygenation as a model for cerebral ischemia [193]. They demonstrated that their model successfully mimicked the ischemic response as evidenced by the upregulated mRNA expressions of the key markers for stroke, S100B, IL-1β and MBP and additionally substantiate the role of transient cell-substrate interactions herein. Lastly, spheroid models have also been exposed to hypoxia to study the integrity of the BBB under pathological conditions. Nzou et al. made cortical spheroids with a functional BBB by mixing human primary brain endothelial cells, pericytes, astrocytes, and human iPSC-derived microglia, oligodendrocytes and neurons at a certain ratio in a hanging drop culture environment. They challenged the spheroids with a hypoxic stimulus and showed that hypoxia resulted in BBB disruption as evidenced by altered localization of tight and adherens junctions [149]. This further indicates the usefulness of the organoid/spheroid model in studying ischemia in a physiologically relevant environment.

Alternative to neurospheroids and organoids, recently also scaffold-based 3D systems have been proposed as a potential *in vitro* model for CNS injury, including stroke. Here, cells are embedded in a polymer-based scaffold that mimics the ECM of the brain. Lin et al. seeded SH-SY5Y cells onto a patterned gelatin scaffold and investigated the neuroprotective effects of resveratrol, an AMP-activated protein kinase (AMPK) activator, when subjected to OGD [194]. Vagaska et al. describe a model consisting of primary human NSCs dispersed in a hydrogel (i.e. Collagen-I/Matrigel) subjected to OGD or to thapsigargin, an inducer of intracellular calcium release [74]. In the same

study, the difference in human NSC phenotype and damage response between 2D and 3D cultures of NSCs was assessed, suggesting that 3D models may be better predictors of the *in vivo* response to damage and compound cytotoxicity.

Finally, these brain spheroids/organoids and scaffold-based 3D cultures of CNS cells can take advantage from microfluidic systems, to generate so called brain-on-a-chip models, forming the final category of existing 3D cell cultures of the brain. Brain-on-a-chip models and microfluidics technology are further discussed in the next section 'microfluidic technology'.

Considering the impact of dimensionality on cells' morphology, proliferation, differentiation and electrophysiological properties under physiological conditions [74, 157], it is not hard to assume that it might as well affect the behaviour of cells in response to pathological stimuli and/or therapeutic compounds. This concept was already demonstrated in the context of hepatotoxicity research, where 3D hepatocyte cultures were less susceptible to cell death when exposed to cytotoxins in comparison with 2D cultures [195]. Within the field of *in vitro* stroke research, important differences between 2D and 3D neural cultures are also becoming apparent. For instance, the earlier mentioned study of Vagaska et al. demonstrated the lower susceptibility to OGD-mediated damage for human NSCs grown in 3D, when compared to their 2D counterpart. The same could be concluded when thapsigargin was used as stimulus, after eliminating the possibility of reduced drug accessibility as a confounding factor [74]. In the context of the development of a 3D cortical spheroid model for cerebral ischemia, Ko et al. confirmed that 3D cell culture models represent better normal brain models, since the neural cells in 3D maintained their healthy physiological morphology of a less activated state and suppressed mRNA expressions of pathological stroke markers S100B, IL1-β and MBP [193]. Also our studies demonstrated different behavioural responses of neural cells in 2D and 3D. More specific, the response to treatment with the pan-caspase inhibitor Z-VAD-FMK during and after OGD differed between NSCs cultured in 2D versus NSC-derived neurospheroids. Where Z-VAD-FMK conferred neuroprotection in 2D, in line with other publications, it failed to protect neurospheroids under OGD [191]. Altogether, these findings further underscore the importance of 3D models in basic as well as applied *in vitro* stroke research to complement conventional 2D cell cultures and *in vivo* animal studies.

2.4.4 Implementation of microfluidics technology in *in vitro* models of ischemic stroke

Besides the factors described above, new technologies may also help to increase the complexity and predictive power of *in vitro* ischemic stroke models (Fig. 1). The newly developed 'brain-on-a-chip' models employ microfluidics technology to create a more physiologically relevant microenvironment for the culture of CNS cells. Through the spatial control over fluids in micro-meter sized channels, microfluidics enable (i) the co-culture of cells in a spatially controlled manner, (ii) generation of and control over (signaling) gradients and (iii) perfusion flow, contributing to an increase in physiological relevance of *in vitro* models [196]. These applications will be further discussed hereafter.

First, microfluidics facilitate physical separation of cellular populations and/or components on a microscale as a basis for mechanistic studies [126]. For instance, using microfluidic devices, the interaction between neuronal populations derived from different brain regions can be studied. This way, cortico-thalamic, cortico-hippocampal interactions and even interactions between three different brain regions (cortex, hippocampus and amygdala) have been established to model the brain's complex neuronal architecture and functionality [126]. The studies using microfluidic systems to investigate brain region interactions are nicely described in the review by Nikolakopoulou et al. [126]. Besides the physical isolation of different cell populations, microfluidics are also used to separately study axons and cell bodies of neurons (Fig. 2). Axons are directed to grow in microgrooves, thereby isolating axons from the cell soma. This platform allows the study of axonal biology, injury, regeneration and myelination but also synapse formation and modulation as well as viral spreading after axonal infection [197-201]. Specifically in the context of stroke, similar microfluidic set-up has been used to study the spreading neurotoxicity into undamaged brain areas [202]. Hereto, hippocampal neurons were cultured in each chamber and synaptically connected via axons traversing the microchannels. An isolated excitotoxic insult (i.e. glutamate) was delivered to neurons in one chamber and spreading toxicity of other synaptically connected neuronal populations could be monitored [202]. This system thus allows to recapitulate focal ischemia, which has been considered difficult to mimic in *in vitro* models.

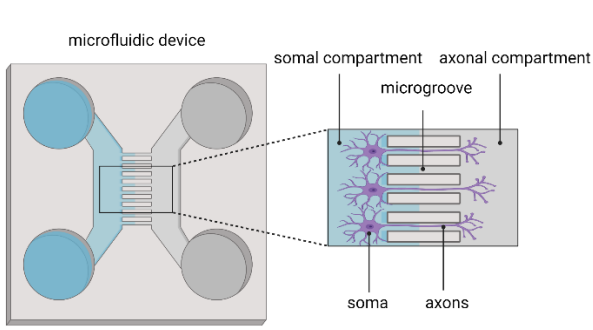

Figure 2 – Microfluidic device for isolating axons from the neuronal soma.

Second, since microfluidics enable spatial control over fluids, gradients can be generated and precisely controlled [196]. This has proven particularly useful for studying angiogenesis, invasion and migration, as all are associated with molecular gradients *in vivo* [196]. Biochemical gradients of growth factors and cytokines also dictate differentiation patterning *in vivo*, making microfluidic devices suitable tools for studying early neurodevelopment [126, 203-205]. Likewise, different microfluidic devices have been developed to establish oxygen gradients in cell and tissue cultures [206-213]. By flowing gas mixtures with desired oxygen concentrations through gas-permeable polydimethylsiloxane (PDMS) gas channels, cellular platforms, including adherent cells, brain slices and even 3D scaffold-based or spheroid models, can be rapidly and efficiently exposed to a range of oxygen concentrations as low as 0.1% O_2 [206-213], which are of relevance for future ischemic stroke research. Compared to a hypoxic chamber, where all cultures are exposed to the same oxygen tension, this microfluidic based system allows to apply multiple oxygen concentrations or gradients to cultures, representing another possible approach to induce focal ischemia by means of microfluidics technology [80, 213].

Last but not least, the compartmentalization of microfluidic devices allows the perfusion of media adjacent or through (3D) cell cultures on microfluidic chips. This perfusion ensures stable nutrient and oxygen supply and removal of waste metabolites and mimics physiological flows, such as interstitial or blood flow. Moreover, accompanying the fluid flow, physiological shear stresses are introduced, which have been shown to be essential for cellular morphology and gene expression of endothelial cells, when modeling vascularity [196]. The perfusion feature of microfluidics has also been exploited to specifically support the perfusion of brain spheroids and organoids generated on a microfluidic chip [214-218]. Evidently, this microfluidic platform is also ideal to recapitulate the BBB, and even the complete NVU, which is of particular

interest for stroke research. The different BBB/NVU models will be described in section 'BBB/NVU models'.

Despite the benefits of microfluidics in creating physiological relevant models and increasing the reproducibility of 3D CNS models [160], these models are nevertheless associated with several disadvantages. The fabrication of microfluidic devices typically rely on multi-step lithographic processes that are time-consuming and complex and require specialized equipment and expertise [148]. This has greatly limited the wide adoption of these systems in research. However, 3D printing might partially solve this issue by providing an alternative fabrication approach [148]. Also, microfluidic platforms are associated with limited scalability [148]. Currently, novel platforms are being developed allowing the culture of multiple chips in parallel [66]. Finally, the use of microfluidics typically requires smaller amounts of media and cells compared to traditional cell culture systems. Though, cost-effective, this also poses a challenge for downstream analysis, requiring highly sensitive instruments [196].

2.4.4.1 BBB/NVU models

Since ischemic stroke is a cerebrovascular disease, the vasculature of the brain plays an essential role in the cause (i.e. obstructed blood flow by blood clot) as well as progress of ischemic stroke. Indeed, stroke is associated with disruption of the BBB, which under physiological conditions tightly controls the entry of molecules from the circulation into the brain, thereby ensuring homeostasis. However, as previously described, *in vitro* stroke models generally lack vasculature and thereby ignore this aspect of ischemic stroke pathology. However, several models to investigate the BBB or broader, the NVU, have been developed over the years and are recently reviewed in detail by Andjelkovic [71]. Here, we will provide a brief overview of current and future BBB/NVU models, with their (potential) application in the context of stroke research.

The BBB is formed by specialized brain endothelial cells with barrier properties, surrounded by astrocytes and pericytes that support and maintain BBB function. The perivascular milieu of the BBB also includes neurons and neuronal endings and transiently present microglia/macrophages, which together with the BBB components are referred to as the NVU [71]. Depending on the availability of model systems and different applications, different BBB/NVU models have been used and developed in *in vitro* stroke research.

The oldest and simplest *in vitro* BBB model consists of a monolayer of brain endothelial cells (BECs). This model allows to unravel specific mechanisms elicited in BECs under stroke-like conditions [132, 135, 219, 220]. For instance, Itoh et al. used this model to determine whether BECs could be a source of free radicals after reperfusion, which are known for its detrimental effects on the brain after transient ischemia [132]. When cultured on semi-permeable membranes, using Transwell systems (Fig. 3), BEC monolayers enable the study of permeability of the BBB. Indeed, different *in vitro* studies examined the role of specific factors or mechanisms associated with OGD-induced barrier dysfunction using this model [133, 134]. However, these represent only poor models of the BBB considering that the formation, maintenance and function of the BBB have been found to depend on intercellular interactions with other CNS cells, with extensive body of evidence for the role of astrocyte-BEC and pericyte-BEC interactions [71, 126, 146-149]. Hereto, co- and tri-culture Transwell systems were developed (Fig. 3), with BECs seeded on the membrane in the upper chamber, while perivascular cells (astrocytes, pericytes and possibly even neuron and microglia) are cultured either on the other side of the membrane or on the bottom of the lower chamber. Comparably to the monoculture systems, these models have been used to study OGD-related mechanisms leading to BBB alterations [221-224].

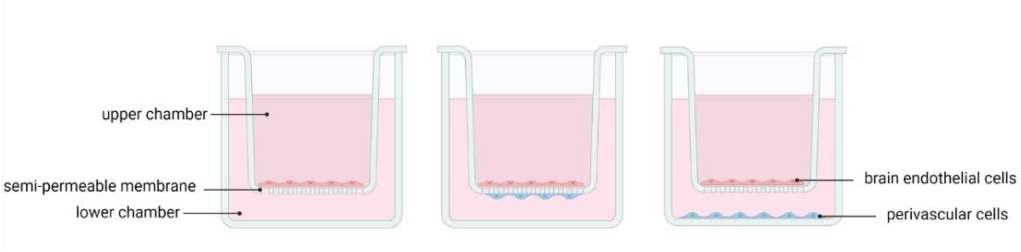

Figure 3 – Schematic representation of BBB/NVU models employing Transwell systems. Brain endothelial cells are seeded on the semi-permeable membrane in the upper chamber. Often perivascular cells, mainly astrocytes and/or pericytes, are cultured on the other side of the membrane or on the bottom of the lower chamber.

Although, the co-culture Transwell systems improved BBB/NVU models to a significant extent, the lack of a 3D structure and the lack of flow and accompanying shear stress, known to be an important factor in inducing and maintaining the BBB-characteristic phenotype of BECs, limits the physiological relevance of these BBB/NVU models [71, 148]. Hence, 3D models of BBB/NVU were developed, including the dynamic *in vitro* model of the BBB (DIV-BBB) and microfluidic BBB/NVU platforms.

The first model of the BBB/NVU able to incorporate flow was the DIV-BBB model (Fig. 4). In this platform, BECs are seeded on the luminal side of artificial capillaries, i.e. microporous pronectin-coated polypropylene hollow fibers, while perivascular cells (mostly astrocytes and pericytes) were grown on the outer surface. By means of a pulsatile pump, intraluminal flow and pressure can be obtained comparable to that found in capillaries *in vivo* [71, 148]. This way, BECs are exposed to flow and shear stress, achieving BBB properties more similar to those *in vivo* than static Transwell co-culture systems. DIV-BBB has been used to mimic an ischemic-like event *in vitro*, by flow cessation and reperfusion in the presence of circulating leukocytes [225-227]. This particular experimental set-up allowed to assess the role of inflammation, including leukocyte activation and associated release of pro-inflammatory cytokines, in BBB failure secondary to an ischemic-like event. Despite their broad applicability in *in vitro* stroke research, these models are costly and require specialized equipment, limiting their adoption in studies and their high-throughput potential [148]. In terms of physiological relevance, the thick membrane (~150µm) of the hollow fiber wall limits direct cell-cell contact between BECs and perivascular cells and limits studies of drug transport and leukocyte transmigration [71]. To this end, microfluidic systems were introduced.

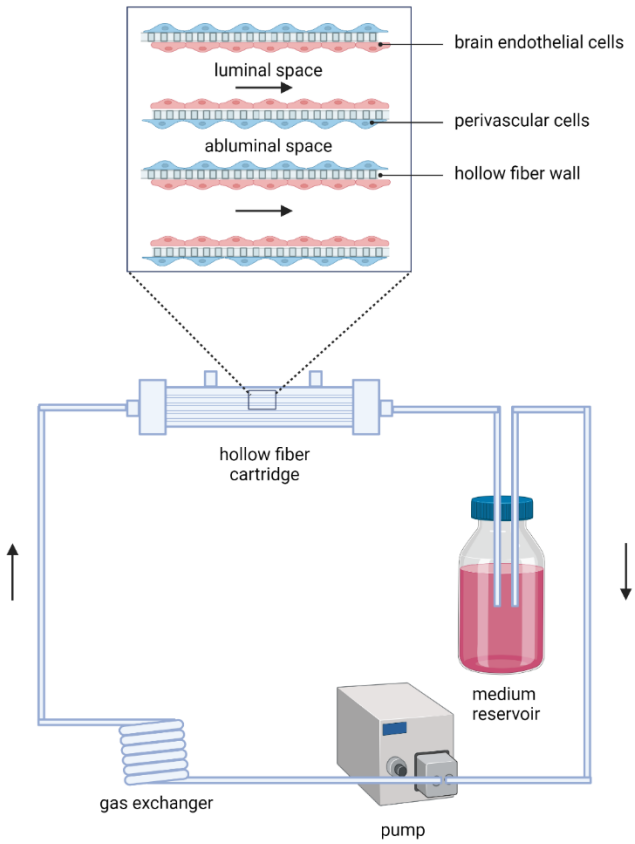

Figure 4 – Schematic representation of the DIV-BBB model. Brain endothelial cells are seeded on the inside of ECM-coated hollow fiber structures. Perivascular cells, mainly astrocytes and/or pericytes, are cultured on the coated outer surface of the hollow fiber wall, i.e. membrane of ~150µm thick. The pulsatile pump enables the establishment of intraluminal flow and pressure comparable to that found in capillaries in vivo. (ECM, extracellular matrix)

Different microfluidic-based BBB/NVU models have been developed and can be roughly categorized into 2D, 2.5D and 3D BBB/NVU models (Fig. 5) [228]. The first BBB/NVU microfluidics-based model was developed by Booth et al. [229], and consists of two perpendicular-crossing channels (one luminal and one abluminal) to introduce dynamic flows, a porous (ECM-coated) membrane at the intersection of the flow channels for cell culture, and even multiple embedded electrodes to monitor the functionality of the barrier (measured by transendothelial electrical resistance or 'TEER'). BECs and astrocytes were cultured on the luminal and abluminal sides of the porous membrane, respectively. The membranes used were much thinner than the hollow fiber walls of the DIV-BBB model, allowing improved cell-cell contact. The model of Booth et al. laid the foundation for the development of other 2D microfluidic BBB

models, generally including two compartments separated by a permeable membrane, where minimum one compartment acts as a flow channel to mimic vascular blood flow [230-233]. These models can differ in terms of cell types, the presence of TEER electrodes or a peristaltic pump. To the best of our knowledge, this model has not yet been used in the context of ischemic stroke research.

2.5D BBB/NVU models refer to microfluidic devices consisting of a compartment containing perivascular cells dispersed in a hydrogel matrix and another compartment containing BEC monolayers grown on ECM-coated rectangular shaped PDMS channels that are exposed to fluid flow (Fig. 5) [234] [66, 235, 236]. Micropillars create distinctions between these channels, allowing hydrogels to be confined to the brain parenchymal channel [234]. Gaps between these micropillars enable direct cell-cell contact in contrast to previously mentioned membrane-based BBB models, improving further the physiological relevance of the BBB. This model, with or without adaptations, has already been applied in the context of ischemic stroke research in three studies, with Cho et al. being the first to suggest the use of their microfluidic BBB/NVU model as an *in vitro* model for ischemic stroke [235]. They developed a BBB model, consisting of a monoculture of rat brain endothelial cell line monolayers on ECM-coated rectangular shaped PDMS channels, without fluid flow or shear stress, and subjected it to ischemia-like conditions by means of replacing the medium with glucose-free medium and incubation in an anaerobic chamber. They confirmed disruption of BBB integrity under these stimuli and used this model to evaluate the protective function of antioxidant and ROCK-inhibitor treatments, which appeared to be limited [235]. Compared to this study, Lyu et al. and Wevers et al. both generated more predictive models of ischemic stroke, by co-culturing human-based neural cells embedded in 3D hydrogels and by incorporating halted perfusion as an additional stimulus to mimic ischemic stroke, next to hypoxia (either by OGD or chemical hypoxia) and hypoglycemia (replacement of media by glucose-free (and serum-free) media) [66, 72]. Lyu et al. developed a microphysiological model of ischemic stroke based on a BBB/NVU model containing human BECs, pericytes, astrocytes, microglia and neurons in order to assess the neurorestorative potential of different therapeutic stem cells after ischemic damage [72]. Wevers et al. described a human NVU on-a-chip model containing primary BECs in co-culture with iPSC-derived astrocytes and neurons that under stroke mimicking conditions showed reduced BBB integrity, mitochondrial membrane potential and ATP, which are common features of ischemic stroke. Moreover, they use a platform allowing the culture of 40 NVU on-a-chip models simultaneously, making the platform suitable for high-throughput applications [66].

Finally, 3D BBB/NVU microfluidic models consist of a 3D hydrogel matrix containing a cylindrical void, generated by using a needle as a mold or by means of a process called viscous fingering, that is lined with BECs on the gel's inner surface (Fig. 5) [237-242]. This allows direct cell-cell contact, without the need for micropillars or membranes. The choice of hydrogel is important since it needs to be able to resist perfusion while providing physiologically relevant cues resembling ECM *in vivo* [228]. So far, this type of microfluidic BBB/NVU model has not been used yet in stroke research, but may become of significant importance in future *in vitro* stroke research.

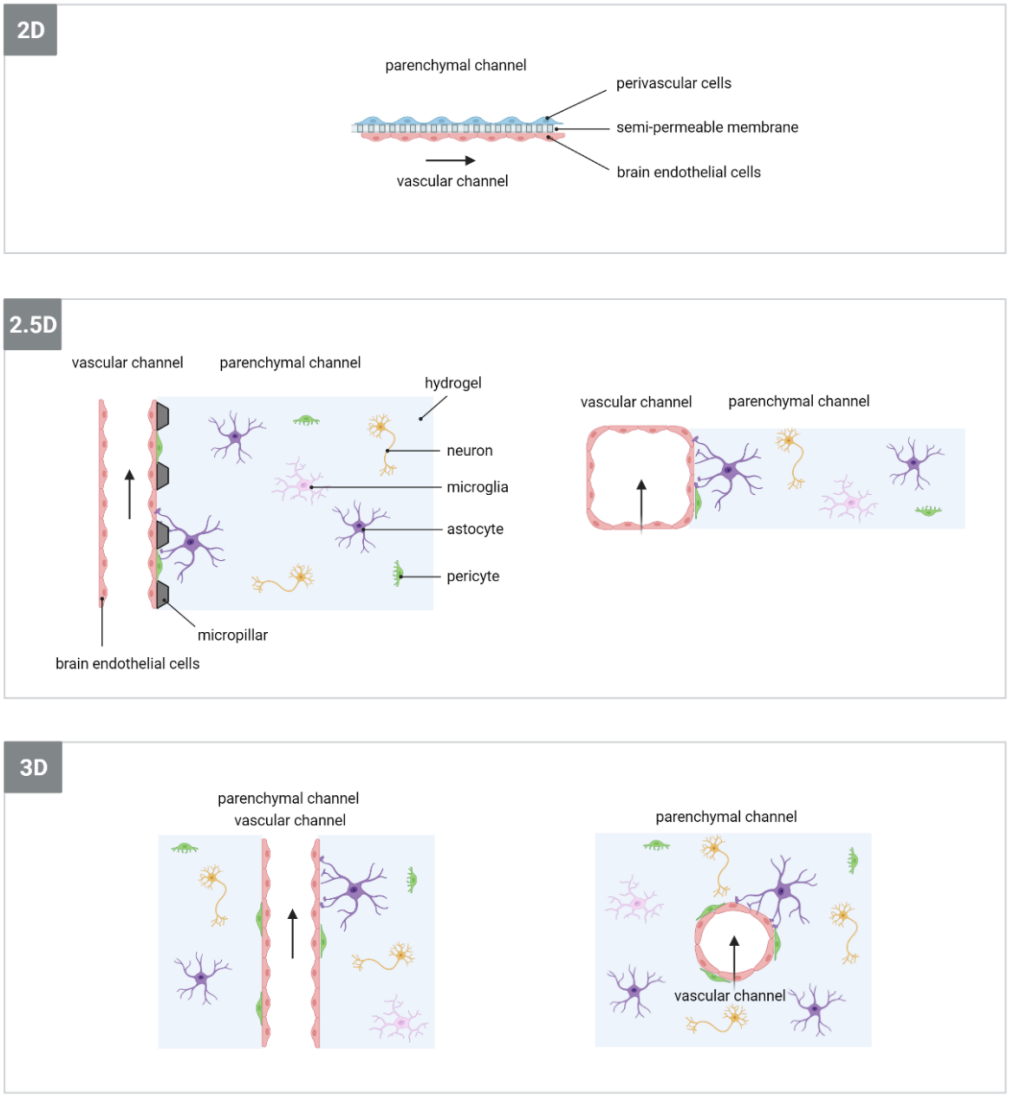

Figure 5 – Schematic representation of 2D, 2.5D and 3D microfluidic-based BBB/NVU models. Perivascular cells indicated in 2D BBB/NVU model mainly consist of astrocytes and/or pericytes. The arrows indicate fluid flow. Figure based on Cameron et al. [228] and Katt et al. [234].

2.5 Conclusion

Human-based 3D models consisting of multiple cell types, either with or without the use of microfluidic technology, may better recapitulate human ischemic responses than current *in vitro* and *in vivo* models. Therefore, their introduction in preclinical research,

next to traditional 2D cultures and animal models, may more accurately predict clinical outcomes, providing more insight into the efficacy of candidate interventions in the human brain eventually aiding the development of urgently needed novel neuroprotective therapies for ischemic stroke.

CHAPTER 3

Luminescent human iPSC-derived neurospheroids enable modelling of neurotoxicity after oxygen-glucose deprivation

This chapter has been published as:

Van Breedam E, Nijak A, Buyle-Huybrecht T, Di Stefano J, Boeren M, Govaerts J, et al. Luminescent Human iPSC-Derived Neurospheroids Enable Modeling of Neurotoxicity After Oxygen-glucose Deprivation. Neurotherapeutics. 2022.

3.1 Abstract

Despite the considerable impact of stroke on both the individual and on society, a neuroprotective therapy for stroke patients is missing. This is partially due to the current lack of a physiologically relevant human *in vitro* stroke model. To address this problem, we have developed a luminescent human iPSC-derived neurospheroid model that enables real-time read-out of neural viability after ischemia-like conditions. We subjected 1- and 4-week-old neurospheroids, generated from iPSC-derived neural stem cells, to 6 hours of oxygen-glucose deprivation (OGD) and measured neurospheroid luminescence. For both, we detected a decrease in luminescent signal due to ensuing neurotoxicity, as confirmed by conventional LDH assay and flow cytometric viability analysis. Remarkably, 1-week-old, but not 4-week-old neurospheroids recovered from OGD-induced injury, as evidenced by their reduced but overall increasing luminescence over time. This underscores the need for more mature neurospheroids, more faithfully recapitulating the *in vivo* situation. Furthermore, treatment of oxygen- and glucose-deprived neurospheroids with the pan-caspase inhibitor Z-VAD-FMK did not increase overall neural survival, despite its successful attenuation of apoptosis, in a human-based 3D environment. Nevertheless, owing to its three-dimensional organisation and real-time viability reporting potential, the luminescent neurospheroids may become readily adopted in high-throughput screens aimed at identification of new therapeutic agents to treat acute ischemic stroke patients.

3.2 Introduction

Stroke is one of the leading causes of death and disability worldwide [49]. Notwithstanding the impact of stroke on the patient's quality of life and on society, the current treatment of ischemic stroke patients is limited to the administration of the thrombolytic agent tissue plasminogen activator or to mechanical clot retrieval by thrombectomy. However, only a small proportion of all acute ischemic stroke patients are eligible for last-mentioned treatments mainly due to the very narrow therapeutic time window after stroke onset [51].

In an urgent need to find new therapies, decades of research resulted in over a thousand of candidate neuroprotective drugs of which none have led to an effective therapy to date. Although considered promising in rodent models, many neuroprotective agents failed when translated to the clinic. Multiple reasons may account for this lack of success, such as deficiencies in animal studies or clinical trial design [52, 53], but it is equally clear that the predictive power of the systems currently used to model ischemic stroke *in vitro* should be questioned.

To study ischemic stroke *in vitro*, ischemic conditions are usually induced by chemical or enzymatic inhibition of metabolism or by more physiologically relevant oxygen and glucose deprivation (OGD), followed by the assessment of the viability and/or cytotoxicity through endpoint assays [56-62]. The vast majority of *in vitro* stroke research is based on the use of rodent cells, with rat primary neurons being the most common. However, as rodents and humans are separated by 80 million years of evolution, cellular and molecular differences exist [53]. In case of stroke, these differences are for instance reflected in a longer duration of excitotoxicity – a part of the ischemic cascade - for humans compared to mice [91]. It is therefore easy to understand that molecular targets identified in rodents might not all be present in humans. The few human-based systems that have been used to date in the field of stroke research, consist mainly of less physiologically relevant cancer cell lines, such as the neuroblastoma cell line, SH-SY5Y [96, 98, 243, 244], and more relevant but difficult to obtain primary human brain slice preparations [100, 101]. Fortunately, the advent of induced pluripotent stem cell (iPSC)-technology has provided another cell source for generating human-based *in vitro* models with the ability to overcome the aforementioned limitations.

Besides the limited number of studies using brain slices, all knowledge acquired from *in vitro* stroke research is based on cells grown as a monolayer. However, it is well

accepted that three-dimensional (3D) models are able to more faithfully recapitulate the *in vivo* human brain in terms of physiology, as compared to traditional 2D cell cultures. In 3D, cells are able to generate 3D projections and establish multiple interactions with other cells and cell types and extracellular matrix in a way that is more representative to the human brain [158]. Moreover, as shown by a recent study [74], the dimensionality of neural culture also seems to affect the response to damage induced by OGD, with 3D models being more resilient. Although 3D brain organoids have found their way into many research fields, their use in *in vitro* stroke research has been largely unexplored territory. Only recently, pioneering studies have exposed brain organoids to low oxygen levels, mainly to investigate the effect of hypoxia on neurodevelopment and corticogenesis [189, 190, 245].

Obviously, the stroke field will benefit from new physiologically relevant *in vitro* models complementing *in vivo* research to eventually improve the clinical translation of promising neuroprotective strategies. In this study, we developed and validated a new human-based model to facilitate *in vitro* stroke research using human iPSC-derived neurospheroid technology (Fig. 1). By means of an incorporated bioluminescent reporter, we have made it possible to directly read out the spheroid culture health condition after the induction of an ischemic-like event in real time. To provide the proof-of-concept of this new model system, 1- and 4-week-old neurospheroids were subjected to OGD and analysed both by luminescence measurements and various conventional methodologies. Furthermore, the (in)effectivity of Z-VAD-FMK, a caspase inhibitor, to confer neuroprotection was evaluated in this human model system.

3.3 Methods

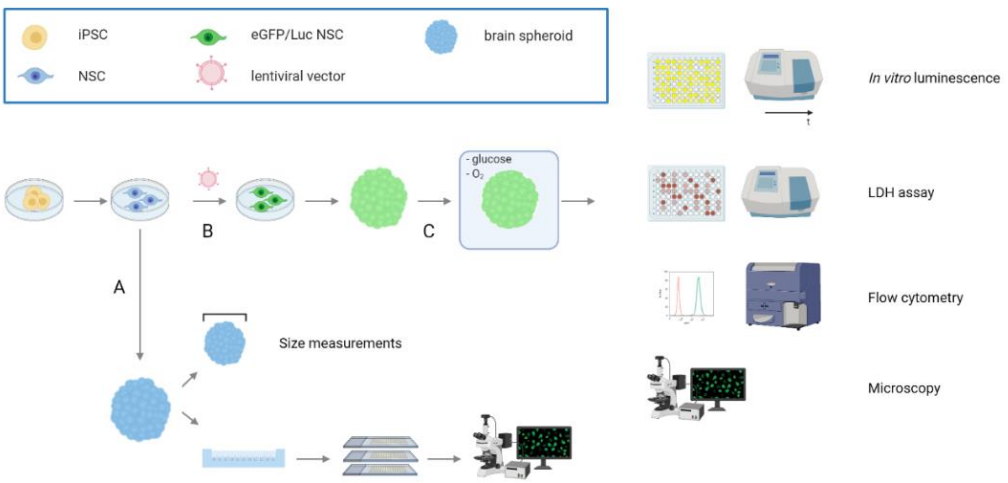

Figure 1 - General overview of the development and characterization of the luminescent neurospheroid model for in vitro stroke research. (A) Neurospheroids were generated starting from human neural stem cells (NSCs) that were differentiated from human iPSCs (hiPSCs). Obtained neurospheroids were characterized for their growth (size measurements) and cell composition (histological quantification using a spheroid array). (B) Luminescent neurospheroids were developed by genetic engineering of the hiPSC-derived NSC population using a lentiviral vector encoding a green fluorescent protein and firefly luciferase reporter open reading frame (ORF) (eGFP-T2A-fLuc) together with a puromycin resistance ORF, by puromycin selection. (C) Luminescent neurospheroids were subjected to OGD and validated as a model for in vitro stroke by luminescence measurements, LDH assay, flow cytometry and histological analysis.

3.3.1 Culture of human neonatal foreskin fibroblasts and embryonic stem cell-derived neural progenitors

Both the neonatal foreskin fibroblasts and the embryonic stem cell-derived neural progenitors used in this study were newly obtained with confirmed origin. Human neonatal foreskin fibroblasts (ATCC, CRL-2522™) were cultured in RPMI supplemented with 15% heat-inactivated fetal bovine serum (FBS, Gibco), 1% sodium pyruvate (Gibco) and 1% penicillin-streptomycin (PS, Gibco). Human embryonic stem cell-derived neural stem cells (ENStem-A^{TM} neural progenitor cells, EMD Millipore) were cultured in ENStem-A^{TM} neural expansion medium supplemented with 2mM L-glutamine (Gibco) and 20ng/ml human fibroblast growth factor-2 (FGF-2, EMD Millipore) on poly-L-

ornithine (20µg/ml, Sigma-Aldrich) and laminin-coated (5µg/ml, Merck Millipore) plates, according to the manufacturer's instructions. Both cultures were maintained at 37°C with 5% CO_2 with medium changes every other day or every 2-3 days for the stem cells and the foreskin fibroblasts, respectively.

3.3.2 Generation and culture of human induced pluripotent stem cells

Human induced pluripotent stem cells (hiPSCs) were generated by the reprogramming of neonatal foreskin fibroblasts (ATCC, CRL-2522™) using CytoTune®-iPS 2.0 Sendai Reprogramming Kit (ThermoFisher) according to the manufacturer's instructions. Obtained hiPSCs were further cultured feeder-free in Essential 8 Flex medium (Life Technologies) on Matrigel (Corning)-coated plates at 37°C with 5% CO_2. Medium was changed every other day.

3.3.3 hPSC ScoreCard assay

Embryoid bodies (EBs) were generated from hiPSCs in Essential 6 medium (Life Technologies) in ultra-low attachment (ULA) 24-well plates (Sigma). RNA was extracted from hiPSC at day 0 and 14 of EB formation using a commercial RNA extraction kit (Zymo). Next, cDNA was prepared using the Super Script III First Strand Synthesis kit (Life Technologies) before the TaqMan™ hPSC ScoreCard™ assay (ThermoFisher) was performed according to the manufacturer's instructions. The accompanying data analysis software was used to quantitatively compare the gene expression profile of the samples to that of a reference set.

3.3.4 Generation and culture of hiPSC-derived neural stem cells

Neural stem cell (NSC) cultures were established from hiPSCs using a commercial Neural Induction Medium (Gibco) according to the manufacturer's instructions with minor modifications. In brief, hiPSCs were plated at a density of 2.5 x 10^5 cells per well of a Matrigel (Corning)-coated 6-well plate. 24h post-seeding, medium was switched to Neural Induction Medium (Neurobasal medium (Gibco), 1x neural induction supplement (Gibco), 1% PS (Gibco)). After seven days of neural induction, obtained hiPSC-derived NSCs (further annotated as hiPSC-NSC) were further cultured in complete Neural Expansion Medium (cNEM) (1:1 Advanced DMEM/F12 (Gibco):Neurobasal medium (Gibco), 1x neural induction supplement (Gibco), 1% PS

(Gibco)) in 6-well plates coated with Geltrex™ (Life Technologies). Cultures were maintained at 37°C with 5% CO_2 with medium changes every other day.

3.3.5 Copy Number Variation sequencing

DNA libraries of hiPSC-NSCs were prepared using the NEXTflex Rapid DNA-seq kit (following option 2, with bead-based size selection prior to polymerase chain reaction amplification) and NEXTflex DNA barcodes (PerkinElmer), starting from 200 ng of DNA. Next, libraries were equimolarly pooled to a concentration of 4-6 nM. Cluster generation was completed using a cBot 2 system (Illumina) and sequencing was performed on a HiSeq 3000 device (Illumina) in a single-read 50-cycle run mode. The minimal number of reads per sample was set at 15 million (mean coverage of 0.25x). Demultiplexing was executed by the bcl2fastq software (Illumina). Reads were mapped to GRCh38 with bwa mem v0.7.17 [246] and duplicate reads were removed with Picard [247] MarkDuplicates v2.21.6. Afterwards, for sWGS, the log2(ratio) was called and processed with WisecondorX [248] v1.1.6 and visualized in Vivar [249] to allow detection of copy number variations (CNVs) larger than 50kb.

3.3.6 Neural differentiation of hiPSC-NSC

Neuronal and astrocyte differentiation was performed based on the protocol of Yan et al. [120], with minor adjustments. For neuronal differentiation, hiPSC-NSCs were grown onto poly-L-ornithine (20µg/ml, Sigma) and laminin (10µg/ml, Sigma)-coated well plates in neuronal differentiation medium (Neurobasal Plus medium (Gibco), 1x B27 plus supplement (Gibco), 2mM L-glutamine (Gibco), 1x CultureOne supplement (Gibco), 200µM ascorbic acid (Sigma), 1% PS (Gibco), 20ng/ml brain-derived neurotrophic factor (BDNF) and glial cell line-derived neurotrophic factor (GDNF) (Immunotools)) for a minimum of 16 days. Medium was changed every 2-3 days. For astrocyte differentiation, hiPSC-NSCs were cultured on Geltrex-coated well plates in astrocyte differentiation medium (DMEM (Gibco), 1x N2 supplement (Gibco), 2mM L-glutamine (Gibco), 1% FBS (Gibco), 1% PS (Gibco)) for a minimum of 22 days. Medium was changed every 2-3 days.

3.3.7 Neurospheroid formation and culture

To generate single neurospheroids of reproducible size, hiPSC-NSCs were seeded at a density of 1.6 x 10^4 cells per well in an ULA 96-well plate (Corning) in cNEM. The second or third day after plating, fresh medium was added. Cultures were maintained at 37°C with 5% CO_2 and from day 3 post-seeding onwards under constant orbital shaking (88 rpm). A half medium change was performed every other day and even every day upon long-term culture.

3.3.8 Spheroid size measurements

The diameter of the neurospheroids was measured every week for five weeks using a Fluovert Leitz microscope with CellSens Entry software v.2.1.

3.3.9 Immunofluorescence of 2D cultures and neurospheroids

All steps described hereafter were performed at room temperature (RT), unless stated otherwise. For the 2D cultures, cells grown on coverslips were fixed with 4% paraformaldehyde (PFA) for 20 min at 4°C. After a washing step with phosphate-buffered saline (PBS), cells were permeabilized for 30 min using 0.1% (v/v) Triton X-100 (Sigma) in Tris-buffered saline (TBS) and blocked with blocking solution consisting of TBS with 20% serum of the corresponding secondary antibody host species for 1h on a shaker. Cells were incubated (4°C) overnight with the primary antibodies diluted in 10% (m/v) milk solution (Sigma) in TBS (Table 1). After a washing step and a subsequent 1h incubation with the secondary antibodies in milk solution on a shaker (Table 2), cells were again washed and counterstained with DAPI (1µg/ml, Sigma) for 10 min at 4°C. After a final washing step with distilled water, the sample was mounted using ProLong® Gold antifade reagent (ThermoFisher).

Table 1 - List of primary antibodies used for immunocytochemistry. (NA, not available)

	Antibody	Host	Source	Final concentration
A	Nanog	Rabbit	Life technologies (PA1-097)	2 µg/ml
B	Oct3/4	Mouse	Santa Cruz (sc-5279)	2 µg/ml
C	Tra-1-60	Mouse	Santa Cruz (sc-21705)	1 µg/ml
D	Tra-1-81	Mouse	Santa Cruz (sc-21706)	1 µg/ml
E	SOX1	Goat	R&D systems (AF3369)	2 µg/ml

F	SOX2	Rabbit	Merck Millipore (AB5603)	2 µg/ml
G	Oct3/4	Rabbit	Santa Cruz (sc-9081)	2 µg/ml
H	Tuj1	Mouse	R&D systems (MAB1195)	2 µg/ml
I	GFAP	Rabbit	Abcam (ab7260)	1-10 µg/ml
J	Ki67	Rabbit	Abcam (ab15580)	5 µg/ml
K	NeuN	Guinea pig	Merck Millipore (ABN90P)	5 µg/ml
L	TBR2	Rabbit	Abcam (ab23345)	2-3 µg/ml
M	PAX6	Mouse	Abcam (ab78545)	20 µg/ml
N	Hop	Mouse	Santa Cruz (sc-398703)	4 µg/ml
O	DCX	Rabbit	Abcam (ab18723)	2 µg/ml
P	Cl. Casp-3	Rabbit	Cell Signaling Technology (9661)	NA – 1/400 dilution

Table 2 – List of secondary antibodies used for immunocytochemistry.

Antibody	Host	Conjugation	Source	Final concentration	In combination with
Anti-goat	Donkey	AF555	Invitrogen (A21432)	10 µg/ml	E
Anti-rabbit	Donkey	AF488	Invitrogen (A21206)	2 µg/ml	A, F, G, J
Anti-mouse	Goat	AF555	Invitrogen (A21425)	2 µg/ml	B, H, M, N
Anti-mouse	Goat	AF555	Invitrogen (A21426)	10 µg/ml	C, D
Anti-rabbit	Goat	FITC	Jackson ImmunoResearch (111-096-045)	7.5 µg/ml	I, L, O
Anti-guinea pig	Donkey	Cy3	Jackson ImmunoResearch (706-165-148)	7.5 µg/ml	K
Anti-rabbit	Donkey	AF555	Invitrogen (A31572)	2 µg/ml	P

Neurospheroids were fixed with 4% PFA for 150 min at RT. To allow high-throughput staining of neurospheroids, we adapted the spheroid micro-array technology described by Ivanov et al. [250] (Fig. 2). The original approach arranges up to 66 spheroids into a gel-based array that subsequently becomes paraffinized and sectioned. However, paraffin embedding does not preserve reporter fluorescence and requires tedious (de)paraffinization and antigen retrieval steps. Therefore, we here describe a new

protocol to generate cryosections of parallel-mounted spheroids, explained in detail hereafter.

A silicone mold was made by imprinting a 3D printed mold-maker (Molecular Spectroscopy research group, University of Antwerp) onto liquid silicone (15 shore A, Henry Schein) (Fig. 2), leaving a mold of either 66 or 35 wells, depending on the mold-maker used for the corresponding size of the neurospheroids. TissueTek-OCT (VWR) was poured into the silicone mold, which was positioned in a metal histology base mold for stabilization. Before loading the neurospheroids, a centrifugation step (100xg for 1 min) ensured that the OCT in the wells was free from air bubbles. Next, the neurospheroids, that had been incubating with 20% sucrose in distilled water overnight for cryoprotection purposes, were pipetted into the OCT in the individual wells. Following a final centrifugation step (100xg for 1 min) to pellet all neurospheroids to the bottom of the wells, the OCT with neurospheroids in the silicone-histology base mold was snap-frozen in isopentane at a fixed temperature of -50°C using liquid N_2. The resulting OCT-block was removed from the silicone mold and turned upside down in the histology base mold (i.e. peaks directing upwards). Another layer of TissueTek-OCT was poured on top of the OCT-peaks and frozen again. Cryosections of 10µm were made on poly-L-lysine (Sigma)-coated glass slides making use of the NX70 cryostar cryostat (Thermo Scientific).

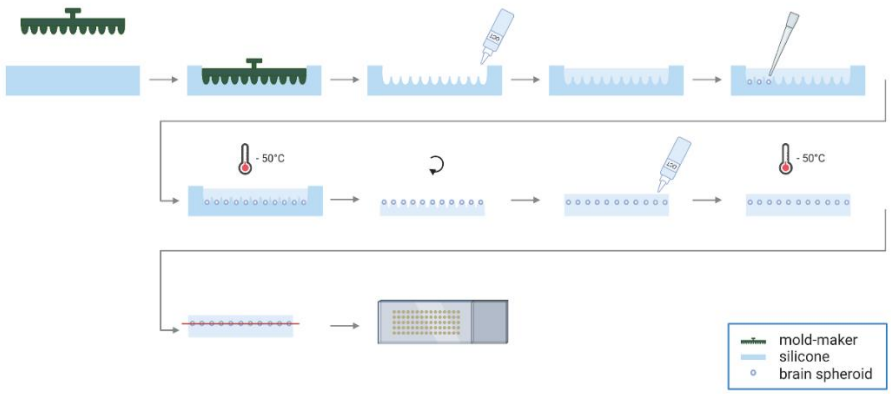

Figure 2 - Procedure of embedding neurospheroids in TissueTek-OCT to make cryosections of multiple neurospheroids arranged in an array.

3.3.10 Hematoxylin and eosin staining

A hematoxylin and eosin (HE) staining of neurospheroid array slices was performed with Carazzi's hematoxylin (0.1% (m/v) dissolved in 1:4 distilled water:glycerol 85% containing 105mM $KAl(SO_4)_2.12\ H_2O$, 0.9mM KIO_3 Sigma) and eosin Y (1% (m/v) in distilled water, Sigma). Slides were stained for 2min with hematoxylin, washed for 5 min with running water, and stained with eosin Y for 5min. After dipping 5 times in distilled water, slides were dehydrated by 95% and 100% ethanol (each for 2min) and xylene (10min) and mounted using Eukitt mounting medium (Sigma).

3.3.11 Microscopy and image analysis

Microscopic images of all 2D cultures were obtained using a BX51 fluorescence microscope equipped with an Olympus DP71 digital camera using a 10x (NA 0.30), 20x (NA 0.50) or 40x (NA 0.75) dry objective lens, except for the images of the hiPSC-NSC neuronal and astrocyte differentiation which were taken with a Leica SP8 confocal microscope using a 60x (NA 1.4) oil objective lens. Microscopic imaging of the neurospheroid arrays was performed using an automated Nikon Eclipse Ti widefield fluorescence microscope using a 20x (NA 0.75) dry objective lens. Fiji image analysis freeware was used for image processing and analysis (http://fiji.sc). Quantification of different markers was performed on a single, complete slice of a neurospheroid composed of stitched 20x images. For nuclear marker (NeuN, Ki67, SOX1, SOX2) quantification, nuclei were segmented to obtain nuclear regions of interest (ROIs) and marker signal intensity was measured using the CellBlocks_v08.ijm ImageJ script (https://github.com/DeVosLab/CellBlocks) [251, 252]. In brief, nuclei were segmented in the DAPI channel after Laplacian-enhancement by means of an automatic threshold setting based on the Triangle algorithm [253]. ROIs were considered positive when exceeding a pre-set intensity threshold. For the quantification of the cytoplasm-based cleaved caspase-3 marker, the percentage of the complete neurospheroid area covered by cleaved caspase-3 staining was determined. To this end, the total area of caspase-3 positive signals was divided by the projected area of the entire slice after manual intensity thresholding.

3.3.12 Genetic engineering of hiPSC-NSC

To generate a hiPSC-NSC line stably expressing the enhanced green fluorescent protein (eGFP) and firefly luciferase (Luc) reporters, the original hiPSC-NSC population was

transduced with the LV_CMV-eGFP-T2A-fLuc-IRES-PuroR lentiviral vector containing the corresponding reporter open reading frames under the control of a constitutive immediate early human CMV (CMVie) promoter, obtained from the Leuven Viral Vector Core (LVCC, KU Leuven, Belgium) (Fig. S1) [254, 255]. The eGFP and luciferase positive hiPSC-NSC population (eGFP/Luc hiPSC-NSC) was enriched by means of a transient puromycin selection of two weeks (increasing the concentration from 0.2 to 2.0 µg/ml).

3.3.13 Flow cytometry

Flow cytometric analyses were performed using the Epics XL-MCL analytical and CytoFLEX (Beckman Coulter) flow cytometer and data were analysed using FlowJo software v.7.2.2. For the validation of eGFP expression by the eGFP/Luc hiPSC-NSC population, dead cells were stained with GelRed (Biotum) and excluded from the analysis. To determine the viability and the mean fluorescence intensity (MFI) of the eGFP signal of the neurospheroids, the neurospheroids were first dissociated by incubation in accutase for 5min at 37°C and subsequent trituration. Dead cells were stained with GelRed.

3.3.14 *In vitro* luminescence measurements

To validate luciferase expression by the eGFP/Luc hiPSC-NSC population, eGFP/Luc hiPSC-NSC and wild-type hiPSC-NSC, serving as a negative control, were plated at equal density in a white 24-well VisiPlate (Perkin Elmer). After reaching confluence, Beetle luciferin (E1601, Promega) was added to the cell culture medium of the wells at a final concentration of 1.5mg/ml for 10 min and the luminescent signal was measured using the GloMax® Discover Microplate Reader (Promega). For eGFP/Luc neurospheroids, luminescent measurements were carried out in black ULA 96-well plates (Corning) after 48h of incubation with 150µg/ml Beetle luciferin. For the luminescence measurements of 2D-cultured eGFP/Luc hiPSC-NSCs in the context of the evaluation of Z-VAD-FMK, cells were incubated for 30min with 150µg/ml Beetle luciferin.

3.3.15 Determination of lactate dehydrogenase release

The degree of cytotoxicity was assessed by colorimetric detection of LDH in culture supernatant after 15-20 min of incubation, using CytoTox 96® Non-Radioactive

Cytotoxicity Assay (Promega) according to the manufacturer's instructions. The culture medium background was subtracted from each measurement.

3.3.16 OGD experiments

To mimic a stroke-like event, eGFP/Luc neurospheroids of 1- or 4-week-old were deprived from glucose and oxygen. The glucose- and oxygen-deficient conditions were achieved by incubating the spheroids in glucose-free cNEM (DMEM/F12 w/o L-glutamine, w/o HEPES, w/o glucose (VWR), 1xB27 (Gibco), human recombinant epidermal growth factor (rhEGF) and rhFGF-2 (20ng/ml, Immunotools)) in a humidified Bactron IV anaerobic chamber (Shel Lab) or Whitley H45 HEPA Hypoxystation (Don Whitley Scientific) containing 5% CO_2, 94.5-95.0% N_2 and 0.0-0.5% O_2. Immediately prior to the OGD at day 0 the luminescent signal of the neurospheroids was measured (i.e. pre-OGD measurement). Thereafter, plates with neurospheroids were placed into the anaerobic/hypoxic chamber and four times a half medium change was performed with the glucose-free cNEM, that had been pre-equilibrating in the chamber overnight. This step ensures the replacement of the oxygenated glucose-containing media by the oxygen- and glucose-free cNEM at the start of the incubation. The neurospheroids were incubated for 6 or 24h. At the end of the OGD, glucose (4.5 mg/ml, Gibco) was administered and the plates were brought back to atmospheric O_2 level (21% O_2). The cultures were maintained for one additional week before they underwent a second *in vitro* luminescence measurement at day 7 after reoxygenation (i.e. post-OGD measurement). Control neurospheroids were subjected to the same manipulations but were kept under normoxia and glucose was added immediately after the medium changes with the glucose-free cNEM.

Obtained luminescence data (in relative light units, RLU) were subsequently processed as follows: for each single neurospheroid, the measured RLU value post-OGD (i.e. post-OGD measurement) was normalized to the calculated mean of pre-OGD RLU values of all neurospheroids of the corresponding condition (i.e. pre-measurement). This approach of data analysis allows to visualize the variation in luminescent signal existing between the individual neurospheres at the start of the experiment, when compared to the approach in which each neurosphere was considered a single entity. The ratio is visualized as 'fold change' in the graphs, thus representing the net fold increase or decrease in signal compared to the pre-OGD measurement. More information on the statistical analysis of these data can be found under 'data representation and statistical analyses' of the material and methods section.

For the evaluation of the caspase inhibitor Z-VAD-FMK (Enzo Lifesciences and Bachem) in the neurospheroid culture, the compound was added to the culture medium at a final concentration of 25µM at the start of OGD until day 2 or until day 7 post-OGD. For the evaluation of Z-VAD-FMK in the 2D culture, eGFP/Luc hiPSC-NSCs were seeded at 2.5 x 10^4 cells/well in a black 96-well plate (Greiner) one day prior to the OGD and kept for a total of 2 days under continuous exposure of Z-VAD-FMK (25µM).

3.3.17 EF5 hypoxia detection

To visualize hypoxia in the neurospheroids, EF5 reconstituted in DMSO (10mg/ml) was added to the culture medium at a final concentration of 200µM at the start of OGD. At the end of OGD, the neurospheroids were immediately fixed and cryosections were obtained as previously described. EF5 adducts were subsequently stained by incubation with EF5 Cy3-conjugated monoclonal antibody ELK3-51 (75µg/ml) for 4h at 4°C, using the EF5 Hypoxia Detection Kit, Cyanine 3 (Merck Millipore) and counterstained with DAPI. The control neurospheroids were handled correspondingly.

3.3.18 Analysis of caspase-3 activity

Lysates were prepared by lysing neurospheroids (n = 15-20 per lysate) in caspase lysis buffer (1% NP-40, 200 mM NaCl, 10 mM Tris-HCl pH 7, 5 mM EDTA, 10% glycerol, freshly supplemented with 1 mM leupeptin, 0.1 mM aprotinin and 1 mM PMSF) followed by collection of the supernatant after a centrifugation step for 15 min at maximum speed at 4°C. The volume of lysates was adjusted to obtain a protein concentration of 2µg/µl. 20µg of protein was further diluted with CFS buffer (10 mM HEPES pH 7.5, 220 mM mannitol, 68 mM sucrose, 2 mM NaCl, 2 mM $MgCl_2$, 2.5 mM KH_2PO_4, freshly supplemented with 1 mM leupeptin, 0.1 mM aprotinin, 1 mM PMSF and 10 mM DTT) containing DEVD-AMC (50µM, PeptaNova) up to a total volume of 150µl. The caspase-3 activity for each lysate was measured using FLUOstar Omega fluorescence plate reader in duplicate or triplicate at intervals of 5min. Lysates of neurospheroids treated with 0.5µM staurosporin (SelleckChem) for 48h were included as a positive control for caspase-3 activity.

3.3.19 Western blot

Lysates of neurospheroids (n = 15-20 per lysate) were prepared as described above. Laemlli buffer was added to the lysate and the mixture was boiled for 10min. Proteins were separated by SDS-PAGE and subsequently transferred to a nitrocellulose membrane through semi-dry blotting. The membrane was blocked using 5% non-fat dry milk solution in TBS buffer with 0.05% Tween20 (TBST) for 1h and incubated with the primary antibody against caspase-3 (1/1000; 9662, Cell Signaling Technology) at 4°C overnight. After TBST washing steps, the membrane was incubated with HRP-conjugated secondary anti-rabbit antibody (1/3000, NA934V, Cytiva Lifesciences) for 1h. Finally, the membrane was developed using Western Lightning Enhanced Chemiluminescence Substrate (Perkin Elmer). The immunoblotting procedure was repeated using a HRP-conjugated anti-β-actin antibody, after a stripping and extensive washing step of the membrane. Lysates of neurospheroids treated with 0.5µM staurosporin (SelleckChem) for 48h were included as a positive control for cleaved caspase-3.

3.3.20 Data representation and statistical analyses

Graphs representing quantitative data were obtained using GraphPad Prism v.8.2.1 software. Statistical analyses were carried out using GraphPad Prism and statistical software JMP® Version 15.1.0 for analysing the mixed-effects models. The choice between a parametric or non-parametric statistical test was based on the sample size (cut off n=10) and the normality of the data (Shapiro-Wilk normality test). Specifically for applying linear mixed-effects models, the conditions on normality of residuals and homoscedasticity were primarily checked to be in an acceptable range to perform this type of analysis. A p-value < 0.05 was considered statistically significant.

To validate the eGFP/Luc hiPSC-NSC population, the produced luminescence of the eGFP/Luc hiPSC-NSC population was compared to that of the wild type hiPSC-NSC population, using a non-parametric Mann-Whitney U test. The same test was used to compare the LDH activity of neurospheroids under control versus OGD conditions. An independent samples t-test was performed for the flow cytometry data to compare the proportion of viable cells and the mean fluorescence intensity of the eGFP-positive cell population between 2- and 5-week-old neurospheroids. For the luminescence in function of the mean diameter, differences in RLU-values between the different diameters were determined by a Kruskal-Wallis test. Growth of the neurospheroids

(size measurements), the marker quantifications, the *in vitro* luminescence data of neurospheroids over time and the flow cytometric data of the OGD experiments were modelled using a linear mixed-effects model, entering the age or condition (i.e. control or 6h OGD) of the neurospheroids as fixed effect. The non-independence between observations within the same experiment was accounted for by entering the independent experiments as random effects. To compare the flow cytometric data between control and OGD conditions with and without Z-VAD-FMK to evaluate this compound, either one-way ANOVA (data from single experiment) or a linear mixed-effects model (data from multiple experiments) was carried out. For the caspase-3 activity assay, an ANCOVA model was fitted to identify differences between conditions for their produced fluorescence over time, followed by pairwise comparisons between conditions of interest. P-values for these pairwise comparisons were corrected for multiple hypothesis testing using the Bonferroni method.

With regard to the luminescence data of the OGD experiments, first significant differences between the RLU fold change of the pre-OGD measurement and post-OGD measurement were determined for every condition (i.e. control or OGD). In case data were derived from a single experiment, a Wilcoxon signed rank test or paired t-test was used to this end. In case data were obtained by multiple experiments, a linear mixed-effects model was fitted entering timepoint of the luminescence measurement as fixed effect and again the independent experiments as random effect. Second, differences between conditions were identified, using the RLU fold $\text{change}_{\text{post-OGD}}$ – RLU fold $\text{change}_{\text{pre-OGD}}$ values (ΔRLU fold change), by means of either one-way ANOVA or Kruskal-Wallis (data from single experiment) or a linear mixed-effects model (data from multiple experiments). For the latter, condition (i.e. control, 6h OGD (+ Z-VAD-FMK)) of the neurospheroids was entered as fixed effect and independent experiments as random effect.

Post-hoc analyses for ANOVA and linear mixed-effects models were carried out with Tukey HSD correction for multiple comparisons. For the post-hoc analysis following the Kruskal-Wallis test, Dunn's correction was used.

3.4 Results

3.4.1 Development and characterization of neurospheroids with reproducible growth and differentiation pattern

In order to develop a platform for *in vitro* stroke research, we set out to generate a robust human iPSC-derived neurospheroid model (Fig. 1a). Hereto, we first established a new hiPSC line from human neonatal foreskin fibroblasts and characterized the resulting hiPSC by means of immunocytochemistry (ICC) and qRT-PCR (Fig. S2). hiPSCs expressed the human pluripotent stem cell markers Oct3/4, SOX2, TRA-1-60, TRA-1-81 and Nanog (Fig. S2a). Trilineage differentiation potential was confirmed after embryoid body formation and subsequent qRT-PCR analysis demonstrating downregulation of pluripotency-associated transcripts and upregulation of ectoderm, mesoderm and endoderm-associated transcripts (hiPSC scorecard assay, Fig. S2b).

Next, the obtained hiPSC line was differentiated into a self-renewable NSC population (further annotated as hiPSC-NSC) and subsequently validated for marker expression, differentiation potential and genetic stability (Fig. 3). First, the marker expression profile of the generated hiPSC-NSCs was compared to that of the corresponding hiPSCs and foreskin fibroblasts from which they had been derived, as well as to a commercially available NSC line derived from human embryonic stem cells (ES-NSCs). By means of ICC (Fig. 3a), we show that the expression of SOX2 is maintained in the hiPSC-NSC population upon differentiation from hiPSC. Moreover, hiPSC-NSCs acquire expression of the neural stem cell marker SOX1 and lose expression of the pluripotency-associated Oct3/4 marker. None of these marker proteins were present in the original foreskin fibroblast population. This $SOX1^+$ $SOX2^+$ $Oct3/4^-$ marker profile is in accordance with the ES-NSC population. As a second validation, the differentiation potential of the hiPSC-NSC into neurons and astrocytes was evaluated (Fig. 3b). The expression of the neuronal marker Tuj1 and the astrocyte marker GFAP was demonstrated after applying specific neuronal and astroglial differentiation protocols, thereby confirming the multipotent differentiation potential of the derived hiPSC-NSCs. Finally, CNV sequencing revealed that the established hiPSC-NSCs did not display large genomic alterations, i.e. CNVs larger than 50kb (Fig. 3c).

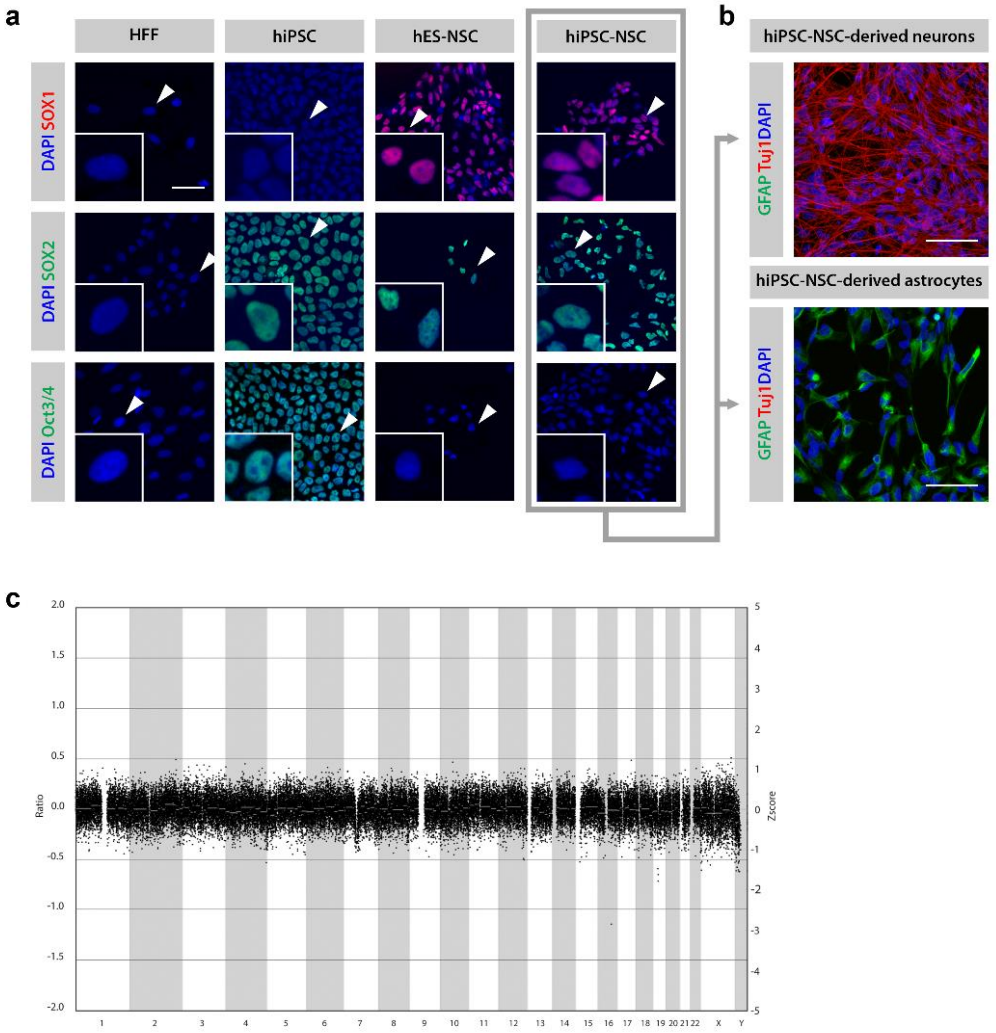

Figure 3 - Validation of the NSC population derived from hiPSC (hiPSC-NSC). (A) Immunofluorescence of hiPSC-NSC. The hiPSC-NSC population is SOX1⁺, SOX2⁺, Oct3/4⁻, in accordance with the commercially available NSC population derived from human embryonic stem cells (hES-NSC). Human neonatal foreskin fibroblasts (HFFs) here represent the negative control for all markers, while hiPSCs were used as a positive control for SOX2 and Oct3/4 expression. This NSC marker profile was confirmed for different passage numbers by at least three different experiments. (B) Immunofluorescence of differentiated hiPSC-NSC. Differentiation of hiPSC-NSCs into neurons (Tuj1⁺) and astrocytes (GFAP⁺) at day 16 and 45, respectively. The differentiation into neurons and astrocytes had been confirmed by at least three additional experiments. (C) CNV sequencing profile of hiPSC-NSC. The CNV sequencing profile of hiPSC-NSC showing the distribution of all bins (indicated as black dots) around ratio 0, indicating a normal genetic constitution. (Deletions would be represented by a ratio of -1, and duplications by a ratio of 0.58.)

We next generated neurospheroids by seeding hiPSC-NSCs at equal density in wells of an ULA 96-well plate. By means of their spontaneous self-assembling capacity, neurospheroids started to form from as early as 1 day post-seeding. Growth of the spheroids was monitored by weekly measurements of their diameter for five consecutive weeks (Fig. 4a, b). Spheroids reached sizes from a mean diameter of 689 ± 22 µm at week 1, up to 2339 ± 96 µm at week 5, growing with an average of 415 ± 9 µm per week (95% CI [380, 450], p=0.0003). Additionally, as can be concluded from Fig. 4b, this procedure of generating neurospheroids was associated with a low level of variability in size between individual neurospheroids. Moreover, the growth of the spheroids was highly reproducible across different independent experiments.

Besides their growth, we characterized the obtained neurospheroids for different markers implicated in proliferation and differentiation into neurons and astrocytes by ICC. The dynamics of these markers were assessed in time by comparison of 2- and 4-week-old neurospheroids. As shown by representative IF images (Fig. 4c), the cells in neurospheroids spontaneously differentiated into neurons, with both immature ($Tuj1^+$, DCX^+) and mature ($NeuN^+$) phenotypes. Quantification of the NeuN-positive cells did however not reveal an increase of this marker over time (p=0.0638) (Fig. 4e). In contrast to neurons, neither 2 nor 4-week-old neurospheroids contained $GFAP^+$ cells, suggesting a lack of astrocytes (Fig. 4c). Nevertheless, the neurospheroids showed a reduction in the $SOX1^+$ (mean difference = 37%, CI[31, 44], p<0.0001) and $SOX2^+$ (mean difference = 40%, CI[35, 46], p<0.0001) NSC population and a decreased proliferation potential, as shown by the reduction in the proliferation marker Ki67 (mean difference = 15%, CI[9, 21], p<0.0001) over time (Fig. 4c, e). Despite the immature phenotype, this suggests ongoing differentiation as further supported by the presence of $TBR2^+$ intermediate progenitors and Hop^+ outer radial glia cells in 2- and 4-week old neurospheroids (Fig. 4f), as well as the disappearance of the radial glia marker PAX6 expression in 4-week old neurospheroids (Fig. 4f). In agreement with ongoing differentiation processes, staining for cleaved caspase-3 indicates ongoing apoptotic events in 2- and 4-week old neurospheroids (Fig. 4c). Also note the distribution of the SOX1-, SOX2- and Ki67-expressing cells within the neurospheroids. Where these marker-expressing cells were widely dispersed in 2-week-old neurospheroids, they were more confined to particular stem cell niches in 4-week-old spheroids. These stem cell niches resemble typical neural rosette structures (Fig. 4d), which can be considered the *in vitro* equivalent of the invaginated neuroectoderm forming the neural tube in embryos.

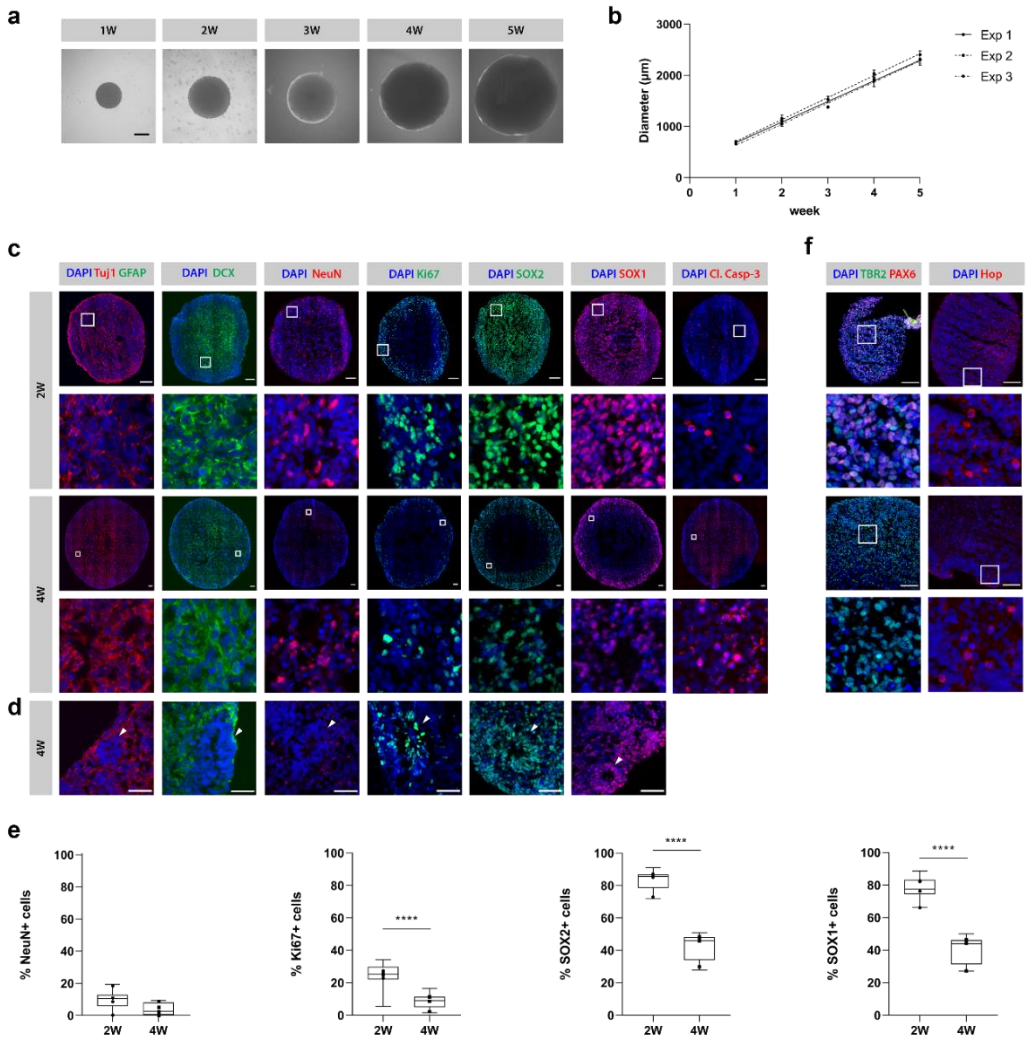

Figure 4 - Characterization of hiPSC-NSC-derived neurospheroids. (A) Representative bright-field microscopic images of 1- to 5-week-old (1-5W) neurospheroids. Scale bar 500µm. (B) Growth of neurospheroids over the course of five weeks by three independent experiments with n=10 per experiment. For each experiment the mean diameter with standard deviation is plotted and a regression line is fitted through the data points. (C) Representative immunofluorescent images (i.e. image with relative number of positive cells closest to the median value of the quantification data shown in fig. E) of 2- and 4-week-old neurospheroids stained for the neuronal markers Tuj1, DCX and NeuN, the astrocyte marker GFAP, the proliferation marker Ki67, the NSC markers SOX1 and SOX2 and for the apoptosis marker cleaved caspase-3 (Cl. Casp-3). Second row represents a 100x100µm inset at the selected region (white square) from upper row images. Scale bar 100µm. (D) Detailed immunofluorescent images of neural rosette structures (arrowheads) present in 4-week-old neurospheroids. Scale bar 50µm. (E) Quantification of NeuN, Ki67, SOX2 and SOX1 markers with respect to the total number of nuclei of 2- and 4-week-old neurospheroids from four independent experiments with n=3 per experiment. The box plots indicate median and

*interquartile range, whiskers indicate the minimum and maximum values of all four independent experiments. The dots indicate the median value of each independent experiment. (F) Representative immunofluorescent images of 2- and 4-week old neurospheroids stained for the radial glia marker PAX6, the intermediate progenitor marker TBR2 and the outer radial glia marker Hop. Second row represents a 100x100µm inset at the selected region (white square) from upper row images. Scale bar 100µm. ****p<0.0001*

3.4.2 Bioluminescence allows real-time monitoring of neurospheroid growth and viability

Most of the traditional cell growth, viability and/or cytotoxicity assays (e.g. 3-(4,5-dimethylthiazol-2-yl)-2,5-diphenyl-2H-tetrazolium bromide (MTT) and lactate dehydrogenase (LDH) assay, flow cytometry, microscopy) are terminal endpoint assays and/or require disruption of neurospheroids into a single cell suspension. To enable a real-time read-out of neurospheroid growth and viability, we therefore stably introduced the firefly luciferase (Luc) reporter into our model through lentiviral vector transduction (Fig. 1b, Fig. 5a). As the construct also contains the fluorescent eGFP reporter (Fig. 5b), the established hiPSC-NSC population will be further referred to as eGFP/Luc hiPSC-NSCs. To evaluate whether the introduced bioluminescent system can be applied to monitor the growth and/or viability of neurospheroids over time, weekly luminescence measurements were performed on the same group of spheroids for five consecutive weeks (Fig. 5c, d). Our results demonstrate that luminescent neurospheroids display a dynamic luminescence pattern, whereby a significant increase in luminescent signal is detected during the first 3 weeks of culture, followed by signal stabilization (week 3-4). When cultured for a longer period, a signal decrease is observed while still leaving a substantially high luminescent signal despite their increase in size over time (Fig. 5c, d, list of p-values provided in Table S1 and S2). The observed decrease in luminescent signal upon long-term culture most likely reflects gradual cell loss due to nutrient deprivation and reduced viability and altered cellular metabolism associated with the transition from immature to more mature neurospheroids (Fig. 4c, e, f). Supporting this hypothesis, flow cytometric analysis of 2-week-old and 5-week-old neurospheroids demonstrated a decrease in the number of viable cells within the neurospheroids (Fig. 5e), as well as a decrease in the level of eGFP expression (Fig. 5f), which may reflect the altered cellular metabolism during the differentiation process. Clearly, the observed decrease in luminescent signal following long-term culture of neurospheroids is a highly complex multifactorial event that may require further investigation. Nevertheless, as the observed luminescent signal pattern displays high similarity over multiple experiments and remains substantially high over

the course of five weeks, its potential use in evaluating spheroid survival following cellular stress will be further evaluated below.

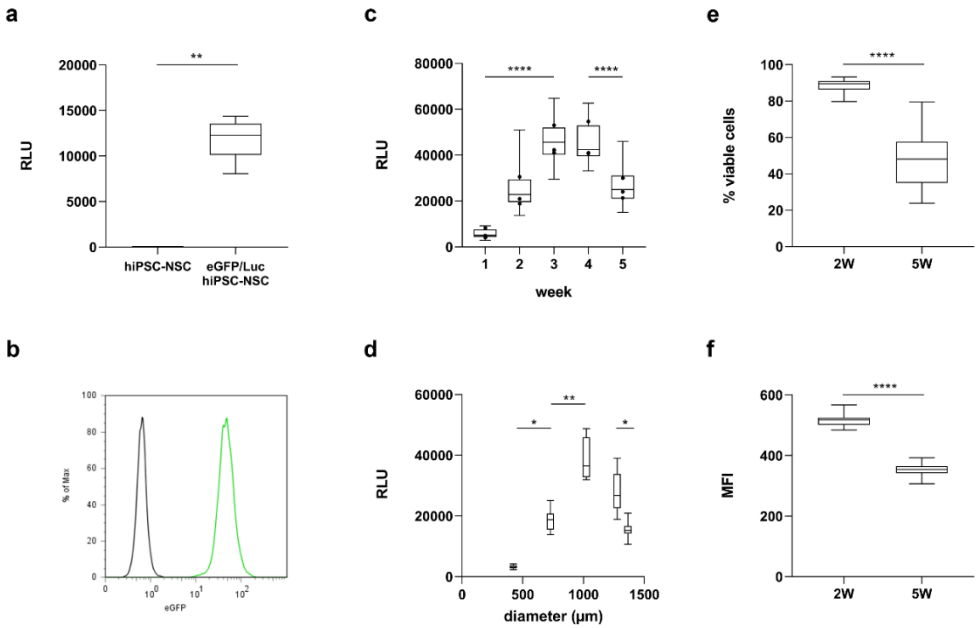

*Figure 5 - Validation of the eGFP- and Luc-positive hiPSC-NSC population (eGFP/Luc hiPSC-NSC) and longitudinal luminescence measurements of eGFP/Luc hiPSC-NSC-derived neurospheroids. (A) Luminescence data of eGFP/Luc hiPSC-NSCs (n=5) versus control hiPSC-NSCs (n=5). (B) Flow cytometry data of eGFP/Luc hiPSC-NSCs (green) versus control hiPSC-NSCs (black) on expression of eGFP. (C) Luminescence data of eGFP/Luc hiPSC-NSC- derived neurospheroids (n=30) over the course of five weeks by three independent experiments. The box plots indicate median and interquartile range, whiskers indicate the minimum and maximum values of all three independent experiments. The dots indicate the median value of each independent experiment (n=30). A list of p-values can be found in Table S1. (D) Luminescence data of eGFP/Luc hiPSC-NSC-derived neurospheroids (n=12) in function of the mean diameter (µm) at week 1-5. A list of p-values can be found in Table S2. (E) Proportion of viable cells in 2-week (2W) (n=12) and 5-week (5W) (n= 35)-old neurospheroids determined by flow cytometry. (F) Mean fluorescence intensity (MFI) of eGFP-positive cell population in 2-week (2W) (n=12) and 5-week (5W) (n= 35) old neurospheroids determined by flow cytometry. **p<0.01, ****p<0.0001 (RLU, relative light units)*

3.4.3 Monitoring of OGD-mediated neurotoxicity using bioluminescence

To evaluate the use of the established luminescent neurospheroids as a model for the investigation of stroke-like events, we subjected 1- and 4-week-old neurospheroids to OGD (0.0-0.5% O_2) (Fig. 1c). At first, neurospheroids were subjected to 6 or 24 hours of OGD with corresponding luminescence measurements immediately before OGD (pre-OGD measurement) and one week after OGD (post-OGD measurement) (Fig. 6). For 1-

week-old neurospheroids (Fig. 6a), control spheroids that did not undergo the OGD event displayed - as expected (see Fig. 5c) - a significant increase in luminescent signal at day 7, while this increase was significantly lower following 6 hours of OGD ($p<0.0001$) (see Table S3 for a complete list of p-values). This was confirmed by four additional experiments (Fig. 7a, Table S4). In contrast, 24 hours of OGD abolished the expected increase in luminescent signal (Fig. 6a). Similarly, for 4-week-old neurospheroids (Fig. 6b), control spheroids that did not undergo the OGD event displayed - as expected (see Fig. 5c) - a significant decrease in luminescent signal at day 7, while this decrease was significantly higher following 6 hours of OGD ($p<0.0001$) (Table S3), as confirmed by six additional experiments (Fig. 7f, Table S4). Again, after 24 hours of OGD virtually all luminescent signal was lost (Fig. 6b, Table S3). Based on these results, we decided to apply 6 hours of OGD to all further experiments since neurospheroids should retain a certain degree of viability when applying a therapeutic intervention.

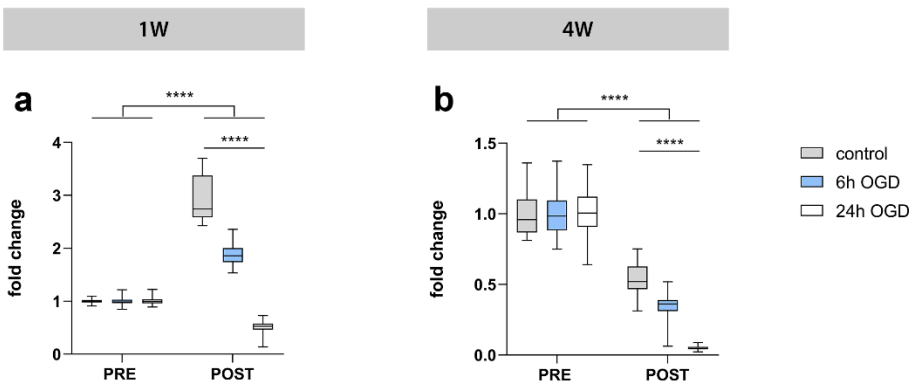

*Figure 6 - Luminescent neurospheroids subjected to different durations of OGD. (A) Luminescence measurements of 1-week-old (1W) neurospheroids subjected to 6h OGD (n=29), 24h OGD (n=30) or control conditions (n=29). The RLU data post-OGD (i.e, day 7) of each condition were normalized to the mean of pre-OGD data of the corresponding condition, represented as 'fold change' in the graph. A complete list of p-values can be found in Table S3. (B) Luminescence measurements of 4-week-old (4W) neurospheroids subjected to 6h OGD (n=30), 24h OGD (n=29) or control conditions (n=30). The RLU data post-OGD (i.e, day 7) of each condition were normalized to the mean of pre-OGD data of the corresponding condition, represented as 'fold change' in the graph. A complete list of p-values can be found in Table S3. ****p<0.0001*

Next, we investigated whether the decrease in luminescent signal post-OGD was related to OGD-induced cytotoxicity. To this end, we first analysed the culture supernatant of OGD neurospheroids after reoxygenation and demonstrate a significant increase in LDH activity as compared to the supernatant of control neurospheroids,

both for 1-week-old (after 4 hours, Fig. 7b) and 4-week-old (after 2 days, Fig. 7g) neurospheroids ($p= 0.0036$ and $p= 0.0063$, respectively). We further confirmed that the OGD-induced increase in LDH activity in the culture supernatant was indeed due to a hypoxic event as both 1- and 4-week-old neurospheroids displayed high immunoreactivity for the hypoxic marker EF5 when analysed by ICC immediately after 6 hours of OGD (Fig. 7c, h). Consequently, the early occurrence of OGD-induced cytotoxicity, as measured by LDH activity and EF5 immunoreactivity, indeed precedes the decreased luminescent signals detected at day 7 post OGD (Fig. 7a, f). Likewise, flow cytometric analysis confirms a significantly decreased cell viability within 1-week-old (Fig. 7d) and 4-week-old (Fig. 7i) neurospheroids at 7 days after OGD as compared to control neurospheroids (resp. 70% ± 18% versus 89% ± 3% and mean of 40% ± 6% versus 54% ± 9%, for both $p<0.0001$). Also note the general difference in cell viability between 1- and 4-week-old neurospheroids, in agreement with our earlier results (Fig. 5e). The latter is also reflected by the loss of spheroid integrity especially for the 4-week-old neurospheroids at 7 days after OGD, visible as less defined edges by classical HE staining (Fig. 7e, j).

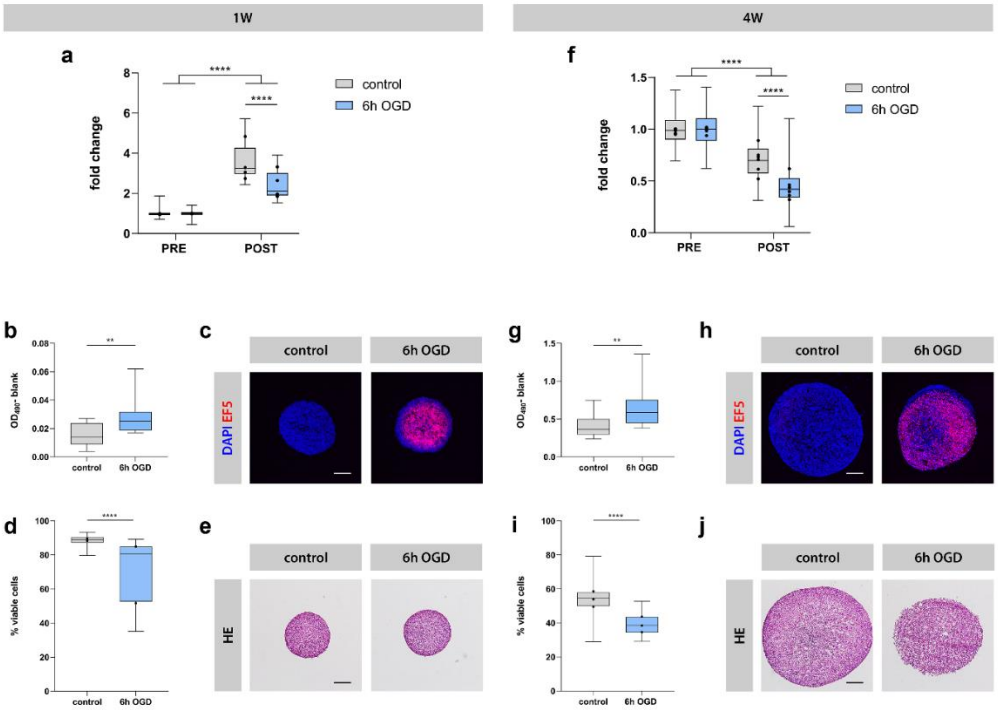

Figure 7 - Luminescent neurospheroids subjected to OGD. Left:1-week-old (1W) neurospheroids (A-E). Right: 4-week-old (4W) neurospheroids (F-J).(A) Luminescence measurements of 1W neurospheroids subjected to 6h OGD (n= 15-30) or control conditions (n= 19-30) from four experiments. The RLU data post-OGD (i.e, day 7) of each condition were normalized to the mean of pre-OGD data of the corresponding condition, represented as 'fold change' in the graph. The box plots indicate median and interquartile range, whiskers indicate the minimum and maximum values of all four experiments. The dots indicate the median value of each independent experiment. A complete list of p-values can be found in Table S4. (B) LDH levels in the culture supernatants of control (n=14) vs. 6h OGD (n= 14) neurospheroids after four hours of reoxygenation. Values represent the measured absorbance at 490 nm corrected for the background absorbance of the culture medium after 20 min. (C) Representative image of control and 6h OGD spheroids stained for EF5 adducts after incubation of neurospheroids with hypoxic marker EF5 during normoxic or ischemia-like conditions, respectively. Scale bar 100µm. (D) Percentage of viable cells determined by flow cytometry at day 7 for control (n= 12-15) and 6h OGD (n=12-15) neurospheroids by two independent experiments. The box plots indicate median and interquartile range, whiskers indicate the minimum and maximum values of two independent experiments. The dots indicate the median value of each independent experiment. (E) Representative light microscopic images of HE-stained control and 6h OGD neurospheroids at day 7. Scale bar 200µm. (F) Luminescence measurements of 4W neurospheroids subjected to 6h OGD (n=29-30) or control conditions (n= 28-30) from six experiments. The RLU data post-OGD (i.e, day 7) of each condition were normalized to the mean of pre-OGD data of the corresponding condition, represented as 'fold change' in the graph. The box plots indicate median and interquartile range, whiskers indicate the minimum and maximum values of all 6 experiments. The dots indicate the median value of each independent experiment. A complete list of p-values can be found in Table S4. (G) LDH levels in the culture supernatants of control (n=15) vs. 6h OGD (n= 12) neurospheroids after two days of reoxygenation. Values represent the measured absorbance at 490 nm corrected for the background absorbance of the culture medium after 15 min. (H)

*Representative image of control and 6h OGD spheroids stained for EF5 adducts after incubation of neurospheroids with hypoxic marker EF5 during normoxic or ischemia-like conditions, respectively. Scale bar 200µm. (I) Percentage of viable cells determined by flow cytometry at day 7 for control (n= 12-15) and 6h OGD (n=12-15) neurospheroids by three experiments. The box plots indicate median and interquartile range, whiskers indicate the minimum and maximum values of all 3 experiments. The dots indicate the median value of each independent experiment. (J) Representative light microscopic images of HE-stained control and 6h OGD neurospheroids at day 7. Scale bar 200µm. **p<0.01, ****p<0.0001*

3.4.4 The pan-caspase inhibitor Z-VAD-FMK is unable to alleviate overall OGD-mediated neurotoxicity in neurospheroids

An important future application for the generated luminescent human neurospheroid model is the evaluation of potential neuroprotective agents and/or therapeutic strategies. Here, we assessed the effect of administration of Z-VAD-FMK to the neurospheroid cultures during OGD. Z-VAD-FMK is a pan-caspase inhibitor that has previously been described to confer neuroprotection in rodent models for cerebral ischemia *in vivo* and *in vitro* [33-35, 256]. Indeed, addition of Z-VAD-FMK to the culture medium of 2D-cultured undifferentiated eGFP/Luc hiPSC-NSCs resulted in a beneficial effect at day 2 post-OGD, as reflected by the smaller decrease in luminescent signal for Z-VAD-FMK-treated cultures compared to the untreated counterpart (p= 0.0004) (Fig. 8). Following confirmation of the beneficial effect of Z-VAD-FMK on cell survival in 2D cultures under OGD, we evaluated this compound in the developed neurospheroid model. In a first experimental setup, Z-VAD-FMK was added to the culture medium of 1-week-old and 4-week-old neurospheroids at the start of OGD until day 2 after reoxygenation. However, neither luminescence analysis (Fig. 9a, e, Table S5) nor flow cytometric analysis (Fig. 9b,f, Table S6) could demonstrate a direct neuroprotective effect on human neurospheroids after OGD. Finally, we also investigated whether addition of Z-VAD-FMK to the culture medium of neurospheroids during the entire course of the experiment (i.e. until day 7 after reoxygenation) could exert a certain degree of neuroprotection. Despite prolonged exposure to Z-VAD-FMK, both luminescence (Fig. 9c, g, Table S5) and flow cytometry (Fig. 9d, h, Table S6) data did not reveal any neuroprotective effect. To investigate whether Z-VAD-FMK was able to interfere with apoptosis specifically, a caspase-3 activity assay and a subsequent western blot for cleaved caspase-3 (in monoplicate on the remaining lysate sample) were performed (Fig. 9i, j, m, n). As can be appreciated from these assays, control neurospheroids of 1-week and 4-weeks old display active caspase-3 activity, indicating a basal level of apoptosis present in neurospheroids. Staurosporin (STS) treatment was used as a positive control for caspase-3 activity. This finding could additionally be

confirmed by quantification of the cleaved caspase-3 immunostaining at day 7 post-reoxygenation (Fig. 9k, l, o, p). Furthermore, Z-VAD-FMK is able to suppress the caspase-3 activity after OGD in both 1-week-old and 4-week-old neurospheroids, when compared to their untreated counterpart (for both $p<0.0001$) (Fig. 9i, m). Similarly, western blot analysis (although not quantified) suggests reduced cleaved caspase-3 upon Z-VAD-FMK treatment (Fig. 9j, n). However, even though reduced caspase-3 activity was observed following Z-VAD-FMK treatment, it did not prevent overall OGD-induced cell death.

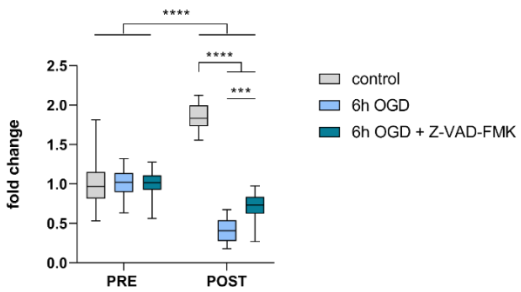

*Figure 8 - Evaluation of Z-VAD-FMK in 2D culture of eGFP/Luc NSCs. Luminescence measurements of eGFP/Luc NSCs under control (n=30) or 6h OGD treated with (n=30) or without (n=30) 25µM Z-VAD-FMK during the OGD until day 2 after reoxygenation. The RLU data post-OGD (i.e, day 2) of each condition were normalized to the mean of pre-OGD data of the corresponding condition, represented as 'fold change' in the graph. ***p<0.001,****p<0.0001.*

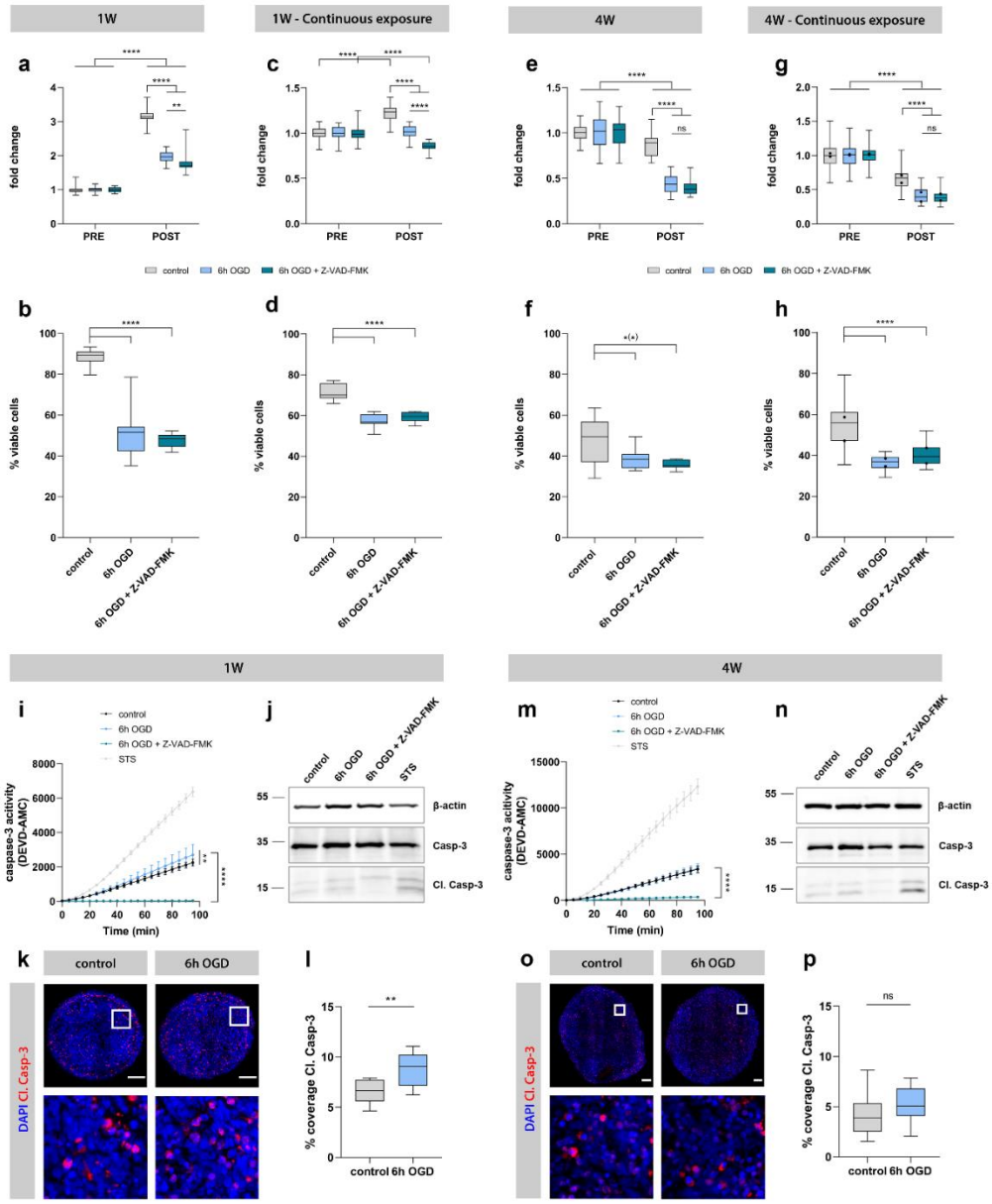

Figure 9 - Evaluation of Z-VAD-FMK in luminescent neurospheroid model. Left and middle-left: 1-week-old (1W) with single administration of Z-VAD-FMK and 1W neurospheroids with daily administration. Middle-right and right: 4-week-old (4W) neurospheroids with single administration and 4W neurospheroids with daily administration of Z-VAD-FMK. (A) Luminescence measurements of 1W neurospheroids under control conditions (n=29) or 6h OGD treated with (n=30) or without (n=29) 25µM Z-VAD-FMK during the OGD until day 2 after reoxygenation. The RLU data post-OGD (i.e, day 7) of each condition were normalized to the mean of pre-OGD data of the corresponding condition, represented as 'fold change' in the graph. A complete list of p-values can be found in Table S5. (B) Percentage of viable cells determined by flow

cytometry at day 7 for control (n= 12) and 6h OGD neurospheroids treated with (n= 12) and without Z-VAD-FMK (n= 12) during the OGD until day 2 after reoxygenation. A complete list of p-values can be found in Table S6. (C) Luminescence measurements of 1W neurospheroids under control conditions (n=29) or 6h OGD treated with (n=28) or without (n=23) 25μM Z-VAD-FMK during the OGD until day 7 after reoxygenation. The RLU data post-OGD (i.e, day 7) of each condition were normalized to the mean of pre-OGD data of the corresponding condition, represented as 'fold change' in the graph. A complete list of p-values can be found in Table S5. (D) Percentage of viable cells determined by flow cytometry at day 7 for control (n= 12) and 6h OGD neurospheroids treated with (n= 12) and without Z-VAD-FMK (n= 12) during the OGD until day 7 after reoxygenation. A complete list of p-values can be found in Table S6. (E) Luminescence measurements of 4W neurospheroids under control conditions (n=30) or 6h OGD treated with (n=30) or without (n=30) 25μM Z-VAD-FMK during the OGD until day 2 after reoxygenation. The RLU data post-OGD (i.e, day 7) of each condition were normalized to the mean of pre-OGD data of the corresponding condition, represented as 'fold change' in the graph. A complete list of p-values can be found in Table S5. (F) Percentage of viable cells determined by flow cytometry at day 7 for control (n= 12) neurospheroids and 6h OGD neurospheroids treated with (n= 7) and without Z-VAD-FMK (n= 12) during the OGD until day 2 after reoxygenation. A complete list of p-values can be found in Table S6. (G) Luminescence measurements of 4W neurospheroids under control conditions (n=30) or 6h OGD treated with (n=29-30) or without (n=30) 25μM Z-VAD-FMK during the OGD until day 7 after reoxygenation from two independent experiments. The RLU data post-OGD (i.e, day 7) of each condition were normalized to the mean of pre-OGD data of the corresponding condition, represented as 'fold change' in the graph. The box plots indicate median and interquartile range, whiskers indicate the minimum and maximum values of all two experiments. The dots indicate the median value of each independent experiment. A complete list of p-values can be found in Table S5. (H) Percentage of viable cells determined by flow cytometry at day 7 for control (n= 12) and 6h OGD neurospheroids treated with (n= 11) and without Z-VAD-FMK (n= 12) during the OGD until day 7 after reoxygenation by two independent experiments. The box plots indicate median and interquartile range, whiskers indicate the minimum and maximum values of two independent experiments. The dots indicate the median value of each independent experiment. A complete list of p-values can be found in Table S6. (I) Caspase-3 activity of lysates derived from 1W neurospheroids under control, 6h OGD or 6h OGD + Z-VAD-FMK conditions at day 2 after reoxygenation using a fluorescent caspase-activity probe (DEVD-AMC). Lysate derived from staurosporin (STS)-treated 1W neurospheroids was included as a positive control for caspase-3 activity. (J) Western blot for caspase-3 of lysates derived from 1W neurospheroids under control, 6h OGD or 6h OGD + Z-VAD-FMK conditions at day 2 after reoxygenation. Lysate derived from STS-treated 1W neurospheroids was included as a positive control for cleaved caspase-3 (Cl. Casp-3). Image of the complete blot can be found in Fig. S3. (K) Representative immunofluorescent images (i.e. image with percentage coverage closest to the median value of the quantification data shown in fig. L) of control and 6h OGD 1W neurospheroids stained for Cl. Casp-3. Second row represents a 100x100μm inset at the selected region (white square) from upper row images. Scale bar 100μm. (L) Quantification of Cl. Casp-3 staining, expressed in percentage coverage, i.e, the percentage of the complete neurospheroid area covered by cleaved caspase-3 staining, of 1W neurospheroids under control or 6h OGD conditions at day 7 after reoxygenation. Data are derived from two independent experiments with n=4 for control and n=5-6 for 6h OGD neurospheroids per experiment. The box plots indicate median and interquartile range, whiskers indicate the minimum and maximum values of all two independent experiments. (M) Caspase-3 activity of lysates derived from 4W neurospheroids under control, 6h OGD or 6h OGD + Z-VAD-FMK conditions at day 2 after reoxygenation using a fluorescent caspase-activity probe (DEVD-AMC). Lysate derived from STS-treated 4W neurospheroids was included as a positive control for caspase-3 activity. (N) Western blot for caspase-3 of lysates derived from 4W neurospheroids under control, 6h OGD or 6h OGD + Z-VAD-FMK conditions at day 2 after reoxygenation. Lysate derived from STS-treated 4W neurospheroids was included as a positive control for Cl. Casp-3. Image of the complete blot can be found in Fig. S3. (O) Representative immunofluorescent images (i.e. image with percentage coverage closest to the median value of the quantification data shown in fig. P) of control and 6h OGD 4W neurospheroids stained for Cl. Casp-3. Second row represents a 100x100μm inset at the

*selected region (white square) from upper row images. Scale bar 100µm. (P) Quantification of Cl. Casp-3 staining, expressed in percentage coverage, i.e, the percentage of the complete neurospheroid area covered by cleaved caspase-3 staining, of 4W neurospheroids under control or 6h OGD conditions at day 7 after reoxygenation. Data are derived from two independent experiments with n=5 for control and n=5-6 for 6h OGD neurospheroids per experiment. The box plots indicate median and interquartile range, whiskers indicate the minimum and maximum values of all two independent experiments. *p<0.05, **p<0.01,****p<0.0001.*

3.5 Discussion

To date, effective therapy for acute ischemic stroke is limited to treatment with tissue plasminogen activator or thrombectomy, which can only be applied in a limited number of patients. The lack of significant progress in finding a neuroprotective therapy for stroke patients can in part be attributed to the absence of physiologically relevant human *in vitro* models. To bridge the translational gap and increase the success rate of potential new therapeutics, *in vitro* stroke research should be shifted from traditional rodent 2D cultures to more relevant human 3D cultures, including neurospheroids/organoids. Although brain organoids have already shown their relevance in modelling brain development, neurodevelopmental and neurodegenerative diseases, only a few articles have been published so far in which brain organoids were subjected to low oxygen tension [189, 190, 245], mainly investigating the effect of hypoxia on neurodevelopment and corticogenesis. In this study, we describe a human luminescent iPSC-derived neurospheroid model as the basis for the development of a new platform suitable for both basic and applied *in vitro* human stroke research. Although the development of brain organoids in particular, is often associated with variations in size, shape and cellular composition [158, 165, 257], the here developed neurospheroid model, based on the spontaneous self-assembling capacity of hiPSC-derived NSCs, showed high reproducibility in terms of size and differentiation. With the culture conditions used in this study, neurospheroids grew over the course of minimum 5 weeks with a growth pattern that is highly reproducible. It should be noted that as the spheroids grow beyond a diameter of 400µm, a necrotic core is present in these models and may be reduced in future studies by means of optimized differentiation media supporting more the differentiation and less the proliferation of the NSC population in the neurospheroids. Nevertheless, the protocol applied here, demonstrated that the neurospheroids had undergone reproducible spontaneous differentiation into neurons from as early as 2 weeks, as determined by their Tuj1, DCX and NeuN immunoreactivity, staining both immature and mature neurons, respectively. Additionally, the proportion of NSCs and proliferative cells

showed a consistent reduction over time, reflecting increasing differentiation of the neurospheroids. One current point of consideration is the lack of astrocytes in the present model. Considering the timeline of the appearance of neurons and astrocytes in the *in vivo* embryonic brain development, these time points may have been too early for the neurospheroids to have spontaneously developed astrocytes under these specific culture conditions. Further supporting this hypothesis, preliminary experiments in which neurospheroids were grown up to 8 weeks of age did, however, reveal the appearance of GFAP+ astrocytes (data not shown). Therefore, future experiments may require even longer periods of culture and/or optimization of the culture conditions to develop neurospheroids that more faithfully recapitulate the *in vivo* situation.

Of note, to characterize the neural spheroids developed here, we adapted an existing protocol for the simultaneous downstream histological processing of multiple spheroids [250]. We modified the protocol to obtain cryosections, making it compatible with spheroids labelled with fluorescence reporter proteins (e.g. eGFP) and omitting the need for the time-consuming (de)paraffinization and subsequent antigen retrieval steps. Techniques to analyse morphology and protein expression of 3D cultures were often considered slow and laborious [165], but with this spheroid microarray technology, the model is well-suited for possible high-throughput drug screening applications.

Common read-outs in different *in vitro* stroke experiments are viability and/or cytotoxicity, which are typically assessed by techniques, such as MTT assay, LDH assay, flow cytometric or microscopic detection of living and/or apoptotic cells. A major drawback associated with these conventional analysis methods is the requirement of a single endpoint. However, to gain more insight into the pathophysiology and/or the effectiveness of candidate neuroprotective compounds, it may be of relevance to study the dynamics in viability and cytotoxicity of the same OGD-treated culture over time. Moreover, some of these methods, in particular flow cytometry, require disruption of the 3D structural organization for analysis. To overcome all aforementioned limitations, we equipped a human iPSC-derived neurospheroid model with intrinsic bioluminescence for an easy and longitudinal follow-up of their growth and overall viability over time. Although still limited, luminescent reporters have been used in 3D cultures for different purposes. Stably expressed luciferase was used before to quantify the outgrowth of mammary epithelial cells propagated within 3D matrices [258] or to determine the cytotoxicity of different hepatotoxicants in primary hepatocyte-derived

spheroids over a long-term [259]. Additionally, when placed under the control of a specific promoter, luminescence can be used to monitor the expression of a specific gene over time. Malik et al. [260] applied luminescence imaging to monitor mPer1 gene expression in mouse neurospheres to study circadian rhythms in adult neurogenesis.

When monitoring the luminescence of the neurospheroid culture over time, a dynamic pattern becomes evident. Initially, their produced luminescent signal exhibited an increase during the first three weeks (Fig. 5c), coinciding with growth of the neurospheroids (Fig. 5d). Although growth continued after three weeks of age, the luminescent signal they generated showed a stagnation and eventually a decrease when cultured for a longer time period. Different reasons might be at the root of this contradiction. First, as the eGFP/Luc hiPSC-NSC population used in this study was generated by lentiviral vector transduction it cannot be excluded that a proportion of transduced cells underwent transgene silencing. The latter may be due to the site of integration being subjected to chromatin remodelling events/epigenetic changes associated with differentiation or due to promoter silencing, as was reported earlier for CMVie [261-263]. These issues may potentially be overcome using CRISPR-based genetic engineering strategies whereby the firefly luciferase reporter ORF is inserted in a ubiquitously active genomic region and/or by the use of other universal (non-viral) promoters (e.g. elongation factor 1α short (EFS) promoter) [264]. Considering the use of long-term cultured, more mature neurospheroids in future experiments, the use of a neuron-specific promoter could also be an interesting approach. Secondly, the increasing differentiation of the cells in the neurospheroids may have reduced the expression of firefly luciferase reporter, despite the use of a constitutive human CMVie promoter, as demonstrated for eGFP by flow cytometry (Fig. 5f). Finally, the increasing hypoxic core associated with growth of the neurospheroids, and the apoptotic events related to the transition of immature to more mature neurospheroids, may affect the overall viability of the neurospheroids, as determined by flow cytometry (Fig. 5e), thereby influencing the observed luminescent signals.

To obtain the proof-of-principle for the use of the aforementioned luminescent model system in *in vitro* stroke research, neurospheroids were subjected to an ischemia-like event, i.e. 6h of oxygen and glucose deprivation. For both 1- and 4-week-old neurospheroids, incubation in an oxygen- and glucose-deprived environment caused a decrease in luminescence when compared to control conditions at day 7 after reoxygenation. This could be attributed to OGD-induced neurotoxicity, as confirmed by the LDH assay shortly after reoxygenation. However, despite the initial damage, the 1-

week-old neurospheroids were able to recover and continued to grow over the course of one week, as demonstrated by a net increase in luminescence. In contrast, the OGD of older, more differentiated 4-week-old neurospheroids caused a damage that remained irreversible, at least without any (therapeutic) intervention as determined here. The ability of the 1-week-old neurospheroids to recover, is most probably the result of the relatively high number of (proliferative) undifferentiated NSCs in the 1-week-old neurospheroids, while the reduced number of NSCs in 4-week-old neurospheroids renders them unable to regenerate (Fig. 4c, e). The latter however resembles a more physiological condition. Moreover, one of the future applications of this model would be the evaluation of neuroprotective compounds. This implies that in order to draw firm conclusions on the effectivity, any recovery or stabilization of deterioration should preferably solely and unambiguously be the result of the potential neuroprotective effect. Therefore, the use of older, more mature neurospheroids is preferred. Apart from the decrease in luminescent signal, flow cytometric analysis confirmed more cell death in OGD-treated neurospheroids at day 7 post-OGD as compared to control conditions, both for 1- and 4-week-old neurospheroids. While considering the recovery of 1-week-old neurospheroids, one might expect to see no difference in viability between control and OGD neurospheroids at day 7. We here hypothesise that initially died cells remained trapped in the neurospheroids by the absence of an immune component able to clear them. A future solution for this will be the use of immune-competent brain organoids containing microglia. Whereas most of the currently used brain spheroids and organoids only contain cells of neuroectodermal lineage, different microglia-containing brain organoids are recently being developed [186, 265, 266], creating a model mimicking the human brain even more closely. Moreover, as microglia have been assigned a key role in the secondary injury after stroke, the use of this model would allow to study both direct and microglia-mediated neurotoxicity after OGD and to evaluate candidate neuroprotective agents based on immunomodulation in the future.

Since the evaluation of candidate neuroprotective drugs is a major application of *in vitro* stroke models, we finally tested the potential neuroprotective pan-caspase inhibitor Z-VAD-FMK in the established luminescent neurospheroid model. As determined by the caspase-3 activity assay and western blot for cleaved caspase-3, Z-VAD-FMK was able to selectively suppress caspase-mediated apoptosis in human neurospheroids. However, this protective effect was not reflected by the luminescence and flow cytometric analysis measuring overall viability, irrespective of treatment duration. The reason for this discrepancy might be explained by other more prominent

cell death mechanisms induced by OGD in this model that mask the attenuation of (ischemic) apoptosis by Z-VAD-FMK, as previously reported by Gottron et al. [256]. Moreover, as evident from the caspase-3 activity assay, corresponding western blot and quantification of cleaved caspase-3 staining, apoptosis present in OGD-treated neurospheroids is mainly the result of basal caspase-3 activity, as demonstrated for control neurospheroids. This suggests that other cell death mechanisms may be responsible for the OGD-mediated neurotoxicity observed by luminescence measurements and conventional analyses in this model. Further research is required to identify cell death types induced by OGD in this model.

Interestingly, when administered to a 2D culture of undifferentiated eGFP/Luc hiPSC-NSCs, Z-VAD-FMK did confer neuroprotection as demonstrated by a smaller decrease in luminescent signal after OGD. This exemplifies how increased complexity of spheroid or organoid models, in terms of cellular heterogeneity and/or dimensionality, may result in a different outcome when testing neuroprotective compounds. Further research is needed to identify the mechanisms, for instance changed susceptibility to neurotoxic stimuli or elicited types of cell death, accounting for this difference in response. Nevertheless, these findings underscore the importance of the introduction of human-based 3D models in the preclinical stage of drug discovery and development, complementing 2D *in vitro* models and *in vivo* models.

3.6 Conclusion

We here present a luminescent human *in vitro* stroke model that can be applied to pathophysiological as well as therapeutic studies in the field of human stroke research. More specifically, the model enables both the study of OGD-associated neurotoxicity and the identification of potential neuroprotective agents by means of its easy read-out of neural survival and health. The high level of reproducibility, the 96-well format development, the easy neurotoxicity read-out and downstream immunocytochemical processing all make this model readily applicable to high-throughput drug screening purposes, which hopefully will lead to the identification of new therapies for acute ischemic stroke patients in the future.

3.7 Supplementary material

Figure S1 - Map of the pCHMWS-eGFP-T2A-fluc-Ires-Puro transfer plasmid used for lentiviral vector production.

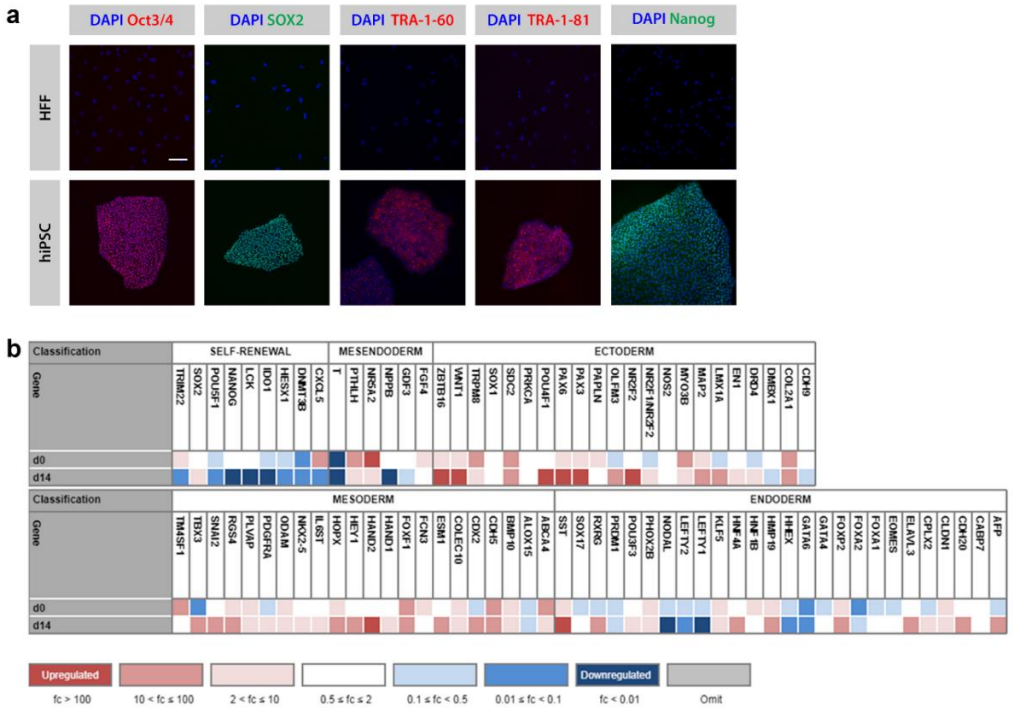

Figure S2 - Characterization of a hiPSC line derived from neonatal foreskin fibroblasts. (A) Immunofluorescence of hiPSC-specific markers. The hiPSC-population derived from neonatal foreskin fibroblasts (HFF) expresses Oct3/4, SOX2, TRA-1-60, TRA-1-81 and Nanog. The original fibroblast culture served as negative control indicating absence of all markers tested. Scale bar 100µm. (B) hPSC ScoreCard analysis. The gene expression of a panel of self-renewal, mesendoderm, ectoderm, mesoderm and endoderm associated genes is represented as the fold change relative to a reference set. hiPSCs derived from 14-day old EBs (d14) show downregulation of self-renewal genes (blue shading), while genes associated with the three germ layers are upregulated (red shading) when compared to undifferentiated hiPSCs at day 0 of EB formation (d0). Colors correlate to the fold change in expression of the indicated gene relative to the undifferentiated reference set.

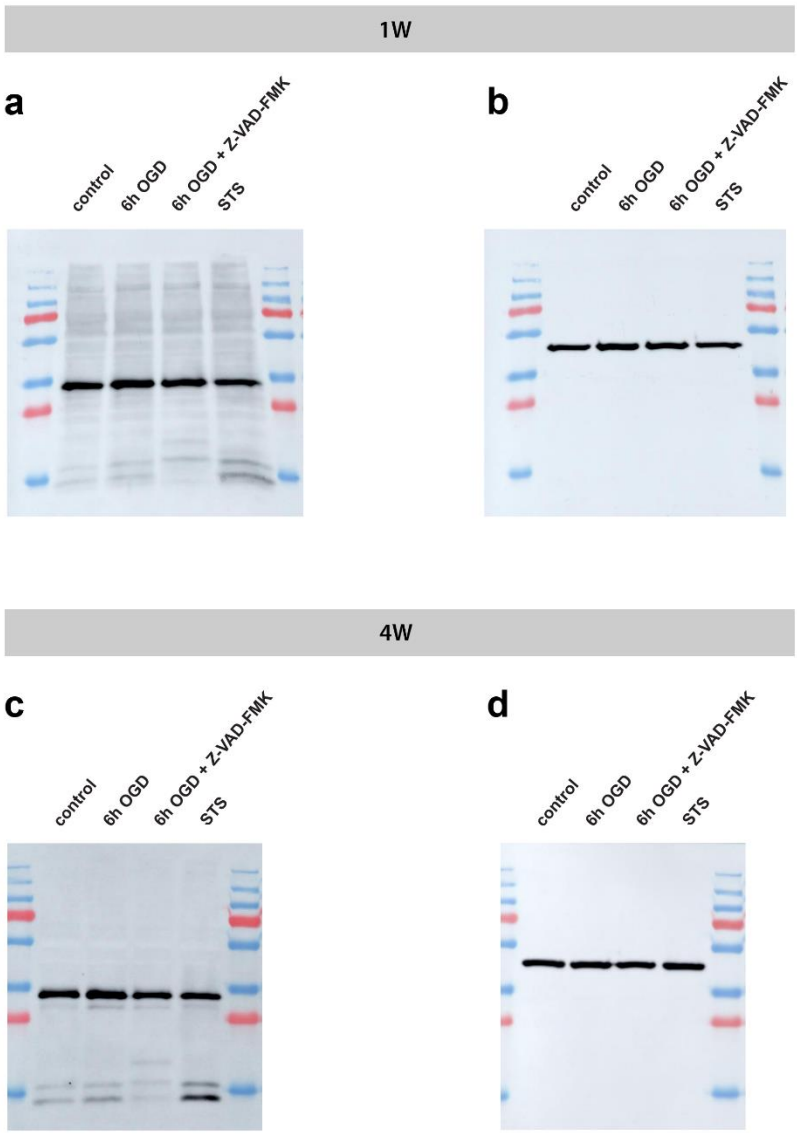

Figure S3 - Western blot for caspase-3. Top: 1-week old (1W) neurospheroids (A-B). Bottom: 4-week old (4W) neurospheroids (C-D). Western blot for caspase-3 (A, C) and β-actin (after a stripping step) (B, D) of lysates derived from neurospheroids under control, 6h OGD or 6h OGD + Z-VAD-FMK conditions at day 2 after reoxygenation. Lysate derived from STS-treated neurospheroids was included as a positive control for cleaved caspase-3.

Table S1 - Statistical output of luminescence data of eGFP/Luc hiPSC-NSC-derived neurospheroids (n=30) over the course of five weeks by three independent experiments, including mean RLU difference, p-value and 95% confidence interval obtained after fitting a linear mixed-effects model.

Age	-age	Mean RLU difference	p-value	Lower 95%	Upper 95%
Week 1	Week 2	-18691	<0.0001	-20961	-16420
Week 2	Week 3	-21153	<0.0001	-23423	-18882
Week 3	Week 4	-52	1.0000	-2323	-2217
Week 4	Week 5	19364	<0.0001	17094	21635

Table S2 - Statistical output of luminescence data of eGFP/Luc hiPSC-NSC-derived neurospheroids (n=12) in function of the mean diameter (µm) at week 1-5, including median RLU difference and p-value obtained by post-hoc analyses for Kruskal-Wallis.

Mean diameter	-Mean diameter	Median RLU difference	p-value	Lower 95%	Upper 95%
Week 1	Week 2	-17019	0.0173	NA	NA
Week 2	Week 3	-25065	0.0070	NA	NA
Week 3	Week 4	17483	>0.9999	NA	NA
Week 4	Week 5	11945	0.0256	NA	NA

Table S3 - Statistical output of luminescence measurements of neurospheroids subjected to different durations of OGD. (A) Median difference in RLU fold change between the post-OGD measurement and pre-OGD measurement for every condition with corresponding p-value obtained by Wilcoxon signed rank test. (B) Median difference (for 1W) or mean difference (for 4W) in ΔRLU fold change between different conditions with corresponding p-values and 95% confidence intervals (for 4W) obtained by post-hoc analyses for Kruskal-Wallis (1W) and One-way ANOVA (4W). (NA, not applicable; 1W, 1-week-old neurospheroids; 4W, 4-week-old neurospheroids)

A

	Median difference (RLU $fold_{POST}$-RLU $fold_{PRE}$)	p-value	Lower 95%	Upper 95%
		1W		
Control	1.78	<0.0001	NA	NA
6h OGD	0.88	<0.0001	NA	NA
24h OGD	-0.48	<0.0001	NA	NA
		4W		
Control	-0.46	<0.0001	NA	NA
6h OGD	-0.65	<0.0001	NA	NA
24h OGD	-0.95	<0.0001	NA	NA

B

Condition	-condition	Median/mean difference ΔRLU fold change between conditions	p-value	Lower 95%	Upper 95%
		1W			
Control	6h OGD	0.90	<0.0001	NA	NA
Control	24h OGD	2.26	<0.0001	NA	NA
6h OGD	24h OGD	1.36	<0.0001	NA	NA
		4W			
Control	6h OGD	0.19	<0.0001	0.10	0.28
Control	24h OGD	0.49	<0.0001	0.40	0.58
6h OGD	24h OGD	0.30	<0.0001	0.20	0.39

Table S4 - Statistical output of luminescence measurements of neurospheroids subjected to OGD by four (for 1W) and six (for 4W) independent experiments. (A) Mean difference in RLU fold change between the post-OGD measurement and pre-OGD measurement for every condition with corresponding p-value and 95% confidence interval obtained after fitting a linear mixed-effects model. (B) Mean difference in ΔRLU fold change between 6h OGD and control neurospheroids, with corresponding p-value and 95% confidence interval obtained after fitting a linear mixed-effects model. (1W, 1-week-old neurospheroids; 4W, 4-week-old neurospheroids)

A

	Mean difference ($RLU\ fold_{POST}$-$RLU\ fold_{PRE}$)	p-value	Lower 95%	Upper 95%
	1W			
Control	2.56	<0.0001	2.42	2.70
6h OGD	1.44	<0.0001	1.33	1.54
	4W			
Control	-0.30	<0.0001	-0.33	-0.27
6h OGD	-0.55	<0.0001	-0.58	-0.52

B

	Mean difference ($\Delta RLU\ fold\ change_{6h\ OGD}$-$\Delta RLU\ fold\ change_{control}$)	p-value	Lower 95%	Upper 95%
1W	-1.13	<0.0001	-1.22	-1.04
4W	-0.26	<0.0001	-0.29	-0.22

Table S5 - Statistical output of luminescence measurements of neurospheroids subjected to OGD with or without Z-VAD-FMK. (A) Median difference or mean difference (for 1W – continuous exposure and 4W – continuous exposure) in RLU fold change between the post-OGD measurement and pre-OGD measurement for every condition with corresponding p-value and 95%confidence interval (for 1W – continuous exposure and 4W – continuous exposure) obtained by Wilcoxon signed rank test, paired t-test (1W- continuous exposure) or by fitting a linear mixed-effects model. (B) Median difference or mean difference (for 1W – continuous exposure and 4W – continuous exposure)in ΔRLU fold change between different conditions with corresponding p-values and 95% confidence intervals (for 1W – continuous exposure and 4W – continuous exposure) obtained by post-hoc analyses for Kruskal-Wallis, one-way ANOVA (1W- continuous exposure) or linear mixed models (4W – continuous exposure). (NA, not applicable; 1W, 1-week-old neurospheroids; 4W, 4-week-old neurospheroids)

A

	Mean/Median difference ($RLU\ fold_{POST}$-$RLU\ fold_{PRE}$)	p-value	Lower 95%	Upper 95%
1W				
Control	2.15	<0.0001	NA	NA
6h OGD	0.99	<0.0001	NA	NA
6h OGD + Z-VAD-FMK	0.74	<0.0001	NA	NA
1W – continuous exposure				
Control	0.22	<0.0001	0.19	0.24
6h OGD	0.01	0.4126	-0.02	0.04
6h OGD + Z-VAD-FMK	-0.15	<0.0001	-0.17	-0.12
4W				
Control	-0.13	<0.0001	NA	NA
6h OGD	-0.57	<0.0001	NA	NA
6h OGD + Z-VAD-FMK	-0.65	<0.0001	NA	NA
4W – continuous exposure				
Control	-0.35	<0.0001	-0.40	-0.29
6h OGD	-0.58	<0.0001	-0.64	-0.53
6h OGD + Z-VAD-FMK	-0.61	<0.0001	-0.65	-0.57

B

Condition	-condition	Mean/Median difference ΔRLU fold change between conditions	p-value	Lower 95%	Upper 95%
		1W			
Control	6h OGD	1.16	<0.0001	NA	NA
Control	6h OGD + Z-VAD-FMK	1.41	<0.0001	NA	NA
6h OGD	6h OGD + Z-VAD-FMK	0.25	0.0024	NA	NA
		1W – continuous exposure			
Control	6h OGD	0.21	<0.0001	0.16	0.25
Control	6h OGD + Z-VAD-FMK	0.36	<0.0001	0.32	0.41
6h OGD	6h OGD + Z-VAD-FMK	0.16	<0.0001	0.11	0.20
		4W			
Control	6h OGD	0.44	<0.0001	NA	NA
Control	6h OGD + Z-VAD-FMK	0.51	<0.0001	NA	NA
6h OGD	6h OGD + Z-VAD-FMK	0.07	0.8982	NA	NA
		4W – continuous exposure			
Control	6h OGD	0.24	<0.0001	0.18	0.29
Control	6h OGD + Z-VAD-FMK	0.27	<0.0001	0.21	0.32
6h OGD	6h OGD + Z-VAD-FMK	0.03	0.3896	-0.02	0.08

Table S6 - Statistical output flow cytometric viability measurements of neurospheroids subjected to OGD with or without Z-VAD-FMK, including mean difference in percentage viable cells between conditions, p-value and 95% confidence interval obtained by post-hoc analyses for one-way ANOVA or linear mixed models (4W – continuous exposure). (NA, not applicable; 1W, 1-week-old neurospheroids; 4W, 4-week-old neurospheroids)

Condition	-condition	Mean Difference % viable cells between conditions	p-value	Lower 95%	Upper 95%
1W					
Control	6h OGD	37.39	<0.0001	30.40	44.38
Control	6h OGD + Z-VAD-FMK	40.95	<0.0001	33.96	47.94
6h OGD	6h OGD + Z-VAD-FMK	3.56	0.4328	-3.427	10.55
1W – continuous exposure					
Control	6h OGD	13.60	<0.0001	10.35	16.85
Control	6h OGD + Z-VAD-FMK	11.97	<0.0001	8.72	15.22
6h OGD	6h OGD + Z-VAD-FMK	-1.63	0.4424	-4.88	1.62
4W					
Control	6h OGD	9.10	0.0178	1.414	16.79
Control	6h OGD + Z-VAD-FMK	11.79	0.0080	2.833	20.74
6h OGD	6h OGD + Z-VAD-FMK	2.69	0.7405	-6.267	11.64
4W – continuous exposure					
Control	6h OGD	18.06	<0.0001	13.42	22.71
Control	6h OGD + Z-VAD-FMK	14,25	<0.0001	9.45	19.05
6h OGD	6h OGD + Z-VAD-FMK	-3.81	0.1282	-8.46	0.83

CHAPTER 4

Towards the development of more mature, multicellular neurospheroids for ischemic stroke research

4.1 Abstract

An increasing body of evidence indicates an important role for astrocytes and microglia in the pathophysiology of ischemic stroke. These glial cells have been ascribed both neurotoxic as well as neuroprotective functions after an ischemic insult, resulting in either exacerbation or recovery of ischemia-induced brain damage. In this chapter, the foundation was laid to further increase the complexity and predictivity of the developed human neurospheroid model by generating more mature, multicellular neurospheroids. In a first set of explorative experiments, culture conditions were optimized in order to obtain neurospheroids with increased maturity and the presence of astrocytes. Hereby, increasing the culture time of the neurospheroids markedly increased neuronal maturity and supported the spontaneous development of astrocytes. It was also noted that culture of neurospheroids in selected differentiation media did not give rise to astrocytes for the evaluated time points, despite their ability to display faster neuronal differentiation and maturation. In a second set of explorative experiments, the integration of hematopoietic progenitors cells into neurospheroids was explored for the future creation of an immune-competent, microglia-enriched neurospheroid model for ischemic stroke. Comparison of different time points for the addition of hematopoietic progenitor cells to neurospheroids, showed higher integration efficiency when added to pre-established neurospheroids and suggest a role for CSF-1 herein.

4.2 Introduction

Ischemic stroke, accounting for ~62% of all stroke cases, is characterized by arterial occlusion due to an embolus or thrombus [1]. The obstructed blood flow gives rise to the formation of an ischemic core and the surrounding penumbra. While the brain tissue denoted as the ischemic core is irreversibly damaged and undergoes necrotic cell death within minutes, the ischemic penumbra contains cells that are less severely affected and that are potentially salvageable from a lethal fate. However, without improved perfusion or therapeutic intervention to improve resistance of cells to injury, the ischemic cascade occurring in the penumbra will result in secondary cerebral damage thereby expanding the infarct core after several hours to days after stroke onset [4-6, 50]. Processes of this ischemic cascade include excitotoxicity, oxidative stress, blood-brain barrier (BBB) dysfunction, inflammation and cell death of neurons, glia and endothelial cells which are triggered by the initial cellular bioenergetic failure as a result of hypoperfusion [5, 50]. It is becoming clear that apart from neurons, other cell types and cell-cell interactions are implicated in aforementioned mechanisms. For instance, with the development of brain injury after ischemia, astrocytes and microglia may acquire a neurotoxic phenotype producing pro-inflammatory factors and chemokines, additionally leading to the infiltration and activation of peripheral immune cells further aggravating brain damage [3, 6, 267]. Furthermore, an important role in the induction of excitotoxicity has been ascribed to astrocytes. While under physiological conditions astrocytes remove excess glutamate from the synaptic cleft, preventing cytotoxic overactivation of glutamatergic neuronal receptors, ischemic conditions impair astrocyte function, contributing to excitotoxic death of neurons [6, 267].

Besides the detrimental role glial cells can play in the pathophysiology of ischemic stroke, astrocytes and microglia have also been ascribed neuroprotective functions aimed at protecting and restoring brain damage. Following ischemic stroke, astrocytes and microglia become activated and release various anti-inflammatory cytokines and neurotrophic factors aimed at protecting the central nervous system (CNS) [3, 6, 267]. Moreover, astrocytes have been shown to alleviate oxidative stress by synthesizing and releasing gluthatione, i.e. an important antioxidant and free radical scavenger, thereby protecting neurons [267]. These examples illustrate the dualistic role of glial and immune cells in the fate of the ischemic penumbra.

Despite the potential role of glial cells, such as astrocytes and microglia, in the exacerbation or recovery of ischemia-induced brain damage, the most commonly used

cellular platform in *in vitro* stroke research consist of neuronal monocultures. Nevertheless, co-culture models consisting of neurons with astrocytes and/or microglia have been reported [56, 59, 151, 152, 156]. Also the recently emerging three-dimensional (3D) models of the brain, such as neurospheroids or organoids, often contain multiple cell types. Next to neurons, astrocytes have demonstrated to spontaneously develop in brain spheroids and organoids generated by different protocols [162, 165, 268, 269]. In contrast to astrocytes, brain spheroids and organoids generally lack microglia due to the mesodermal origin from microglia, compared to neuroectoderm-derived neurons, astrocytes and oligodendrocytes [157, 160, 161, 178, 179]. Recently developed differentiation protocols of iPSC-derived microglia [112-116] are paving the way for development of state-of-the-art immune-competent brain organoids and spheroids [184-186].

Last-mentioned technologies enable the development of fully human multicellular models, which is of particular importance considering the increasing evidence of differences between rodent and human glial cells. For instance, human astrocytes have previously been shown to differ from rodent astrocytes in terms of morphology, diversity and velocity of calcium wave propagation [270]. Even though the astrocytic gene expression is largely conserved between human and mouse, some species-specific differences exist in the expression of genes involved in cytokine signaling [271]. Furthermore, human astrocytes have been shown to respond differently toward certain stimuli including glutamate, oxidative stress and even hypoxia [270-272]. With regard to the latter, hypoxia has been shown to induce a molecular program for neural repair in murine astrocytes, potentially underlying the greater functional recovery occurring in mouse models of ischemic stroke compared to human stroke patients [271]. Similarly, differences between human and rodent microglia have previously been reported [93]. Whereas human and rodent microglia have a highly similar expression profile, human microglia have been shown to express higher levels of immune genes as compared to their murine counterpart [273]. In addition, distinct transcriptional changes were demonstrated for human versus rodent microglia during aging and in response to amyloidosis [273, 274], which is of particular relevance in the context of neurodegenerative diseases. Hence, the species-specific intrinsic as well as behavioral differences of glial cells underscore the importance of studying ischemic stroke in fully human systems.

The neurospheroid model described in chapter 3 already increases the complexity and physiological relevance by providing a 3D microenvironment for the neural cells

compared to traditional 2D cultures. However, the oldest neurospheroids of 4-week-old only contain very few NeuN+ mature neurons and more importantly lack glial cells. In this chapter, I report on our latest developments in generating more mature, multicellular neurospheroids better resembling the human brain that are able to eventually improve predictivity of human ischemic responses and the efficacy of candidate neuroprotective agents. In a first part of this chapter, the culture conditions were optimized to increase the maturity and to allow the spontaneous development of astrocytes in these neurospheroids. In a second part of this chapter, avenues were explored to integrate hematopoietic progenitor cells into these neurospheroids for the future creation of an immune-competent, microglia-enriched neurospheroid model for ischemic stroke research.

4.3 Methods

4.3.1 Neurospheroid formation and culture

HiPSC-NSCs were seeded at a density of 1.6 x 10^4 cells per well in an ULA 96-well plate (Corning) in cNEM. The third day after plating, fresh cNEM (i.e. control condition of chapter 3) or differentiation medium (i.e. new experimental condition) was added. The selection of differentiation media (Table 1 and table S1) was based on the different media types previously used for differentiation of the brain organoids and spheroids in different studies. The main components of the different differentiation media are given in Table 1. For a more detailed overview of the composition, we refer to table S1. Cultures were maintained at 37°C with 5% CO_2 and from day 3 post-seeding onwards under constant orbital shaking (88 rpm). A half to two-third medium change was performed every other day. To allow continuous growth of the neurospheroids over time, the neurospheroids were transferred to an ULA 6-well plate (Corning) containing a higher volume of medium, after 2 or 5 weeks of culture for cNEM or the differentiation media, respectively.

Table 1 – Medium composition of different media types evaluated in this chapter. (BDNF, brain-derived growth factor; GDNF, glial-derived neurotrophic factor)

	Neuro-basal medium	Advanced DMEM/ F12	Neuro-basal Electro medium	BrainPhys medium	B27	N2	BDNF	GDNF	Neural induction supplement
Medium 1	X	X			X	X			
Medium 2	X	X			X	X	X	X	
Medium 3			X		X				
Medium 4			X		X		X	X	
Medium 5				X	X	X			
Medium 6				X	X	X	X	X	
Medium 7 (cNEM)	X	X							X

4.3.2 Spheroid size measurements

The size of the neurospheroids was determined every week for 8 consecutive weeks. To this end, brightfield images were taken using a Zeiss microscope with 5x (NA 0.15) objective lens or a Fluovert Leitz microscope with 4x (NA 0.12) objective lens. Fiji image analysis freeware (http://fiji.sc) was used for image analysis. The size of the neurospheroids was determined using an ImageJ macro for automated spheroid size determination developed by Ivanov et al. [275, 276]. In brief, a specific threshold was used to discriminate between the neurospheroids and the background. From the selected region of the neurospheroid, the area (μm^2) was determined.

4.3.3 Immunofluorescence of neurospheroids

Neurospheroids were fixed with 4% paraformaldehyde (PFA) for 150 min at RT. Following a washing step with phosphate-buffered saline (PBS), neurospheroids were incubated with 20% sucrose in distilled water overnight. Next, neurospheroids were embedded in TissueTek-OCT (VWR) to generate cryosections of multiple neurospheroids arranged in a micro-array according to the protocol described in detail in chapter 3. Cryosections of parallel-mounted neurospheroids were subjected to a permeabilization step of 30 min using 0.1% (v/v) Triton X-100 (Sigma) in Tris-buffered saline (TBS) and blocked with blocking solution consisting of TBS with 20% serum of the corresponding secondary antibody host species for 1h on a shaker. Slices were

incubated (4°C) overnight with the primary antibodies diluted in 10% (m/v) milk solution (Sigma) in TBS (Table 1). After a washing step and a subsequent 1h incubation with the secondary antibodies in milk solution on a shaker (Table 2), slices were again washed and counterstained with DAPI (1µg/ml, Sigma) or TOPRO (5µM, Life Technologies) for 10 min or 20 min at 4°C, respectively. After a final washing step with distilled water, the slices were mounted using ProLong® Gold antifade reagent (ThermoFisher).

Table 2 - List of primary antibodies used for immunocytochemistry. (NA, not available)

	Antibody	Host	Source	Final concentration
A	SOX2	Rabbit	Merck Millipore (AB5603)	2 µg/ml
B	Tuj1	Mouse	R&D systems (MAB1195)	2 µg/ml
C	GFAP	Rabbit	Abcam (ab7260)	1-10 µg/ml
D	NeuN	Guinea pig	Merck Millipore (ABN90P)	5 µg/ml
E	S100β	Rabbit	Abcam (ab52642)	3.1 µg/ml
F	CD45-PE	Mouse	BD (560975)	NA – 1/10 dilution
G	Iba-1	Rabbit	Wako (019-19741)	1-1.4 µg/ml

Table 3 - List of secondary antibodies used for immunocytochemistry.

Antibody	Host	Conjugation	Source	Final concentration	In combination with
Anti-rabbit	Donkey	AF488	Invitrogen (A21206)	2 µg/ml	A
Anti-mouse	Goat	AF555	Invitrogen (A21425)	0.5 µg/ml	B
Anti-rabbit	Goat	FITC	Jackson ImmunoResearch (111-096-045)	7.5 µg/ml	C, E, G
Anti-guinea pig	Donkey	Cy3	Jackson ImmunoResearch (706-165-148)	7.5 µg/ml	D
Anti-rabbit	Donkey	AF555	Invitrogen (A31572)	2 µg/ml	G

4.3.4 Microscopy and image processing

Microscopic imaging was performed using a BX51 fluorescence microscope equipped with an Olympus DP71 digital camera using a 10 x (NA 0.30) and 20 x (NA 0.50) dry objective lens. Images were further processed using Fiji image analysis freeware (http://fiji.sc).

4.3.5 CSF-1 ELISA

The supernatant of neurospheroid cultures (n=3) grown in cNEM for 48h was collected every week for eight weeks and analysed by a CSF-1 ELISA kit (Sigma), according to the manufacturer's instructions.

4.3.6 Supplementation of neurospheroids with hematopoietic progenitor cells

Hematopoietic progenitor cells or hematopoietic progenitor cells pre-directed towards microglia differentiation, resuspended in 100µl cNEM (medium 7) or Brainphys medium (medium 5), were either added to an equal number of NSCs or to single neurospheroids cultured in cNEM or Brainphys medium in an ULA 96-well plate at different timepoints. Hematopoietic progenitor cells were differentiated from hiPSC using STEMdiff™ Hematopoietic Kit (STEMCELL Technologies), according to manufacturer's instructions (for experiments shown in figure 8A, C and D), or were kindly provided by Johanna Van den Daele (Laboratory of Cell biology and Histology, University of Antwerp) [113] (for experiment shown in figure 7). In some of the experiments (Fig. 8C and D), the establishment of hematopoietic progenitor cells was followed by an 8-day pre-direction period. For the latter, the generated hematopoietic progenitor cells were cultured on ULA-plates in medium (DMEM/F12 (Gibco), 0,5% N2 (Gibco), 0,5% B27 (Gibco)) supplemented with 100ng/ml IL-34 (PeproTech), 5ng/ml M-CSF (Immunotools), 5µg/ml insulin (Sigma) for the first 2 days and with 10ng/ml IL-34 and 10ng/ml M-CSF, for the remaining days, based on the protocol of Konttinen et al. [115].

4.3.7 Data Representation and Statistical Analyses

Graphs representing quantitative data were obtained using GraphPad Prism v.8.2.1 software. Statistical analyses were carried out using GraphPad Prism. For the size

measurement data, a non-parametric Kruskal-Wallis test was used, followed by a Mann-Whitney U test for the pairwise comparisons of interest. The obtained p-values were adjusted for multiple testing using the post-hoc Bonferroni correction. To compare the size of neurospheroids grown in differentiation media to the original medium, a Bonferroni correction of 48 was used, to correct for the number of pairwise comparisons of interest and the number of time points (6 and 8, resp.). To compare the size of 1-week-old and 8-week-old neurospheroids for each medium type, a Mann-Whitney U test was used with a Bonferroni correction of 7, i.e. the number of medium types. A p-value <0.05 was considered statistically significant.

4.4 Results

4.4.1 Neurospheroids show increased maturation and spontaneous development of astrocytes over time

With the aim of developing more mature, multicellular neurospheroids, we first evaluated neurospheroids grown under the same conditions, i.e. cNEM, as in chapter 3 for their maturity and the presence of astrocytes at 2, 4, 6 and 8 weeks of culture.

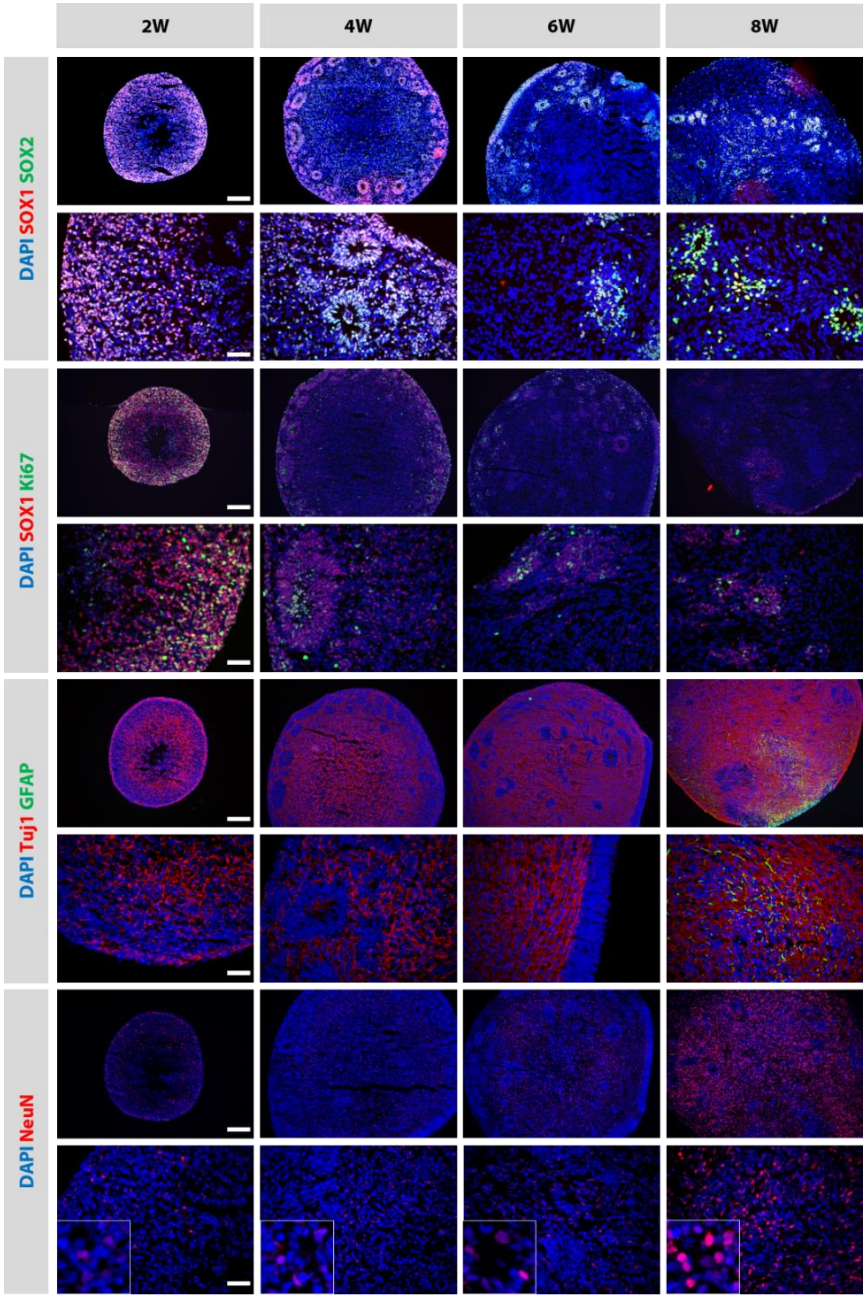

Figure 1 - Representative immunofluorescent images of 2, 4, 6 and 8-week-old neurospheroids immunostained for the NSC markers SOX1 and SOX2, the proliferation marker Ki67, the neuronal markers Tuj1 and NeuN, and for the astrocyte marker GFAP. For each staining, an overview image at 10x magnification (upper row), and a more detailed image at 40x (lower row) are represented. Representative images chosen from 12 individual neurospheroids obtained over 3-4 independent experiments. Scale bar upper row 200µm, lower row 50µm. (2-8W, 2-8-week-old neurospheroid)

By means of immunocytochemistry, it became clear that the results obtained in chapter 3 for the comparison of 2- and 4-week-old neurospheroids could be extended to the data collected here, including 6- and 8-week-old neurospheroids. While 2-week-old neurospheroids showed a high proportion of SOX1+ SOX2+ NSCs, the number of NSCs reduced with increasing age of the neurospheroids (Fig. 1). Likewise, the number of proliferative cells decreased over time, as can be deduced from the sporadic presence of Ki67+ cells in 8-week-old neurospheroids as compared to the high abundance of this marker in 2-week-old neurospheroids (Fig. 1). Furthermore, starting from 4 weeks onward, undifferentiated and proliferative NSCs increasingly assembled in neural rosettes (Fig. 1).

In agreement with earlier results, neurospheroids spontaneously developed neurons as shown by the appearance of Tuj1+ and NeuN+ cells. Although cells in the neurospheroids spontaneously developed neurons within 2 weeks of culture, the number and intensity of mature NeuN+ cells was only markedly present in 8-week-old neurospheroids (Fig. 1).

Next to the increased maturation of neurons, at 8 weeks of age, neurospheroids also showed GFAP positive cells, indicative for the spontaneous generation of astrocytes in these neurospheroids (Fig. 1). This differentiation pattern, in which first neurons are formed and at later age astrocytes, recapitulates the *in vivo* embryonic brain development.

4.4.2 Testing different media compositions for balanced proliferation and differentiation of neurospheroids

As can be concluded from abovementioned results, neurospheroids grown in cNEM show increased maturation and spontaneous development of astrocytes over time. However, as cNEM is medium primarily optimized for the expansion of neural stem and progenitor cells, we here investigated whether other media compositions can accelerate the differentiation into neurons and astrocytes and thereby reduce the proliferation of neural stem and progenitor cells, minimizing the formation of a hypoxic, necrotic core. To this end, neurospheroids were grown in different media types without (medium 1, 3, 5) and with (medium 2, 4, 6) the supplementation of neurotrophic factors BDNF and GDNF and subsequently characterized for their size at a weekly interval and their cellular composition at weeks 2, 4, 6 and 8-weeks of age.

At first, the size of the neurospheroids was measured weekly (Fig. 2). For the original medium 7, the size of the neurospheroids significantly increased until week 8 ($p = 0.0014$, table S2), where the neurospheroids eventually reached a size of 3319036 μm^2 or a theoretical diameter of 2056 µm, as derived from the formula of the area of a circle. Also for the differentiation media, a significant increase in size can be observed over a 8-week growth period (for all $p \leq 0.0014$, table S2). Nevertheless, neurospheroids grown in differentiation media remain smaller than those cultured in medium 7, with a significant difference in size detected from week 2 onwards (for all $p < 0.0048$, table S2). For example, at week 8 the biggest neurospheroids of medium 4 and the smallest neurospheroids of medium 5 only reached a median size of 1067893 μm^2 or 562222 μm^2 (i.e. theoretical diameter of 1166 µm or 846 µm), respectively. Although not visible on the provided images, the neurospheroids cultured in the differentiation media still potentially develop a hypoxic, necrotic core, despite their significant smaller sizes. Indeed, already at week 1, the median theoretical diameters of the neurospheroids grown in the different differentiation media (media 1-6) exceed diameters of 400µm, which is the maximum diameter before neurospheroids start to develop a hypoxic core, considering the diffusion limit of oxygen (i.e. 200µm) [277].

Next, we assessed whether these differentiation media were able to accelerate the differentiation of cells in the neurospheroids. When compared to cNEM (medium 7), 2-week-old neurospheroids grown in the various differentiation media (media 1-6) appear to display a much higher relative number of NeuN-expressing mature neurons (Fig. 3). These results suggest that neurospheroids grown in differentiation media differentiated and matured relatively faster compared to medium 7 where a widespread, high proportion of NeuN positive cells is only established at 8 weeks of age. In agreement with these results, neurospheroids grown in medium 7 appear to retain a larger number of SOX2-expressing NSCs between weeks 2 and 6 as compared to the other 6 types of differentiation media (Fig. 3). Interestingly, together with the lower number of NSCs, the typical neural rosette structures which are present in neurospheroids of medium 7 from week 4 onwards, are completely absent in the neurospheroids grown in the differentiation media (media 1-6).

Furthermore, the Tuj1 staining, indicating neurons including those with a more immature phenotype, is for all media types (medium 1-7) present from 2 weeks onwards and shows a widely dispersed pattern (Fig. 4). Of note, the various types of differentiation media (media 1-6) displayed a slightly brighter staining for Tuj1 at weeks

2 and 4, compared to medium 7, possibly reflecting a higher number of neurons at these early time points in the neurospheroids cultured in differentiation media (Fig. 4).

Finally, the neurospheroids cultured in the different media types were also stained for GFAP, a marker representative for astrocytes. As can be appreciated from figure 5, GFAP staining is almost exclusively present in 8-week-old neurospheroids grown in medium 7, except for the sporadically present GFAP positive cells occurring at the periphery of neurospheroids cultured in differentiation medium 1 and 2. Upon longer term culture of neurospheroids in medium 7, the GFAP staining expands, suggesting a wide spread distribution of an increasing population of astrocytes (Fig. 6A). Confirming these results, s100β positive cells, reflecting more mature astrocytes, are present at 8-weeks of age and increase over time (Fig. 6B).

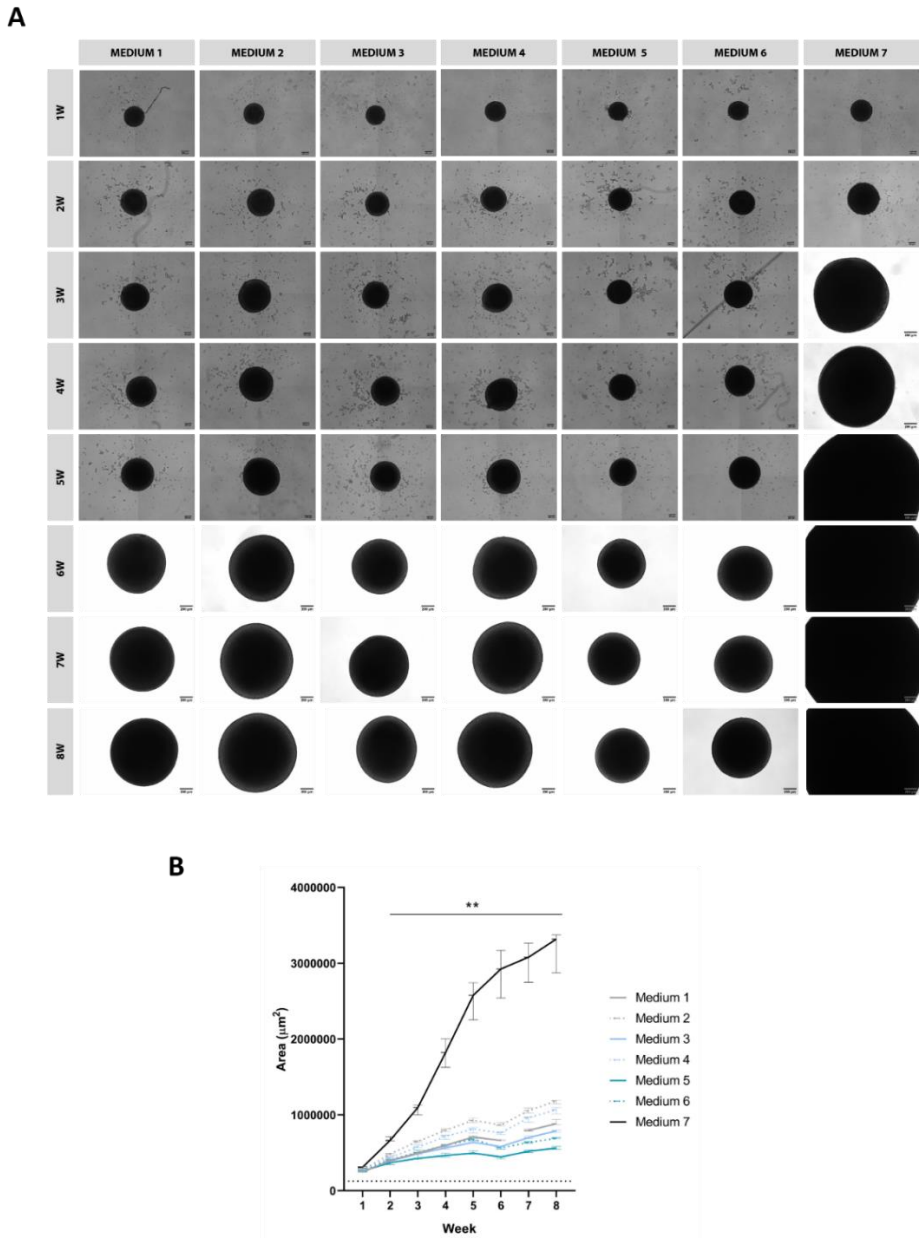

*Figure 2 – Size measurements of neurospheroids over the course of 8 weeks. (A) Representative brightfield images (i.e. image with measured area closest to the median value shown in B) of neurospheroids grown in various types of differentiation media (medium 1-6) and cNEM (medium 7). Scale bar 200µm. (B) The median area of the neurospheroids grown in different media types over the course of 8 weeks (n= 6-10 per medium type). Error bars represent the interquartile range. Note that for medium type 1 two subsets of neurospheroids were used for these weekly measurements, shown by two individual curves. The horizontal black dotted line represents the threshold area for the development of a hypoxic core and corresponds to a theoretical diameter of 400µm. ** $p < 0.01$*

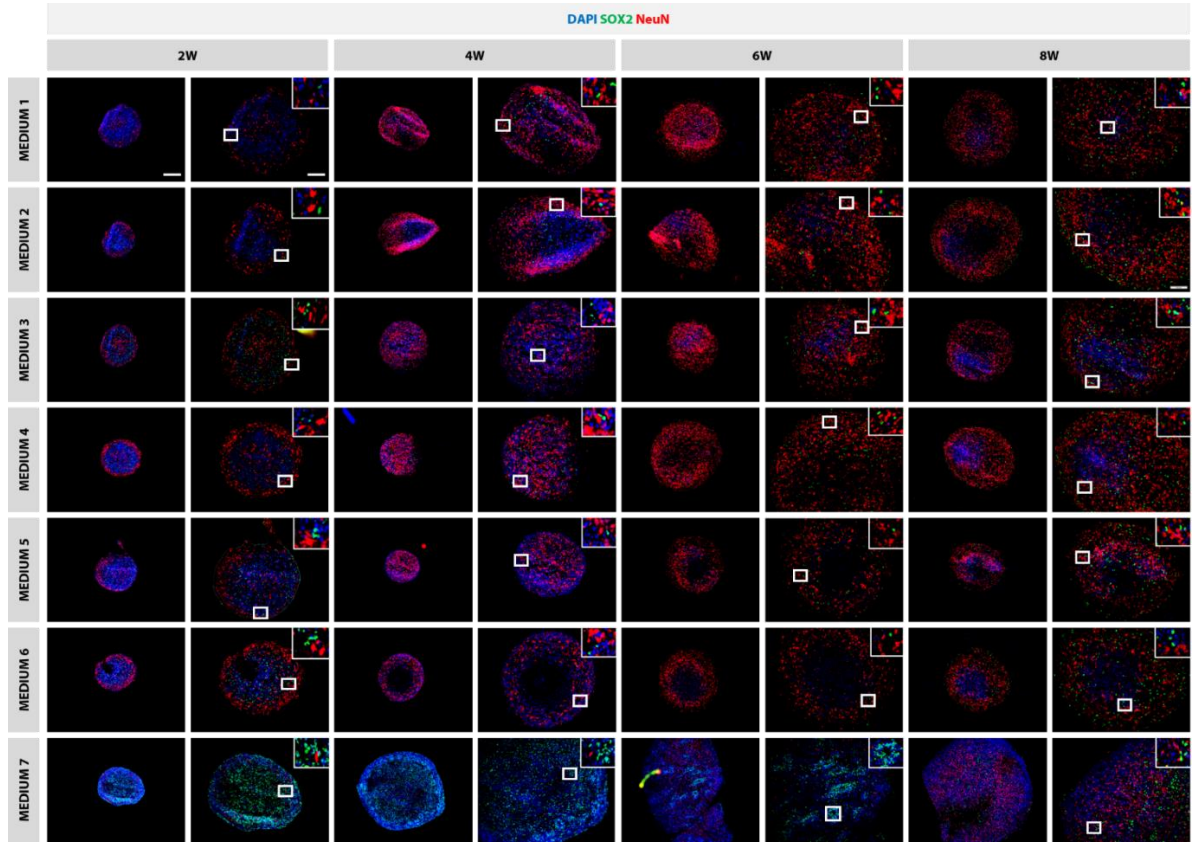

Figure 3 - Representative immunofluorescent images of 2, 4, 6 and 8-week-old neurospheroids immunostained for the NSC marker SOX2 and mature neuron marker NeuN. For each medium condition, an overview image at 10x magnification (left) and a more detailed image at 20x (right) are represented per time point. Representative images chosen from 3 individual neurospheroids. Scale bar left image 200 µm (10x), scale bar right image 100 µm (20x). An inset shows higher level of detail at the selected region (white square) from right images (20x). (2-8W, 2-8-week-old neurospheroid)

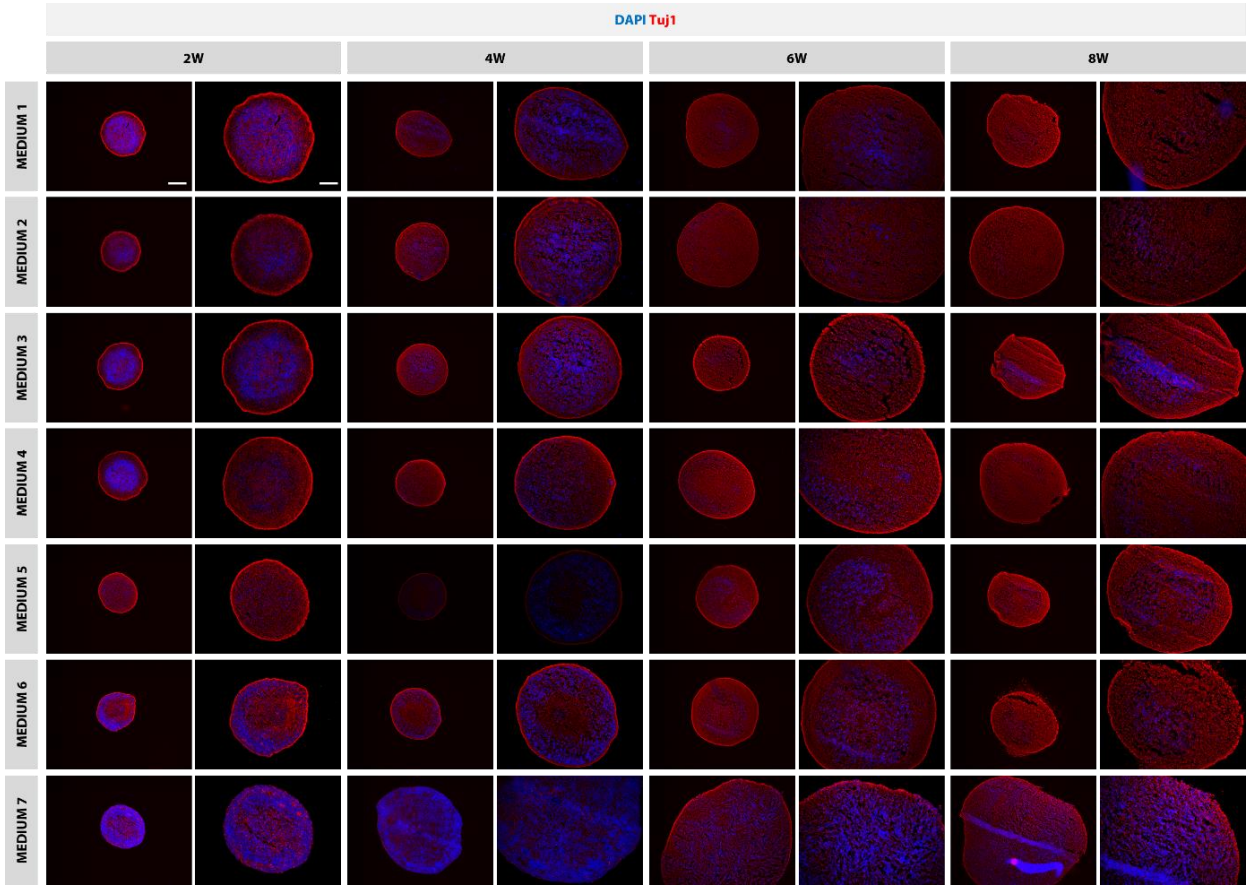

Figure 4 - Representative immunofluorescent images of 2, 4, 6 and 8-week-old neurospheroids immunostained for the neuronal marker Tuj1. For each medium condition, an overview image at 10x magnification (left) and a more detailed image at 20x (right) are represented per time point. Representative images chosen from 3 individual neurospheroids. Scale bar left image 200 µm (10x), scale bar right image 100 µm (20x). (2-8W, 2-8-week-old neurospheroid)

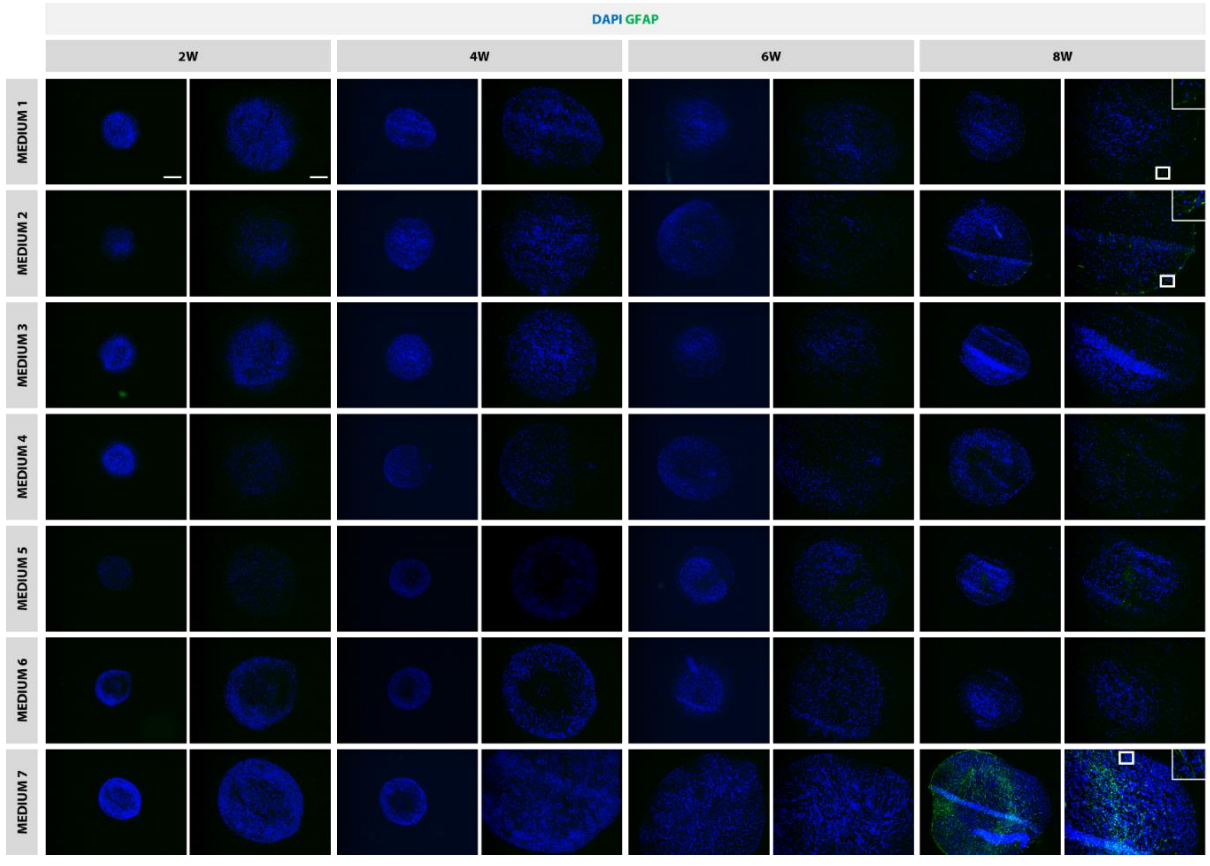

Figure 5 - Representative immunofluorescent images of 2, 4, 6 and 8-week-old neurospheroids immunostained for the astrocyte marker GFAP. For each medium condition, an overview image at 10x magnification (left) and a more detailed image at 20x (right) are represented per time point. Representative images chosen from 3 individual neurospheroids. Scale bar left image 200 µm (10x), scale bar right image 100 µm (20x). An inset shows higher level of detail at the selected region (white square) from right images (20x). (2-8W, 2-8-week-old neurospheroid)

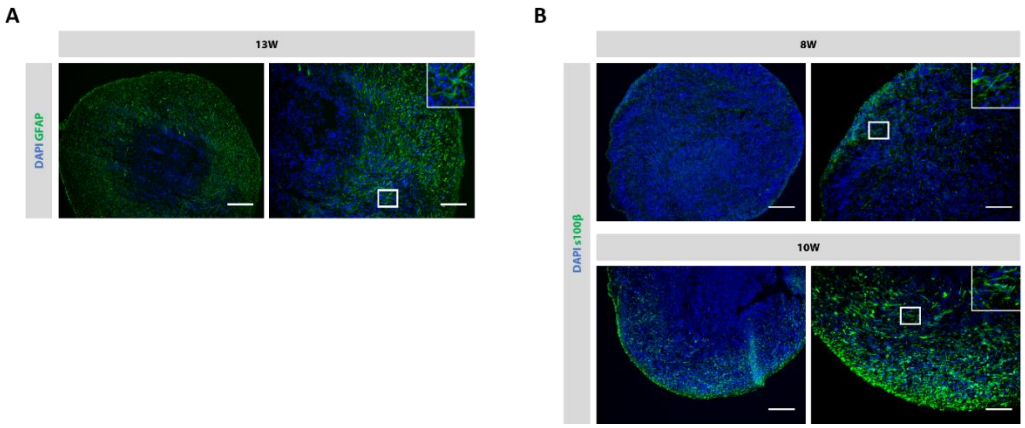

Figure 6 - Representative immunofluorescent images of neurospheroids grown in medium 7 immunostained for astrocyte markers. (A) Neurospheroid of 13-weeks-old immunostained for the astrocyte marker GFAP. An overview image at 10x magnification (left) and a more detailed image at 20x (right) are depicted. Representative image chosen from 3 individual neurospheroids. Scale bar left image 200 µm (10x), scale bar right image 100 µm (20x). An inset shows higher level of detail at the selected region (white square) from right images (20x). (B) Neurospheroid of 8- and 10-weeks-old immunostained for the more mature astrocyte marker s100β. An overview image at 10x magnification (left) and a more detailed image at 20x (right) are depicted. Representative images chosen from 2 individual neurospheroids. Scale bar left image 200 µm (10x), scale bar right image 100 µm (20x). An inset shows higher level of detail at the selected region (white square) from right images (20x). (8-13W, 8-13-week-old neurospheroids)

4.4.3 Integration of hematopoietic progenitor cells in neurospheroids for the creation of microglia-enriched neurospheroids

Besides astrocytes, the presence of microglia in the neurospheroids would greatly improve the resemblance of the model to human brain tissue and would allow to more accurately mimic the secondary cerebral damage occurring after stroke. To this end, we conducted explorative studies aiming at the integration of hematopoietic progenitor cells in these neurospheroids, which is a critical step for the development of microglia-containing neurospheroids.

In a first experiment, we added hematopoietic progenitor cells to 1-week-old neurospheroids in medium based on the Brainphys medium (medium 5). After a co-culture period of 2 weeks, a CD45 staining, indicative of hematopoietic cells, shows the integration of the hematopoietic progenitor cells in these neurospheroids (Fig. 7). Although, integration of hematopoietic progenitor cells was successful, the consideration that this medium type does not give rise to the spontaneous

development of astrocytes in a short time frame of 8 weeks, a similar strategy was applied for neurospheroids continuously grown in cNEM (medium 7).

Multiple explorative experiments were performed to estimate the preferred timing for the addition of hematopoietic progenitor cells. In a first experiment, hematopoietic progenitor cells were directly mixed with neural stem cells from the beginning before the formation of a neurospheroid. As can be concluded from the Iba-1 staining, defining microglia and macrophages, this strategy is associated with a very low integration efficiency of these hematopoietic progenitor cells after 1 week in co-culture. Indeed, figure 8A shows only the sporadic presence of Iba-1 positive cells within these spheroids. Moreover, a lot of hematopoietic progenitor cells surrounded the neurospheroid and eventually detached upon further processing for embedding and staining, as can be seen by the Iba-1 positive patch at the right side of the image. One hypothesis for the failure of this particular strategy might be the absence of environmental cues that normally are provided by neural tissue. One such cue is the cytokine CSF-1, which is considered to be implicated in the development, steady state maintenance and migration of microglia in the CNS [278, 279]. By means of a CSF-1 ELISA we show increasing endogenous production of this factor by the neurospheroids over time (Fig. 8B). Taking into account this observation, we conducted a second experiment where we added hematopoietic progenitor cells to 10-week-old neurospheroids. After 2 weeks of culture, the marked presence of Iba-1 positive cells confirmed that the hematopoietic progenitor cells integrated into the neurospheroid. Interestingly, the progenitors are more located at the periphery of the neurospheroid (Fig. 8C). In an attempt to more evenly distribute the hematopoietic progenitors in the neurospheroid, we added the hematopoietic progenitors at an earlier time point of 4 weeks in a final experiment. Although some Iba-1 positive cells localize more in the center of the neurospheroid, the large majority of hematopoietic progenitor cells is still located at the periphery of the neurospheroid at 4 weeks of co-culture (Fig. 8D).

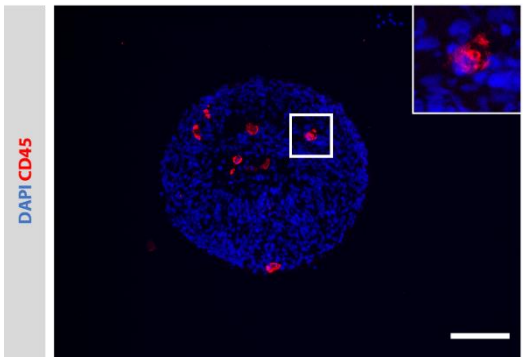

Figure 7 - Representative immunofluorescent image of neurospheroid after the addition of hematopoietic progenitor cells in Brainphys medium. 3-week-old neurospheroid stained for the hematopoietic cell marker CD45 after the addition of 1.2 x10^4 hematopoietic progenitor cells at week 1. Representative image chosen from 4 individual neurospheroids. Inset shows higher level of detail at the selected region (white square). Scale bar 100µm.

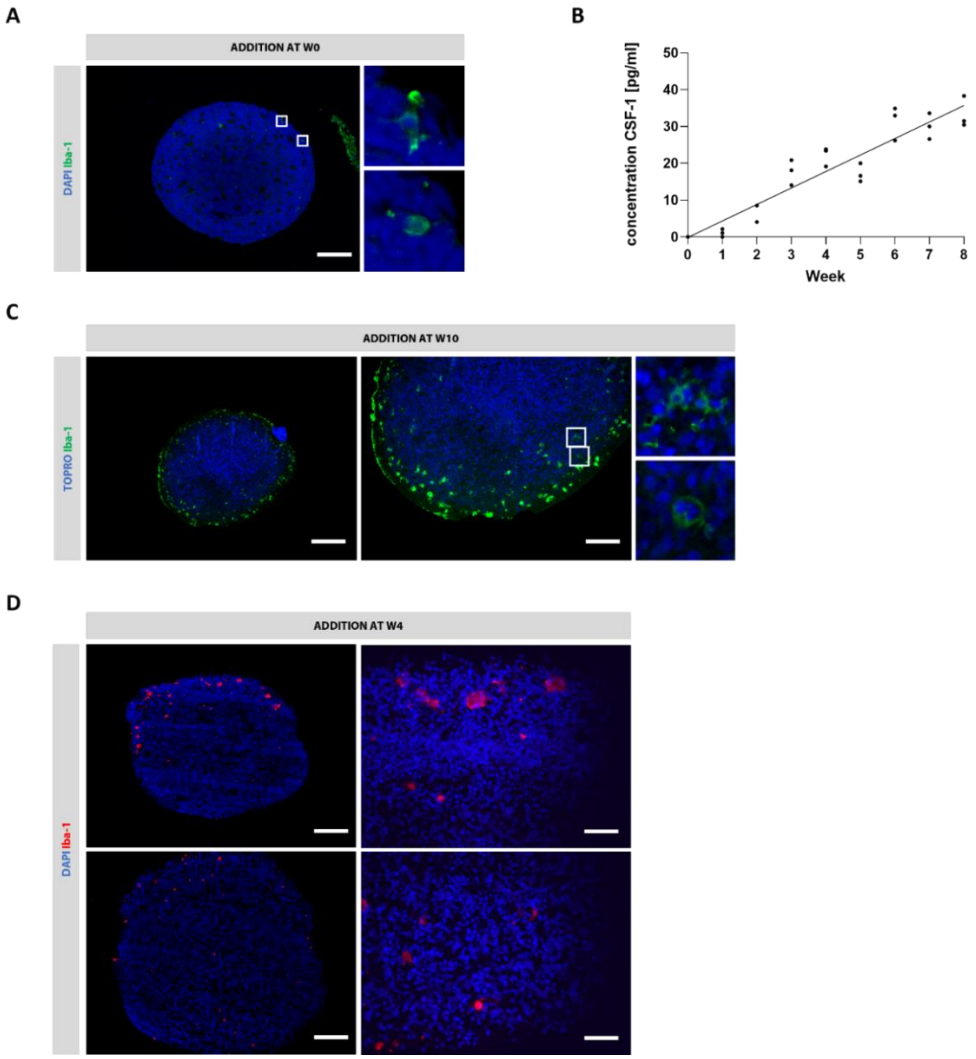

Figure 8 - Representative immunofluorescent image of neurospheroid after the addition of hematopoietic progenitors in cNEM medium at different time points. (A) 1-week-old neurospheroid stained for the microglia/macrophage marker Iba-1 after the addition of 1.6 x10^4 hematopoietic progenitor cells at week 0, i.e. time point of seeding the neural stem cells. Representative image chosen from 2 individual neurospheroids. Scale bar 100µm. (B) The concentration of CSF-1 measured in the supernatant of neurospheroids at different timepoints (week 0-8) (n=3 per timepoint). Each dot is an independent observation. A curve of best fit was plotted on the graph. (C) 12-week-old neurospheroid stained for the microglia/macrophage marker Iba-1 after the addition of 2.0 x10^5 hematopoietic progenitor cells at week 10. An overview image at 10x magnification (left) and a more detailed image at 20x (right) are depicted. Representative image chosen from 2 individual neurospheroids. Scale bar left image 200 µm (10x), scale bar right image 100 µm (20x). An inset shows higher level of detail at the selected region (white square) from right images (20x). (D) 8-week-old neurospheroid, sliced at two different depths, stained for the

microglia/macrophage marker Iba-1 after the addition of 1.2 x10^5 hematopoietic progenitor cells at week 4. An overview image at 10x magnification (left) and a more detailed image at 40x (right) are depicted. Representative image chosen from 3 individual neurospheroids obtained over 2 independent experiments. Scale bar left image 200 µm (10x), scale bar right image 50 µm (40x).

4.5 Discussion

To model human ischemic responses more accurately *in vitro*, the ischemic stroke field would greatly benefit from more mature neurospheroids containing multiple cell types, including astrocytes and microglia next to neurons and its progenitors. The general lack of astrocytes and microglia in neurospheroid or organoid models for ischemic stroke research not only ignores the contribution of these glial cells in the progression of ischemia-induced brain damage, but also excludes the possibility to evaluate neuroprotective strategies based on immunomodulation. In this chapter we aimed to add another level of complexity to the neurospheroid model described in chapter 3, by exploring ways to introduce astrocytes and microglia to this model as well as to increase its maturity.

In the first part of this chapter, we examined whether increasing the culture time of the neurospheroids under the same conditions as described in chapter 3, could increase maturation and spontaneous development of astrocytes over an 8-week period. Although no histological quantification was performed, one could appreciate the increased maturation of neurons and the presence of astrocytes at an 8-week time point. The latter is in line with embryonic brain development, where glial differentiation is initiated later than neuronal differentiation. Clearly, whether the neurons are functionally mature remains to be determined by means of electrophysiological measurements, for example through the use of multi-electrode arrays (MEAs), a project which will be actively pursued in our future research. Though, given the increased proportion of mature neurons and the presence of astrocytes – which have previously demonstrated to improve the functional maturation of neurons in 2D cultures [139-142] - at the 8-week time point, the presence of neuronal activity is conceivable. Also, the astrocytes still would need to be functionally characterized for its ability to produce cytokines and glutamate uptake.

With the aim of accelerating the differentiation and maturation of the neurospheroids, we examined different media types that have previously been used for the culture of brain organoids and spheroids. As expected, these differentiation media appear to expedite the differentiation and maturation, as evidenced by the prominent

appearance of mature neurons at 2 weeks of age, compared to 8 weeks when using the original cNEM. This difference in differentiation dynamics between the different media types and cNEM was also reflected in their corresponding growth profiles. Whereas neurospheroids grown in the original medium kept on growing at a significant rate, the expedited differentiation of the neurospheroids in differentiation media caused the proliferation potential to be reduced already at earlier stages, overall resulting in smaller sized neurospheroids. Nonetheless, their acquired size still suggest the potential development of a hypoxic, necrotic core. With regard to astrocyte development, the selected media types have previously demonstrated to allow astrocyte differentiation in different studies [162, 165, 269, 280]. However, in our hands, besides medium 1 and 2, which are based on the neurobasal and DMEM/F12 media type supplemented with N2 and B27, that showed sporadic appearance of astrocytes at the periphery of the neurospheroids, the majority of differentiation media in these preliminary experiments did not give rise to astrocytes, at least not in this short time frame of 8 weeks. Hence, for the generation of astrocyte-containing neurospheroids, the original medium, cNEM, is superior to the other media types. Moreover, despite the delay compared to specific differentiation media, a marked population of mature neurons is present at the time point of astrocyte appearance (i.e. 8 weeks). Nevertheless, neurospheroids grown in the original medium develop a relative larger necrotic core. In the future, this may be circumvented by using a combination of cNEM with one of the evaluated medium types above and/or by the use of bioreactors tailored for 3D cultures. Of note, the results obtained in these explorative experiments need to be confirmed by additional experiments further supplemented with data on the quantification of the different markers. Furthermore, to draw firm conclusions concerning the maturity level of the neurospheroids grown in the different media types, the electrophysiological activity of the neurospheroids should be measured.

In the second part of this chapter, we tried to introduce hematopoietic progenitor cells into the neurospheroid model as a first step to develop state-of-the-art microglia-enriched neurospheroids. In contrast to other CNS cell types that know a neuroectodermal origin, microglia are derived from the mesodermal lineage and eventually invade the developing brain. Therefore one of the biggest shortcomings of current brain organoids and spheroids has been the lack of microglia cells. Despite this general concept, protocols have recently been developed that support the innate development of microglia in brain organoids [266, 281]. However, these protocols compass cerebral organoids that are directly derived from human iPSCs and rely on the

spontaneous stochastic appearance of microglia, making it impossible to control the ratio of microglia in these organoids. Therefore, we here applied another strategy, similar to other studies that are recently are being published [112, 115, 116, 184-186, 265, 282, 283], where we add hematopoietic progenitors cells to NSCs before the initiation of neurospheroid formation or to pre-established neurospheroids. This concept would mimic the in vivo migration of progenitors into the developing brain where they further develop into mature microglia. As can be concluded from the experiments conducted here, hematopoietic progenitor cells are able to successfully migrate in 1-week-old neurospheroids cultured in Brainphys-based medium. However, with the aim of developing multicellular neurospheroids containing neurons, microglia and astrocytes, further experiments were carried out it with cNEM. Different time points of addition of hematopoietic progenitor cells to the neurospheroids were evaluated. Addition to neural stem cells before the formation of neurospheroids resulted in a very low integration efficiency, which might be explained by the lack of the necessary neural environmental cues. Microglia development, but also migration and steady state maintenance of microglia, rely on the presence of certain factors provided by the neural environment. Supporting this hypothesis, hematopoietic progenitor cells added at later timepoints (i.e. weeks 10 and 4) show more successful integration possibly due to the CSF-1 gradient generated endogenously by neurons and/or astrocytes in the developing neurospheroids. Despite the successful integration, an important point of consideration is the continuous growth of the neurospheroid in cNEM, as shown by the size measurements (Fig. 2), eventually leading to the dilution of hematopoietic progenitor cells over time. Furthermore, the bigger the size of the neurospheroids the less hematopoietic progenitor cells are evenly distributed over the neurospheroid, for the same distance they migrate in smaller neurospheroids, as can noticed when comparing figures 7 and 8. To this end, key of future experiments would be to optimize the media composition, as suggested earlier, and to optimize the time point of addition to balance between the addition to young neurospheroids, which are smaller and older neurospheroids that are capable of providing the necessary environmental signals. A second step towards the development of microglia-enriched neurospheroids would be to increase the co-culture time and subsequently validate the development of mature microglia by means of immunocytochemistry for microglia-specific markers (e.g. TMEM119 and P2RY12) and single cell RNA sequencing, combined with assessments of their functionality to secrete cytokines and their phagocytic capacity upon stimulation.

Of note, future experiments aimed at confirming the integration of microglia-like cells and the distribution of CNS cell types in the neurospheroids in general, would greatly benefit from 3D imaging. Whereas here, slices of neurospheroids at various depths are used to conclude something about the distribution of cells, 3D imaging would allow to capture the complete distribution in the neurospheroid, providing more accurate data.

Altogether, the preliminary data presented in this chapter demonstrate the feasibility of generating astrocyte- and microglia-progenitor-containing neurospheroids and represent an important first step towards the development of multicellular neurospheroids that when subjected to hypoxic and hypoglycemic stimuli may model human ischemic stroke with greater accuracy.

4.6 Supplementary material

Table S1 – Detailed overview of all components of the different differentiation media (medium 1-6) and cNEM (medium 7) for a total volume of 50ml per medium type. For medium types 2,4 and 6 additionally BDNF and GDNF are added at a final concentration of 2 ng/ml. (BDNF, brain-derived growth factor; GDNF, glial-derived neurotrophic factor)

	Components	Volume (µl)	Source
MEDIUM 1-2	Neurobasal medium (1:1)	24000	Gibco
	Advanced DMEM/F12 (1:1)	24000	Gibco
	N2 (1/100)	500	Gibco
	B27 (1/50)	1000	Gibco
	L-glutamine (1/100 = 1%)	500	Gibco
MEDIUM 3-4	Neurobasal Electro Medium	48500	Gibco
	B27 (Electro, 1/50)	1000	Gibco
	L-glutamine (1/100 = 1%)	500	Gibco
MEDIUM 5-6	BrainPhys Medium	48000	Stemcell Technologies
	N2 (1/100)	500	Gibco
	B27 (1/50)	1000	Gibco
	L-glutamine (1/100 = 1%)	500	Gibco
MEDIUM 7	Neurobasal medium	24500	Gibco
	Advanced DMEM/F12	24500	Gibco
	Neural Induction Supplement	1000	Gibco

Table S2 – Statistical output of size measurements of neurospheroids grown in different differentiation media types (medium 1-6) or cNEM (medium 7). (A) Adjusted p-values for comparison of the size of neurospheroids grown in differentiation media to the original medium 7 obtained by Mann Withney U test for the pairwise comparisons of interest and Bonferroni correction. (B) Adjusted p-values for comparison of 1-week-old and 8-week-old neurospheroids for each medium type obtained by Mann Withney U test for the pairwise comparisons of interest and Bonferroni correction.

A

	Week 1	Week 2	Week 3	Week 4	Week 5	Week 6	Week 7	Week 8
Medium 1-7	0,1056	< 0,0048	< 0,0048	< 0,0048	< 0,0048	< 0,0048	< 0,0048	< 0,0048
Medium 2-7	3,1152	< 0,0048	< 0,0048	< 0,0048	< 0,0048	< 0,0048	< 0,0048	< 0,0048
Medium 3-7	0,1056	< 0,0048	< 0,0048	< 0,0048	< 0,0048	< 0,0048	< 0,0048	< 0,0048
Medium 4-7	0,1056	< 0,0048	< 0,0048	< 0,0048	< 0,0048	< 0,0048	< 0,0048	< 0,0048
Medium 5-7	3,1152	< 0,0048	< 0,0048	< 0,0048	< 0,0048	< 0,0048	< 0,0048	< 0,0048
Medium 6-7	0,1056	< 0,0048	< 0,0048	< 0,0048	< 0,0048	< 0,0048	< 0,0048	< 0,0048

B

	Medium 1	Medium 2	Medium 3	Medium 4	Medium 5	Medium 6	Medium 7
Week 1-8	0,0014	0,0007	0,0007	0,0014	0,0007	0,0007	0,0014

CHAPTER 5

General discussion and future perspectives

5.1 Enhancing clinical translation of neuroprotective therapies for ischemic stroke

Decades of research resulted in over a thousand of candidate neuroprotective agents of which none have led to an effective therapy for ischemic patients to date. Despite being considered promising in preclinical setting, many neuroprotective agents failed when translated to the clinic. Apart from possible reasons with regard to clinical trial design, deficiencies in animal studies have also been identified. With the purpose of increasing the chance of success of clinical translation of neuroprotective agents, specific guidelines were hereto formulated [9, 284-287]. For instance, researchers are strongly encouraged to conduct short- as well as long-term functional assessments of the animals, next to measurements of the infarct volume which has long been used as the main readout [9, 284, 287]. More recently, also the animal models themselves are being improved. From all different rodent ischemic stroke models, the middle cerebral artery occlusion (MCAO) rodent model is most often used as it is able to closely simulate human ischemic stroke, that often originates from occlusion of this artery [54]. While highly relevant, studies are mostly conducted in young animals without comorbidities. To increase translatability, it is recommended to include assessment of the candidate neuroprotective agent in experimental models of stroke with co-morbidities and advanced age in both sexes before moving to clinical trials [9]. In this regard, the preclinical evaluation of statins for instance, included the use of rodent models of ischemic stroke with hypertension [288]. Despite the improvements in animal studies, failures as a result of species-specific differences cannot be ruled out by means of these measures. It would therefore be of equal importance to validate the neuroprotective agents also in a human *in vitro* context before initiating clinical trials. At current, the use of human-based models in preclinical ischemic stroke research is rare because of the ignorance of species-specific differences, the difficult access of primary brain tissue and the lack of physiological relevance of easy accessible transformed cell lines. The field of ischemic stroke would greatly benefit from the implementation of more complex *in vitro* models with improved physiological relevance to model human-ischemic responses and thus clinical outcomes with greater accuracy. To this end, in this doctoral dissertation, I developed and characterized a human neurospheroid model, generated by the spontaneous self-assembling capacity of hiPSC-derived NSCs. In what follows, I will briefly summarize the main technological

and scientific findings during my PhD research, as well as provide important future follow-up research directions.

5.2 Technological achievements

Data presented in this thesis demonstrate that the established neurospheroid culture protocol results in neurospheroids with **reproducible size, growth and differentiation pattern** (see Chapter 3). Heterogeneity in terms of size, shape and composition, have often been considered a limitation of organoids [179, 187, 188]. Most of the 3D neurospheroid and organoid models are directly derived from iPSCs that self-assemble into embryoid bodies and are embedded in martigel droplets as part of the applied differentiation protocol [164]. Although protocols based on this approach give rise to neural organoids with high level of complexity, which is of particular relevance in neurodevelopment research, they are often associated with high variability [158, 165, 257, 289]. Here, neurospheroids were developed starting from NSCs that were previously derived from hiPSC, without the use of Matrigel to support 3D culture. This approach allows to surpass potential sources of variability, by ensuring the exclusive development of cells of neuroectodermal origin and avoiding undefined factors present in natural hydrogels [157, 169, 187, 289].

Furthermore, the neurospheroid model was equipped with intrinsic **bioluminescence** that allows for an easy and longitudinal follow-up of the viability after OGD (see Chapter 3). Most *in vitro* stroke studies determine the viability and/or cytotoxicity after OGD by techniques such as MTT assay, LDH assay, flow cytometric or microscopic detection of living and/or apoptotic cells, that require a single endpoint and/or disruption of the neurospheroids. Bioluminescence overcomes aforementioned limitations, thereby enabling to monitor the dynamics in viability and cytotoxicity of the same (OGD-treated) culture over time, possibly providing more insight into the pathophysiology of ischemic stroke and/or the effectiveness of candidate neuroprotective compounds. However, given the decrease in luminescent signal over time under control conditions in our study, the genetic engineering strategy and the promoter type may need to be modified for future experiments.

In addition, the neurospheroid generation protocol and analysis tools set out in this thesis support the **high-throughput potential** of the described neurospheroids (see Chapter 3). As mentioned earlier, protocols for generating cerebral organoids often contain cumbersome matrix-embedding steps and result in complex, non-uniform

organoids, rendering them less suitable for applications such as drug screening [158, 165, 257]. However, the rather simple protocol, the 96-well format development and the reproducibility of the neurospheroids, together with easy read-out of viability of single neurospheroids by means of bioluminescence, presented in this thesis, make this model compatible with high-throughput screening applications in the future. In addition, the spheroid microarray technology, adapted from Ivanov et al. [250], further supports the histological processing and microscopic imaging to be carried out in (semi-)high-throughput.

5.3 Scientific findings

In chapter 3, the applicability of the luminescence-based read-out to detect OGD-induced neurotoxicity within neurospheroids was demonstrated. Using this approach, distinct dynamics of 1-week-old and 4-week-old neurospheroids after OGD were observed. By comparing 1-week-old with 4-week-old neurospheroids, containing relatively more undifferentiated NSCs or intermediate progenitors/immature neurons, respectively, it was demonstrated that 1-week-old neurospheroids were able to completely and spontaneously recover from the initial OGD-induced damage over the course of one week, unlike 4-week-old neurospheroids. This is in line with other studies, also using human brain organoids, where NSCs have demonstrated to be relative resilient to hypoxic injury, as compared to other neuroprogenitor cell subtypes, and even maintain their proliferation potential [189, 190]. Moreover, one of these studies observed the induction of a compensatory mechanism in these NSCs to replenish the stem cell pool after hypoxia [190]. Considering that the adult human brain mainly consists of mature neurons and glial cells and displays limited spontaneous recovery after ischemic stroke, underscores the need for older, more mature neurospheroids for *in vitro* stroke research. Besides, this would at the same time facilitate the evaluation of neuroprotective compounds, where any recovery or stabilization of deterioration could be solely attributed to the neuroprotective compound, enabling to draw firm conclusions.

A second important scientific finding obtained in this thesis was the different behavioral response of NSCs cultured in 2D versus NSC-derived neurospheroids towards treatment with the pan-caspase inhibitor Z-VAD-FMK during and after OGD (see Chapter 3). In 2D, Z-VAD-FMK conferred neuroprotection, in agreement with other publications [33-35]. Though significant, the effect of Z-VAD-FMK was rather limited. It is plausible that besides apoptosis other cell death mechanisms are underlying OGD-

induced neurotoxicity [7]. Whether changes in concentration and/or administration time may influence the magnitude of neuroprotection by Z-VAD-FMK, remains to be further investigated. Nevertheless, concentrations as low as 20 µM Z-VAD-FMK administered during and after OGD have previously demonstrated to be neuroprotective in mouse neuronal cultures [290]. In contrast to 2D, Z-VAD-FMK failed to improve the overall viability of neurospheroids under OGD. This exemplifies how increased complexity of spheroid or organoid models, in terms of cellular heterogeneity and/or dimensionality, may result in a different outcome when evaluating neuroprotective compounds. The concept that dimensionality can affect the cell's behavior is in line with other studies demonstrating that cells cultured in a 3D environment can show changes in morphology, survival, proliferation, differentiation, gene expression and even function (e.g. electrophysiological network properties) when compared to cells cultured in 2D on plastic surfaces [74, 157]. Likewise, differences in response to pathological stimuli and/or therapeutic compounds have been observed in different fields of research. For instance, in hepatoxicity research, 3D hepatocyte cultures have been shown to be less susceptible to cell death when exposed to cytotoxins in comparison with 2D cultures [195]. Similar findings are emerging in the field of *in vitro* stroke research. For instance, Vagaska et al. demonstrated the lower susceptibility to OGD-mediated damage for human NSCs grown in 3D, when compared to their 2D counterpart. The same could be concluded when thapsigargin was used as stimulus, after eliminating the possibility of reduced drug accessibility as a confounding factor [74]. Additionally, Ko et al. confirmed that 3D cell culture models represent better normal brain models, since the neural cells in 3D maintained their healthy physiological morphology of a less activated state and suppressed mRNA expressions of pathological stroke markers S100B, IL1-β and MBP [193]. Nevertheless, it remains to be investigated how the increased complexity of the neurospheroid model in this thesis affected the difference in response, for instance by changing susceptibility to neurotoxic stimuli or elicited types of cell death. To this end, it may be of relevance to extend the experiments in this thesis with inhibitors of specific cell death mechanisms, such as autophagy or ferroptosis. Additionally, to confirm whether these cell death mechanisms are due to the OGD stimulus, a double staining could be performed for the hypoxic marker EF5 and a specific marker for cell death, for instance cleaved caspase-3 or 4-hydroxynonenal (4-HNE) to identify apoptosis or ferroptosis, respectively. Altogether, these findings further underscore the importance of 3D models in basic as well as applied *in vitro* stroke research to complement conventional 2D cell cultures and *in vivo* animal studies.

5.4 Opportunities for model improvement

While the here described neurospheroid model already increased the complexity and physiological relevance by providing a 3D microenvironment for the neural cells, the presence of glial cells, such as astrocytes and microglia, and increased maturation would enable the model to mimic human ischemic responses with greater accuracy. Moreover, it would allow candidate neuroprotective agents targeting the inflammatory and excitotoxic component of ischemic stroke to be evaluated. Here, the foundation was laid for the development of more mature, multicellular neurospheroids (see Chapter 4). Obtained results demonstrate that longer term culture of neurospheroids in cNEM can give rise to more mature, astrocyte-containing neurospheroids. However, whether the neurons are functionally mature remains to be determined by means of electrophysiological measurements, for example through the use of multi-electrode arrays (MEAs). Likewise, the astrocytes still would need to be functionally characterized for its ability to produce cytokines and glutamate uptake. Furthermore, it was demonstrated in Chapter 4 that hematopoietic progenitor cells are able to successfully integrate into neurospheroids grown in cNEM and suggest a role of CSF-1 herein. However, further optimization of the protocol is needed to develop microglia-enriched neurospheroids, where microglia will be phenotypically and functionally characterized.

Although the feasibility of developing more mature, multicellular neurospheroids is provided here, the protocol for development of this model still requires optimization and validation. The use of cNEM supports the growth of the neurospheroids to significant extent. This might not only imply that the eventual microglia number and distribution may be suboptimal, but also that the necrotic, ischemic core can take significant proportions. The latter is of particular importance when these immune cells are added, as it may potentially cause their activation prior to their subjection to OGD. Therefore, a combination of cNEM with one of the evaluated differentiation media may be considered, that would allow the development of astrocytes, while suppressing the proliferation by inducing neuronal differentiation and maturation. Together with the use of bioreactor systems, the multicellular model may be improved on short-term.

On the long-term, vascularization of the neurospheroids would be an ideal approach, not only to prevent the necrotic core, but also to incorporate a blood-brain barrier (BBB) in this model. By this means the BBB dysfunction associated with ischemic stroke pathophysiology can be modelled, as well as the contribution of brain endothelial cells and neurovascular interactions in the exacerbation of ischemic damage can be investigated. For instance, brain endothelial cells have been indicated to be a potential

source of detrimental free radicals after reperfusion [132]. Efforts to vascularize brain organoids have been undertaken. Multiple studies report on the development of tube-like vascular structures after co-culturing human brain organoids with vascular cells, such as iPSC-derived endothelial cells, HUVECs, or embryonic stem cells in which the ETV2 gene - known to directly convert fibroblasts to endothelial cells – was engineered to be expressed in the presence of doxycycline [180, 181, 291]. Despite the absence of perfusion of the vessel-like structures, the vascularized brain organoids showed improved growth, attenuated apoptosis and accelerated neuronal maturation in comparison to non-vascularized brain organoids [180, 181, 291]. Moreover, the endothelial cells in these organoids developed BBB-characteristics, as evidenced by their expression of BBB related markers, including P-glycoprotein, ZO-1 and occludin [180, 181]. One of the aforementioned studies even suggests the improvement of the hypoxic state in the human brain organoids upon this non-functional vascularization by the detected decrease in HIF-1 positive cells [181]. However, to take full advantage of vascularized brain organoids, the vessel like-structures need to be perfused, allowing the delivery of oxygen and nutrients to all cells of the brain organoid. To achieve this, several groups have transplanted these pre-vascularized brain organoids into highly vascular tissues in immunodeficient mice often resulting in successful functional perfusion with blood of the host (i.e. mouse) [180, 181, 291]. Although interesting, the required transplantation negates the benefits of (i) the *in vitro* identity of brain organoids and spheroids and thereby the controllability and potential scalability, and (ii) the pure human origin of those models, as the capillaries in the transplanted organoid are constituted of both mouse-derived endothelial cells and the human endothelial cells (e.g. HUVECs) and have murine blood flowing through them.

A better approach to establish the neurospheroids with a functional vasculature in the future would rely on microfluidics technology. Microfluidic devices have been used before to perfuse lung fibroblast spheroids through HUVEC-derived vessels (Fig. 1) [292]. Hereto, spheroids containing HUVECs were cultivated in a central nonfluid channel filled with fibrin-collagen gel mimicking the extracellular matrix. HUVECs were also seeded in the channels adjacent and parallel to the central channel. Angiogenic sprouts were formed from HUVECs in the microchannels and reached the vessel-like structures in the spheroid to form a continuous lumen, enabling perfusion. Although this approach has not been applied yet to human brain organoids [292], this would be an appropriate strategy to allow *in vitro* perfusion of the here established luminescent neurospheroid model in the future. Besides the delivery of oxygen and nutrients to the interior of the neurospheroid, the increased maturation and the formation of a BBB,

this system would also allow to control the perfusion flow, enabling the interrupted blood flow and possible reperfusion associated with ischemic stroke to be recapitulated, allowing to mimic *in vivo* stroke even more closely. To take this even further, this model would open up new possibilities to study the infiltration of leukocytes and to investigate their dual role in the progression of ischemia-induced damage [3, 40].

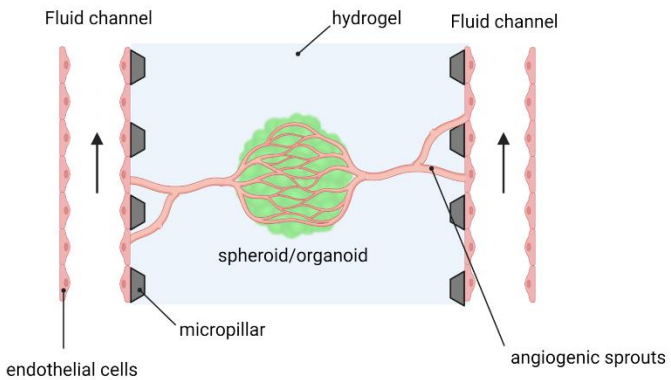

Figure 1 – Schematic overview to obtain vascularized, perfused spheroids/organoids using a microfluidic device. The spheroid/organoid containing endothelial cells is cultivated in a central channel filled with hydrogel. Adjacent to the central channel are two channels containing endothelial monolayers exposed to fluid flow. Endothelial cells generate angiogenic sprouts, induced by secreted VEGF from the spheroid/organoid, that eventually bridge the fluid channel and the spheroid/organoid enabling the establishment of a functional vascular network, perfusing the spheroid/organoid. The arrows indicate fluid flow.

5.5 Implications of human multicellular neurospheroids in ischemic stroke research

The human neurospheroid model described here has the potential to complement 2D *in vitro* models and animal models, each having their own advantages and limitations, to gain more insight into the pathophysiology of ischemic stroke and even other neurological pathologies. Once optimized and after thorough phenotypic and functional validation, RNA-sequencing of the more mature, multicellular human neurospheroids – where cells are allowed to interact with other cells and cell types in a 3D manner (i.e. multicellularity and dimensionality) - will enable to uncover the main pathways up- or downregulated when subjected to OGD and reoxygenation. While RNA-sequencing of human cerebral organoids after OGD and subsequent

reoxygenation has already been reported, the rather young organoids used in this study lack microglia and probably also astrocytes, resulting in a rather restricted image of all transcriptional changes that occur in ischemic stroke [192]. Additionally, the optimized human neurospheroid model would allow to allocate the specific contribution of microglia in the secondary damage after stroke, by comparing the luminescent signal of neurospheroids with and without incorporated microglia.

Furthermore, in general, the extension of the *in vitro* armamentarium for ischemic stroke research with 3D models will also entail the implementation and development of a new set of technologies tailored for 3D models. For example, application of tissue clearance and subsequent 3D imaging will become more important as it would allow to image the complete spheroid or organoid [289, 293], and thereby capture the complete distribution of particular cell types and/or specific markers across the spheroid or organoid. Furthermore, emerging 3D MEAs and 3D flexible bioelectronics, will enable the measurement of the activity of neurons located across the brain spheroids or organoids as compared to 2D MEAs, where the electrophysiological measurement is limited to the neurons at the bottom of the brain organoids [294]. With regard to multicellular spheroids or organoids, measurement of the cytokine response of individual spheroids may possibly require more sensitive detection methods than conventional ELISA, given the rather low number of glial cells present in a single spheroid. Development of such technologies would allow to take full advantage of 3D models.

Ultimately, besides their future role in unraveling the pathophysiological mechanisms, the introduction of the human multicellular neurospheroid model in the preclinical phase of drug discovery and development, would allow to bridge the translational gap between preclinical studies and clinical trials, increasing chances of success for the agents to be effective in clinical setting. Nevertheless, as human PSC-derived 3D models in general are a rather recent development, it remains to be demonstrated whether these models are actually better at predicting human ischemic responses and clinical outcomes when evaluating new agents prior to their integration in the preclinical *in vitro* armamentarium. Therefore, a side-to-side evaluation of rodent neurospheroid models with their *in vivo* counterpart and a validation by means of ischemic stroke patient-derived blood and cerebral spinal fluid samples, may provide more insight on their translational value. In this regard, it may also be of interest to re-evaluate certain neuroprotective compounds in these models that have been tested before in clinical setting. The latter would also allow to investigate whether species-specific differences

are at the root of certain clinical failures. Nonetheless, still with much fundamental research ahead, all evidence points toward a clear future for advanced human PSC-derived multicellular 3D models, such as the here developed neurospheroid model, in fundamental and translational ischemic stroke research.

References

1. World Stroke Organization. Global Stroke Fact Sheet 2022.
2. Dirnagl U, Iadecola C, Moskowitz MA. Pathobiology of ischaemic stroke: an integrated view. Trends in neurosciences. 1999;22(9):391-7.
3. Amantea D, Greco R, Micieli G, Bagetta G. Paradigm Shift to Neuroimmunomodulation for Translational Neuroprotection in Stroke. Front Neurosci. 2018;12:241.
4. Woodruff TM, Thundyil J, Tang SC, Sobey CG, Taylor SM, Arumugam TV. Pathophysiology, treatment, and animal and cellular models of human ischemic stroke. Molecular neurodegeneration. 2011;6(1):11.
5. Brouns R, De Deyn PP. The complexity of neurobiological processes in acute ischemic stroke. Clin Neurol Neurosurg. 2009;111(6):483-95.
6. Jayaraj RL, Azimullah S, Beiram R, Jalal FY, Rosenberg GA. Neuroinflammation: friend and foe for ischemic stroke. Journal of neuroinflammation. 2019;16(1):142.
7. Tuo QZ, Zhang ST, Lei P. Mechanisms of neuronal cell death in ischemic stroke and their therapeutic implications. Med Res Rev. 2022;42(1):259-305.
8. Venkat P, Shen Y, Chopp M, Chen J. Cell-based and pharmacological neurorestorative therapies for ischemic stroke. Neuropharmacology. 2018;134(Pt B):310-22.
9. Paul S, Candelario-Jalil E. Emerging neuroprotective strategies for the treatment of ischemic stroke: An overview of clinical and preclinical studies. Experimental neurology. 2021;335:113518.
10. Kuriakose D, Xiao Z. Pathophysiology and Treatment of Stroke: Present Status and Future Perspectives. Int J Mol Sci. 2020;21(20).
11. Patel RAG, McMullen PW. Neuroprotection in the Treatment of Acute Ischemic Stroke. Prog Cardiovasc Dis. 2017;59(6):542-8.
12. Cheng YD, Al-Khoury L, Zivin JA. Neuroprotection for ischemic stroke: two decades of success and failure. NeuroRx. 2004;1(1):36-45.
13. Danton GH, Dietrich WD. The search for neuroprotective strategies in stroke. AJNR Am J Neuroradiol. 2004;25(2):181-94.
14. Hoyte L, Barber PA, Buchan AM, Hill MD. The rise and fall of NMDA antagonists for ischemic stroke. Curr Mol Med. 2004;4(2):131-6.
15. Albers GW, Goldstein LB, Hall D, Lesko LM, Aptiganel Acute Stroke I. Aptiganel hydrochloride in acute ischemic stroke: a randomized controlled trial. JAMA. 2001;286(21):2673-82.
16. Davis SM, Albers GW, Diener HC, Lees KR, Norris J. Termination of Acute Stroke Studies Involving Selfotel Treatment. ASSIST Steering Committed. Lancet. 1997;349(9044):32.

17. Elting JW, Sulter GA, Kaste M*, et al.* AMPA antagonist ZK200775 in patients with acute ischemic stroke: possible glial cell toxicity detected by monitoring of S-100B serum levels. Stroke. 2002;33(12):2813-8.
18. Walters MR, Kaste M, Lees KR*, et al.* The AMPA antagonist ZK 200775 in patients with acute ischaemic stroke: a double-blind, multicentre, placebo-controlled safety and tolerability study. Cerebrovasc Dis. 2005;20(5):304-9.
19. Turski L, Huth A, Sheardown M*, et al.* ZK200775: a phosphonate quinoxalinedione AMPA antagonist for neuroprotection in stroke and trauma. Proceedings of the National Academy of Sciences of the United States of America. 1998;95(18):10960-5.
20. Bielenberg GW, Beck T. The Effects of Dizocilpine (Mk-801), Phencyclidine, and Nimodipine on Infarct Size 48 H after Middle Cerebral-Artery Occlusion in the Rat. Brain Research. 1991;552(2):338-42.
21. Gelmers HJ, Gorter K, de Weerdt CJ, Wiezer HJ. A controlled trial of nimodipine in acute ischemic stroke. N Engl J Med. 1988;318(4):203-7.
22. Sze KH, Sim TC, Wong E, Cheng S, Woo J. Effect of nimodipine on memory after cerebral infarction. Acta Neurol Scand. 1998;97(6):386-92.
23. Gelmers HJ. The effects of nimodipine on the clinical course of patients with acute ischemic stroke. Acta Neurol Scand. 1984;69(4):232-9.
24. Martinez-Vila E, Guillen F, Villanueva JA*, et al.* Placebo-controlled trial of nimodipine in the treatment of acute ischemic cerebral infarction. Stroke. 1990;21(7):1023-8.
25. Franke CL, Palm R, Dalby M*, et al.* Flunarizine in stroke treatment (FIST): a double-blind, placebo-controlled trial in Scandinavia and the Netherlands. Acta Neurol Scand. 1996;93(1):56-60.
26. Sydserff SG, Borelli AR, Green AR, Cross AJ. Effect of NXY-059 on infarct volume after transient or permanent middle cerebral artery occlusion in the rat; studies on dose, plasma concentration and therapeutic time window. Br J Pharmacol. 2002;135(1):103-12.
27. Kuroda S, Tsuchidate R, Smith ML, Maples KR, Siesjo BK. Neuroprotective effects of a novel nitrone, NXY-059, after transient focal cerebral ischemia in the rat. J Cereb Blood Flow Metab. 1999;19(7):778-87.
28. Marshall JW, Duffin KJ, Green AR, Ridley RM. NXY-059, a free radical--trapping agent, substantially lessens the functional disability resulting from cerebral ischemia in a primate species. Stroke. 2001;32(1):190-8.
29. Marshall JW, Cummings RM, Bowes LJ, Ridley RM, Green AR. Functional and histological evidence for the protective effect of NXY-059 in a primate model of stroke when given 4 hours after occlusion. Stroke. 2003;34(9):2228-33.
30. Lees KR, Zivin JA, Ashwood T*, et al.* NXY-059 for acute ischemic stroke. N Engl J Med. 2006;354(6):588-600.
31. Shuaib A, Lees KR, Lyden P*, et al.* NXY-059 for the treatment of acute ischemic stroke. N Engl J Med. 2007;357(6):562-71.

32. Antonic A, Dottori M, Macleod MR, Donnan GA, Howells DW. NXY-059, a Failed Stroke Neuroprotectant, Offers No Protection to Stem Cell-Derived Human Neurons. J Stroke Cerebrovasc Dis. 2018;27(8):2158-65.
33. Le DA, Wu Y, Huang Z*, et al.* Caspase activation and neuroprotection in caspase-3- deficient mice after in vivo cerebral ischemia and in vitro oxygen glucose deprivation. Proceedings of the National Academy of Sciences of the United States of America. 2002;99(23):15188-93.
34. Wiessner C, Sauer D, Alaimo D, Allegrini PR. Protective effect of a caspase inhibitor in models for cerebral ischemia in vitro and in vivo. Cell Mol Biol (Noisy-le-grand). 2000;46(1):53-62.
35. Endres M, Namura S, Shimizu-Sasamata M*, et al.* Attenuation of delayed neuronal death after mild focal ischemia in mice by inhibition of the caspase family. J Cereb Blood Flow Metab. 1998;18(3):238-47.
36. Zhang RL, Chopp M, Li Y*, et al.* Anti-ICAM-1 antibody reduces ischemic cell damage after transient middle cerebral artery occlusion in the rat. Neurology. 1994;44(9):1747-51.
37. Zhang RL, Chopp M, Jiang N*, et al.* Anti-intercellular adhesion molecule-1 antibody reduces ischemic cell damage after transient but not permanent middle cerebral artery occlusion in the Wistar rat. Stroke. 1995;26(8):1438-42; discussion 43.
38. Enlimomab Acute Stroke Trial I. Use of anti-ICAM-1 therapy in ischemic stroke: results of the Enlimomab Acute Stroke Trial. Neurology. 2001;57(8):1428-34.
39. Furuya K, Takeda H, Azhar S*, et al.* Examination of several potential mechanisms for the negative outcome in a clinical stroke trial of enlimomab, a murine anti-human intercellular adhesion molecule-1 antibody: a bedside-to-bench study. Stroke. 2001;32(11):2665-74.
40. Kanazawa M, Ninomiya I, Hatakeyama M, Takahashi T, Shimohata T. Microglia and Monocytes/Macrophages Polarization Reveal Novel Therapeutic Mechanism against Stroke. Int J Mol Sci. 2017;18(10).
41. Garcia-Bonilla L, Campos M, Giralt D*, et al.* Evidence for the efficacy of statins in animal stroke models: a meta-analysis. Journal of neurochemistry. 2012;122(2):233-43.
42. Ni Chroinin D, Callaly EL, Duggan J*, et al.* Association between acute statin therapy, survival, and improved functional outcome after ischemic stroke: the North Dublin Population Stroke Study. Stroke. 2011;42(4):1021-9.
43. Yoshimura S, Uchida K, Daimon T*, et al.* Randomized Controlled Trial of Early Versus Delayed Statin Therapy in Patients With Acute Ischemic Stroke: ASSORT Trial (Administration of Statin on Acute Ischemic Stroke Patient). Stroke. 2017;48(11):3057-63.
44. Flint AC, Kamel H, Navi BB*, et al.* Statin use during ischemic stroke hospitalization is strongly associated with improved poststroke survival. Stroke. 2012;43(1):147-54.

45. Hypothermia after Cardiac Arrest Study G. Mild therapeutic hypothermia to improve the neurologic outcome after cardiac arrest. N Engl J Med. 2002;346(8):549-56.
46. van der Worp HB, Sena ES, Donnan GA, Howells DW, Macleod MR. Hypothermia in animal models of acute ischaemic stroke: a systematic review and meta-analysis. Brain. 2007;130(Pt 12):3063-74.
47. Kuczynski AM, Marzoughi S, Al Sultan AS*, et al.* Therapeutic Hypothermia in Acute Ischemic Stroke-a Systematic Review and Meta-Analysis. Curr Neurol Neurosci Rep. 2020;20(5):13.
48. Sun YJ, Zhang ZY, Fan B, Li GY. Neuroprotection by Therapeutic Hypothermia. Front Neurosci. 2019;13:586.
49. Benjamin EJ, Blaha MJ, Chiuve SE*, et al.* Heart Disease and Stroke Statistics-2017 Update: A Report From the American Heart Association. Circulation. 2017;135(10):e146-e603.
50. Moskowitz MA, Lo EH, Iadecola C. The science of stroke: mechanisms in search of treatments. Neuron. 2010;67(2):181-98.
51. Writing Group M, Mozaffarian D, Benjamin EJ*, et al.* Executive Summary: Heart Disease and Stroke Statistics--2016 Update: A Report From the American Heart Association. Circulation. 2016;133(4):447-54.
52. Holloway PM, Gavins FN. Modeling Ischemic Stroke In Vitro: Status Quo and Future Perspectives. Stroke. 2016;47(2):561-9.
53. Antonic A, Sena ES, Donnan GA, Howells DW. Human in vitro models of ischaemic stroke: a test bed for translation. Transl Stroke Res. 2012;3(3):306-9.
54. Fluri F, Schuhmann MK, Kleinschnitz C. Animal models of ischemic stroke and their application in clinical research. Drug Des Devel Ther. 2015;9:3445-54.
55. Sommer CJ. Ischemic stroke: experimental models and reality. Acta Neuropathol. 2017;133(2):245-61.
56. Hu X, Li P, Guo Y*, et al.* Microglia/macrophage polarization dynamics reveal novel mechanism of injury expansion after focal cerebral ischemia. Stroke. 2012;43(11):3063-70.
57. Datta A, Park JE, Li X*, et al.* Phenotyping of an in vitro model of ischemic penumbra by iTRAQ-based shotgun quantitative proteomics. J Proteome Res. 2010;9(1):472-84.
58. Tasca CI, Dal-Cim T, Cimarosti H. In vitro oxygen-glucose deprivation to study ischemic cell death. Methods in molecular biology. 2015;1254:197-210.
59. Goldberg MP, Choi DW. Combined oxygen and glucose deprivation in cortical cell culture: calcium-dependent and calcium-independent mechanisms of neuronal injury. The Journal of neuroscience : the official journal of the Society for Neuroscience. 1993;13(8):3510-24.
60. Ryou MG, Mallet RT. An In Vitro Oxygen-Glucose Deprivation Model for Studying Ischemia-Reperfusion Injury of Neuronal Cells. Methods in molecular biology. 2018;1717:229-35.

61. Kaneko Y, Pappas C, Tajiri N, Borlongan CV. Oxytocin modulates GABAAR subunits to confer neuroprotection in stroke in vitro. Scientific reports. 2016;6:35659.
62. Wang JH, Wan D, Wan GR, Wang JH, Zhang JH, Zhu HF. Catalpol induces cell activity to promote axonal regeneration via the PI3K/AKT/mTOR pathway in vivo and in vitro stroke model. Ann Transl Med. 2019;7(23).
63. Sun MS, Jin H, Sun X*, et al.* Free Radical Damage in Ischemia-Reperfusion Injury: An Obstacle in Acute Ischemic Stroke after Revascularization Therapy. Oxid Med Cell Longev. 2018;2018:3804979.
64. Arumugam TV, Chan SL, Jo DG*, et al.* Gamma secretase-mediated Notch signaling worsens brain damage and functional outcome in ischemic stroke. Nature medicine. 2006;12(6):621-3.
65. Kim MJ, Hur J, Ham IH*, et al.* Expression and activity of the na-k ATPase in ischemic injury of primary cultured astrocytes. Korean J Physiol Pharmacol. 2013;17(4):275-81.
66. Wevers NR, Nair AL, Fowke TM*, et al.* Modeling ischemic stroke in a triculture neurovascular unit on-a-chip. Fluids Barriers CNS. 2021;18(1):59.
67. Park HS, Han KH, Shin JA, Park JH, Song KY, Kim DH. The neuroprotective effects of carnosine in early stage of focal ischemia rodent model. J Korean Neurosurg Soc. 2014;55(3):125-30.
68. Zitta K, Peeters-Scholte C, Sommer L, Parczany K, Steinfath M, Albrecht M. Insights into the neuroprotective mechanisms of 2-iminobiotin employing an in-vitro model of hypoxic-ischemic cell injury. Eur J Pharmacol. 2016;792:63-9.
69. Zitta K, Meybohm P, Bein B*, et al.* Hypoxia-induced cell damage is reduced by mild hypothermia and postconditioning with catalase in-vitro: application of an enzyme based oxygen deficiency system. Eur J Pharmacol. 2010;628(1-3):11-8.
70. Mueller S, Millonig G, Waite GN. The GOX/CAT system: a novel enzymatic method to independently control hydrogen peroxide and hypoxia in cell culture. Adv Med Sci. 2009;54(2):121-35.
71. Andjelkovic AV, Stamatovic SM, Phillips CM, Martinez-Revollar G, Keep RF. Modeling blood-brain barrier pathology in cerebrovascular disease in vitro: current and future paradigms. Fluids Barriers CNS. 2020;17(1):44.
72. Lyu Z, Park J, Kim KM*, et al.* A neurovascular-unit-on-a-chip for the evaluation of the restorative potential of stem cell therapies for ischaemic stroke. Nat Biomed Eng. 2021;5(8):847-63.
73. von Engelhardt J, Coserea I, Pawlak V*, et al.* Excitotoxicity in vitro by NR2A- and NR2B-containing NMDA receptors. Neuropharmacology. 2007;53(1):10-7.
74. Vagaska B, Gillham O, Ferretti P. Modelling human CNS injury with human neural stem cells in 2- and 3-Dimensional cultures. Scientific reports. 2020;10(1):6785.
75. Akaneya Y, Enokido Y, Takahashi M, Hatanaka H. In vitro model of hypoxia: basic fibroblast growth factor can rescue cultured CNS neurons from oxygen-deprived cell death. J Cereb Blood Flow Metab. 1993;13(6):1029-32.

76. Xu SY, Hu YF, Li WP*, et al.* Intermittent hypothermia is neuroprotective in an in vitro model of ischemic stroke. Int J Biol Sci. 2014;10(8):873-81.
77. Luo HC, Yi TZ, Huang FG, Wei Y, Luo XP, Luo QS. Role of long noncoding RNA MEG3/miR-378/GRB2 axis in neuronal autophagy and neurological functional impairment in ischemic stroke. J Biol Chem. 2020;295(41):14125-39.
78. le Feber J, Tzafi Pavlidou S, Erkamp N, van Putten MJ, Hofmeijer J. Progression of Neuronal Damage in an In Vitro Model of the Ischemic Penumbra. PloS one. 2016;11(2):e0147231.
79. Humpel C. Organotypic brain slice cultures: A review. Neuroscience. 2015;305:86-98.
80. Jorfi M, D'Avanzo C, Kim DY, Irimia D. Three-Dimensional Models of the Human Brain Development and Diseases. Adv Healthc Mater. 2018;7(1).
81. Li Q, Han X, Wang J. Organotypic Hippocampal Slices as Models for Stroke and Traumatic Brain Injury. Mol Neurobiol. 2016;53(6):4226-37.
82. Bonde C, Noraberg J, Noer H, Zimmer J. Ionotropic glutamate receptors and glutamate transporters are involved in necrotic neuronal cell death induced by oxygen-glucose deprivation of hippocampal slice cultures. Neuroscience. 2005;136(3):779-94.
83. Laake JH, Haug FM, Wieloch T, Ottersen OP. A simple in vitro model of ischemia based on hippocampal slice cultures and propidium iodide fluorescence. Brain Res Brain Res Protoc. 1999;4(2):173-84.
84. Noraberg J, Poulsen FR, Blaabjerg M*, et al.* Organotypic hippocampal slice cultures for studies of brain damage, neuroprotection and neurorepair. Curr Drug Targets CNS Neurol Disord. 2005;4(4):435-52.
85. Richard MJ, Saleh TM, El Bahh B, Zidichouski JA. A novel method for inducing focal ischemia in vitro. Journal of neuroscience methods. 2010;190(1):20-7.
86. Gertz CC, Lui JH, LaMonica BE, Wang X, Kriegstein AR. Diverse behaviors of outer radial glia in developing ferret and human cortex. The Journal of neuroscience : the official journal of the Society for Neuroscience. 2014;34(7):2559-70.
87. Kawaguchi A. Neuronal Delamination and Outer Radial Glia Generation in Neocortical Development. Front Cell Dev Biol. 2020;8:623573.
88. Syvanen S, Lindhe O, Palner M*, et al.* Species differences in blood-brain barrier transport of three positron emission tomography radioligands with emphasis on P-glycoprotein transport. Drug Metab Dispos. 2009;37(3):635-43.
89. Warren MS, Zerangue N, Woodford K*, et al.* Comparative gene expression profiles of ABC transporters in brain microvessel endothelial cells and brain in five species including human. Pharmacol Res. 2009;59(6):404-13.
90. Williams SM, Sullivan RK, Scott HL*, et al.* Glial glutamate transporter expression patterns in brains from multiple mammalian species. Glia. 2005;49(4):520-41.
91. Davalos A, Castillo J, Serena J, Noya M. Duration of glutamate release after acute ischemic stroke. Stroke. 1997;28(4):708-10.

92. Seok J, Warren HS, Cuenca AG*, et al.* Genomic responses in mouse models poorly mimic human inflammatory diseases. Proceedings of the National Academy of Sciences of the United States of America. 2013;110(9):3507-12.
93. Smith AM, Dragunow M. The human side of microglia. Trends in neurosciences. 2014;37(3):125-35.
94. Sharp FR, Jickling GC. Modeling immunity and inflammation in stroke: differences between rodents and humans? Stroke. 2014;45(9):e179-80.
95. Du Y, Deng W, Wang Z*, et al.* Differential subnetwork of chemokines/cytokines in human, mouse, and rat brain cells after oxygen-glucose deprivation. J Cereb Blood Flow Metab. 2017;37(4):1425-34.
96. Chang R, Algird A, Bau C, Rathbone MP, Jiang S. Neuroprotective effects of guanosine on stroke models in vitro and in vivo. Neuroscience letters. 2008;431(2):101-5.
97. Lorenz L, Dang J, Misiak M, Tameh Abolfazl A, Beyer C, Kipp M. Combined 17beta-oestradiol and progesterone treatment prevents neuronal cell injury in cortical but not midbrain neurones or neuroblastoma cells. J Neuroendocrinol. 2009;21(10):841-9.
98. Liu Y, Eaton ED, Wills TE, McCann SK, Antonic A, Howells DW. Human Ischaemic Cascade Studies Using SH-SY5Y Cells: a Systematic Review and Meta-Analysis. Transl Stroke Res. 2018;9(6):564-74.
99. Marcoli M, Bonfanti A, Roccatagliata P*, et al.* Glutamate efflux from human cerebrocortical slices during ischemia: vesicular-like mode of glutamate release and sensitivity to A(2A) adenosine receptor blockade. Neuropharmacology. 2004;47(6):884-91.
100. Marcoli M, Cervetto C, Castagnetta M, Sbaffi P, Maura G. 5-HT control of ischemia-evoked glutamate efflux from human cerebrocortical slices. Neurochem Int. 2004;45(5):687-91.
101. Werth JL, Park TS, Silbergeld DL, Rothman SM. Excitotoxic swelling occurs in oxygen and glucose deprived human cortical slices. Brain Res. 1998;782(1-2):248-54.
102. Mitsios N, Gaffney J, Krupinski J*, et al.* Expression of signaling molecules associated with apoptosis in human ischemic stroke tissue. Cell Biochem Biophys. 2007;47(1):73-86.
103. Mitsios N, Saka M, Krupinski J*, et al.* A microarray study of gene and protein regulation in human and rat brain following middle cerebral artery occlusion. BMC Neurosci. 2007;8:93.
104. Mitsios N, Pennucci R, Krupinski J*, et al.* Expression of cyclin-dependent kinase 5 mRNA and protein in the human brain following acute ischemic stroke. Brain Pathol. 2007;17(1):11-23.
105. Liu Y. Human in vitro Models of Ischaemic Stroke: New Strategies for Neuroprotection. Australia: University of Melbourn; 2018.
106. Takahashi K, Tanabe K, Ohnuki M*, et al.* Induction of pluripotent stem cells from adult human fibroblasts by defined factors. Cell. 2007;131(5):861-72.

107. Staerk J, Dawlaty MM, Gao Q*, et al.* Reprogramming of human peripheral blood cells to induced pluripotent stem cells. Cell Stem Cell. 2010;7(1):20-4.
108. Lippmann ES, Azarin SM, Kay JE*, et al.* Derivation of blood-brain barrier endothelial cells from human pluripotent stem cells. Nature biotechnology. 2012;30(8):783-91.
109. Tcw J, Wang M, Pimenova AA*, et al.* An Efficient Platform for Astrocyte Differentiation from Human Induced Pluripotent Stem Cells. Stem cell reports. 2017;9(2):600-14.
110. Gunhanlar N, Shpak G, van der Kroeg M*, et al.* A simplified protocol for differentiation of electrophysiologically mature neuronal networks from human induced pluripotent stem cells. Mol Psychiatry. 2018;23(5):1336-44.
111. Gonzalez R, Garitaonandia I, Abramihina T*, et al.* Deriving dopaminergic neurons for clinical use. A practical approach. Scientific reports. 2013;3:1463.
112. Abud EM, Ramirez RN, Martinez ES*, et al.* iPSC-Derived Human Microglia-like Cells to Study Neurological Diseases. Neuron. 2017;94(2):278-93 e9.
113. Haenseler W, Sansom SN, Buchrieser J*, et al.* A Highly Efficient Human Pluripotent Stem Cell Microglia Model Displays a Neuronal-Co-culture-Specific Expression Profile and Inflammatory Response. Stem cell reports. 2017;8(6):1727-42.
114. McQuade A, Coburn M, Tu CH, Hasselmann J, Davtyan H, Blurton-Jones M. Development and validation of a simplified method to generate human microglia from pluripotent stem cells. Molecular neurodegeneration. 2018;13(1):67.
115. Konttinen H, Cabral-da-Silva MEC, Ohtonen S*, et al.* PSEN1DeltaE9, APPswe, and APOE4 Confer Disparate Phenotypes in Human iPSC-Derived Microglia. Stem cell reports. 2019;13(4):669-83.
116. Muffat J, Li Y, Yuan B*, et al.* Efficient derivation of microglia-like cells from human pluripotent stem cells. Nature medicine. 2016;22(11):1358-67.
117. Krencik R, Zhang SC. Directed differentiation of functional astroglial subtypes from human pluripotent stem cells. Nature protocols. 2011;6(11):1710-7.
118. Shaltouki A, Peng J, Liu Q, Rao MS, Zeng X. Efficient generation of astrocytes from human pluripotent stem cells in defined conditions. Stem Cells. 2013;31(5):941-52.
119. Shi Y, Kirwan P, Livesey FJ. Directed differentiation of human pluripotent stem cells to cerebral cortex neurons and neural networks. Nature protocols. 2012;7(10):1836-46.
120. Yan Y, Shin S, Jha BS*, et al.* Efficient and rapid derivation of primitive neural stem cells and generation of brain subtype neurons from human pluripotent stem cells. Stem cells translational medicine. 2013;2(11):862-70.
121. Ehrlich M, Mozafari S, Glatza M*, et al.* Rapid and efficient generation of oligodendrocytes from human induced pluripotent stem cells using transcription factors. Proceedings of the National Academy of Sciences of the United States of America. 2017;114(11):E2243-E52.

122. Juntunen M, Hagman S, Moisan A, Narkilahti S, Miettinen S. In Vitro Oxygen-Glucose Deprivation-Induced Stroke Models with Human Neuroblastoma Cell- and Induced Pluripotent Stem Cell-Derived Neurons. Stem Cells Int. 2020;2020:8841026.
123. Patel R, Page S, Al-Ahmad AJ. Isogenic blood-brain barrier models based on patient-derived stem cells display inter-individual differences in cell maturation and functionality. Journal of neurochemistry. 2017;142(1):74-88.
124. DeStefano JG, Xu ZS, Williams AJ, Yimam N, Searson PC. Effect of shear stress on iPSC-derived human brain microvascular endothelial cells (dhBMECs). Fluids Barriers CNS. 2017;14(1):20.
125. Linville RM, DeStefano JG, Sklar MB*, et al.* Human iPSC-derived blood-brain barrier microvessels: validation of barrier function and endothelial cell behavior. Biomaterials. 2019;190-191:24-37.
126. Nikolakopoulou P, Rauti R, Voulgaris D, Shlomy I, Maoz BM, Herland A. Recent progress in translational engineered in vitro models of the central nervous system. Brain. 2020;143(11):3181-213.
127. Mukda S, Tsai CY, Leu S, Yang JL, Chan SHH. Pinin protects astrocytes from cell death after acute ischemic stroke via maintenance of mitochondrial anti-apoptotic and bioenergetics functions. J Biomed Sci. 2019;26(1):43.
128. Sun X, Jung JH, Arvola O*, et al.* Stem Cell-Derived Exosomes Protect Astrocyte Cultures From in vitro Ischemia and Decrease Injury as Post-stroke Intravenous Therapy. Front Cell Neurosci. 2019;13:394.
129. Alluri H, Anasooya Shaji C, Davis ML, Tharakan B. Oxygen-glucose deprivation and reoxygenation as an in vitro ischemia-reperfusion injury model for studying blood-brain barrier dysfunction. Journal of visualized experiments : JoVE. 2015(99):e52699.
130. Xu J, He L, Ahmed SH*, et al.* Oxygen-glucose deprivation induces inducible nitric oxide synthase and nitrotyrosine expression in cerebral endothelial cells. Stroke. 2000;31(7):1744-51.
131. Salvador E, Burek M, Forster CY. Stretch and/or oxygen glucose deprivation (OGD) in an in vitro traumatic brain injury (TBI) model induces calcium alteration and inflammatory cascade. Front Cell Neurosci. 2015;9:323.
132. Itoh Y, Takaoka R, Ohira M, Abe T, Tanahashi N, Suzuki N. Reactive oxygen species generated by mitochondrial injury in human brain microvessel endothelial cells. Clin Hemorheol Microcirc. 2006;34(1-2):163-8.
133. Kokubu Y, Yamaguchi T, Kawabata K. In vitro model of cerebral ischemia by using brain microvascular endothelial cells derived from human induced pluripotent stem cells. Biochem Biophys Res Commun. 2017;486(2):577-83.
134. Chen J, Sun L, Ding GB*, et al.* Oxygen-Glucose Deprivation/Reoxygenation Induces Human Brain Microvascular Endothelial Cell Hyperpermeability Via VE-Cadherin Internalization: Roles of RhoA/ROCK2. J Mol Neurosci. 2019;69(1):49-59.
135. Neuhaus W, Burek M, Djuzenova CS*, et al.* Addition of NMDA-receptor antagonist MK801 during oxygen/glucose deprivation moderately attenuates the

upregulation of glucose uptake after subsequent reoxygenation in brain endothelial cells. Neuroscience letters. 2012;506(1):44-9.
136. Pannasch U, Vargova L, Reingruber J*, et al.* Astroglial networks scale synaptic activity and plasticity. Proceedings of the National Academy of Sciences of the United States of America. 2011;108(20):8467-72.
137. Rouach N, Koulakoff A, Abudara V, Willecke K, Giaume C. Astroglial metabolic networks sustain hippocampal synaptic transmission. Science. 2008;322(5907):1551-5.
138. Chandrasekaran A, Avci HX, Leist M, Kobolak J, Dinnyes A. Astrocyte Differentiation of Human Pluripotent Stem Cells: New Tools for Neurological Disorder Research. Front Cell Neurosci. 2016;10:215.
139. Kuijlaars J, Oyelami T, Diels A*, et al.* Sustained synchronized neuronal network activity in a human astrocyte co-culture system. Scientific reports. 2016;6:36529.
140. Tang X, Zhou L, Wagner AM*, et al.* Astroglial cells regulate the developmental timeline of human neurons differentiated from induced pluripotent stem cells. Stem cell research. 2013;11(2):743-57.
141. Odawara A, Saitoh Y, Alhebshi AH, Gotoh M, Suzuki I. Long-term electrophysiological activity and pharmacological response of a human induced pluripotent stem cell-derived neuron and astrocyte co-culture. Biochem Biophys Res Commun. 2014;443(4):1176-81.
142. Johnson MA, Weick JP, Pearce RA, Zhang SC. Functional neural development from human embryonic stem cells: accelerated synaptic activity via astrocyte coculture. The Journal of neuroscience : the official journal of the Society for Neuroscience. 2007;27(12):3069-77.
143. Kierdorf K, Prinz M. Microglia in steady state. The Journal of clinical investigation. 2017;127(9):3201-9.
144. Haenseler W, Rajendran L. Concise Review: Modeling Neurodegenerative Diseases with Human Pluripotent Stem Cell-Derived Microglia. Stem Cells. 2019;37(6):724-30.
145. De Vocht N, Praet J, Reekmans K*, et al.* Tackling the physiological barriers for successful mesenchymal stem cell transplantation into the central nervous system. Stem Cell Res Ther. 2013;4(4):101.
146. Blanchette M, Daneman R. Formation and maintenance of the BBB. Mech Dev. 2015;138 Pt 1:8-16.
147. Janzer RC, Raff MC. Astrocytes induce blood-brain barrier properties in endothelial cells. Nature. 1987;325(6101):253-7.
148. Sivandzade F, Cucullo L. In-vitro blood-brain barrier modeling: A review of modern and fast-advancing technologies. J Cereb Blood Flow Metab. 2018;38(10):1667-81.
149. Nzou G, Wicks RT, Wicks EE*, et al.* Human Cortex Spheroid with a Functional Blood Brain Barrier for High-Throughput Neurotoxicity Screening and Disease Modeling. Scientific reports. 2018;8(1):7413.

150. Desestret V, Riou A, Chauveau F*, et al.* In vitro and in vivo models of cerebral ischemia show discrepancy in therapeutic effects of M2 macrophages. PloS one. 2013;8(6):e67063.
151. Kaushal V, Schlichter LC. Mechanisms of microglia-mediated neurotoxicity in a new model of the stroke penumbra. The Journal of neuroscience : the official journal of the Society for Neuroscience. 2008;28(9):2221-30.
152. Lai AY, Todd KG. Differential regulation of trophic and proinflammatory microglial effectors is dependent on severity of neuronal injury. Glia. 2008;56(3):259-70.
153. Mai N, Prifti V, Kim M, Halterman MW. Characterization of neutrophil-neuronal co-cultures to investigate mechanisms of post-ischemic immune-mediated neurotoxicity. Journal of neuroscience methods. 2020;341:108782.
154. Chaitanya GV, Minagar A, Alexander JS. Neuronal and astrocytic interactions modulate brain endothelial properties during metabolic stresses of in vitro cerebral ischemia. Cell Commun Signal. 2014;12:7.
155. Shindo A, Maki T, Mandeville ET*, et al.* Astrocyte-Derived Pentraxin 3 Supports Blood-Brain Barrier Integrity Under Acute Phase of Stroke. Stroke. 2016;47(4):1094-100.
156. Ryu S, Kwon J, Park H*, et al.* Amelioration of Cerebral Ischemic Injury by a Synthetic Seco-nucleoside LMT497. Exp Neurobiol. 2015;24(1):31-40.
157. Centeno EGZ, Cimarosti H, Bithell A. 2D versus 3D human induced pluripotent stem cell-derived cultures for neurodegenerative disease modelling. Molecular neurodegeneration. 2018;13(1):27.
158. Rothenbucher TSP, Martinez-Serrano A. Human cerebral organoids and neural 3D tissues in basic research, and their application to study neurological diseases. Futur Neurol. 2019;14(1).
159. Kelava I, Lancaster MA. Dishing out mini-brains: Current progress and future prospects in brain organoid research. Dev Biol. 2016;420(2):199-209.
160. Gong J, Meng T, Yang J, Hu N, Zhao H, Tian T. Three-dimensional in vitro tissue culture models of brain organoids. Experimental neurology. 2021;339:113619.
161. Brawner AT, Xu R, Liu D, Jiang P. Generating CNS organoids from human induced pluripotent stem cells for modeling neurological disorders. Int J Physiol Pathophysiol Pharmacol. 2017;9(3):101-11.
162. Pasca AM, Sloan SA, Clarke LE*, et al.* Functional cortical neurons and astrocytes from human pluripotent stem cells in 3D culture. Nature methods. 2015;12(7):671-8.
163. Lancaster MA, Knoblich JA. Generation of cerebral organoids from human pluripotent stem cells. Nature protocols. 2014;9(10):2329-40.
164. Lancaster MA, Renner M, Martin CA*, et al.* Cerebral organoids model human brain development and microcephaly. Nature. 2013;501(7467):373-9.
165. Pamies D, Barreras P, Block K*, et al.* A human brain microphysiological system derived from induced pluripotent stem cells to study neurological diseases and toxicity. ALTEX. 2017;34(3):362-76.

166. Jo J, Xiao Y, Sun AX*, et al.* Midbrain-like Organoids from Human Pluripotent Stem Cells Contain Functional Dopaminergic and Neuromelanin-Producing Neurons. Cell Stem Cell. 2016;19(2):248-57.
167. Muguruma K, Nishiyama A, Kawakami H, Hashimoto K, Sasai Y. Self-organization of polarized cerebellar tissue in 3D culture of human pluripotent stem cells. Cell Rep. 2015;10(4):537-50.
168. Sakaguchi H, Kadoshima T, Soen M*, et al.* Generation of functional hippocampal neurons from self-organizing human embryonic stem cell-derived dorsomedial telencephalic tissue. Nat Commun. 2015;6:8896.
169. Qian X, Nguyen HN, Song MM*, et al.* Brain-Region-Specific Organoids Using Mini-bioreactors for Modeling ZIKV Exposure. Cell. 2016;165(5):1238-54.
170. Huang WK, Wong SZH, Pather SR*, et al.* Generation of hypothalamic arcuate organoids from human induced pluripotent stem cells. Cell Stem Cell. 2021;28(9):1657-70 e10.
171. Mariani J, Coppola G, Zhang P*, et al.* FOXG1-Dependent Dysregulation of GABA/Glutamate Neuron Differentiation in Autism Spectrum Disorders. Cell. 2015;162(2):375-90.
172. Dang J, Tiwari SK, Lichinchi G*, et al.* Zika Virus Depletes Neural Progenitors in Human Cerebral Organoids through Activation of the Innate Immune Receptor TLR3. Cell Stem Cell. 2016;19(2):258-65.
173. Garcez PP, Loiola EC, Madeiro da Costa R*, et al.* Zika virus impairs growth in human neurospheres and brain organoids. Science. 2016;352(6287):816-8.
174. Lee HK, Velazquez Sanchez C, Chen M*, et al.* Three Dimensional Human Neuro-Spheroid Model of Alzheimer's Disease Based on Differentiated Induced Pluripotent Stem Cells. PloS one. 2016;11(9):e0163072.
175. Raja WK, Mungenast AE, Lin YT*, et al.* Self-Organizing 3D Human Neural Tissue Derived from Induced Pluripotent Stem Cells Recapitulate Alzheimer's Disease Phenotypes. PloS one. 2016;11(9):e0161969.
176. Leite PEC, Pereira MR, Harris G*, et al.* Suitability of 3D human brain spheroid models to distinguish toxic effects of gold and poly-lactic acid nanoparticles to assess biocompatibility for brain drug delivery. Part Fibre Toxicol. 2019;16(1):22.
177. Zeng Y, Tin-Tin W-S, Tomohiro I, Hideko S. A three-dimensional neurosphere system using human stem cells for nanotoxicology studies. 2018.
178. Lee CT, Bendriem RM, Wu WW, Shen RF. 3D brain Organoids derived from pluripotent stem cells: promising experimental models for brain development and neurodegenerative disorders. J Biomed Sci. 2017;24(1):59.
179. Hartley BJ, Brennand KJ. Neural organoids for disease phenotyping, drug screening and developmental biology studies. Neurochem Int. 2017;106:85-93.
180. Cakir B, Xiang Y, Tanaka Y*, et al.* Engineering of human brain organoids with a functional vascular-like system. Nature methods. 2019;16(11):1169-75.
181. Shi Y, Sun L, Wang M*, et al.* Vascularized human cortical organoids (vOrganoids) model cortical development in vivo. PLoS Biol. 2020;18(5):e3000705.

182. Kook MG, Lee SE, Shin N*, et al.* Generation of Cortical Brain Organoid with Vascularization by Assembling with Vascular Spheroid. Int J Stem Cells. 2022;15(1):85-94.
183. Ginhoux F, Prinz M. Origin of microglia: current concepts and past controversies. Cold Spring Harb Perspect Biol. 2015;7(8):a020537.
184. Fagerlund I, Dougalis A, Shakirzyanova A*, et al.* Microglia-like Cells Promote Neuronal Functions in Cerebral Organoids. Cells. 2021;11(1).
185. Xu R, Boreland AJ, Li X*, et al.* Developing human pluripotent stem cell-based cerebral organoids with a controllable microglia ratio for modeling brain development and pathology. Stem cell reports. 2021;16(8):1923-37.
186. Abreu CM, Gama L, Krasemann S*, et al.* Microglia Increase Inflammatory Responses in iPSC-Derived Human BrainSpheres. Front Microbiol. 2018;9:2766.
187. Wang Z, Wang SN, Xu TY, Miao ZW, Su DF, Miao CY. Organoid technology for brain and therapeutics research. CNS Neurosci Ther. 2017;23(10):771-8.
188. Koo B, Choi B, Park H, Yoon KJ. Past, Present, and Future of Brain Organoid Technology. Mol Cells. 2019;42(9):617-27.
189. Kim MS, Kim DH, Kang HK, Kook MG, Choi SW, Kang KS. Modeling of Hypoxic Brain Injury through 3D Human Neural Organoids. Cells. 2021;10(2).
190. Daviaud N, Chevalier C, Friedel RH, Zou H. Distinct Vulnerability and Resilience of Human Neuroprogenitor Subtypes in Cerebral Organoid Model of Prenatal Hypoxic Injury. Front Cell Neurosci. 2019;13:336.
191. Van Breedam E, Nijak A, Buyle-Huybrecht T*, et al.* Luminescent Human iPSC-Derived Neurospheroids Enable Modeling of Neurotoxicity After Oxygen-glucose Deprivation. Neurotherapeutics. 2022.
192. Iwasa N, Matsui TK, Iguchi N*, et al.* Gene Expression Profiles of Human Cerebral Organoids Identify PPAR Pathway and PKM2 as Key Markers for Oxygen-Glucose Deprivation and Reoxygenation. Front Cell Neurosci. 2021;15:605030.
193. Ko E, Poon MLS, Park E, Cho Y, Shin JH. Engineering 3D Cortical Spheroids for an In Vitro Ischemic Stroke Model. ACS Biomater Sci Eng. 2021;7(8):3845-60.
194. Lin CH, Nicol CJB, Cheng YC, Yen C, Wang YS, Chiang MC. Neuroprotective effects of resveratrol against oxygen glucose deprivation induced mitochondrial dysfunction by activation of AMPK in SH-SY5Y cells with 3D gelatin scaffold. Brain Res. 2020;1726:146492.
195. Bokhari M, Carnachan RJ, Cameron NR, Przyborski SA. Culture of HepG2 liver cells on three dimensional polystyrene scaffolds enhances cell structure and function during toxicological challenge. J Anat. 2007;211(4):567-76.
196. van Duinen V, Trietsch SJ, Joore J, Vulto P, Hankemeier T. Microfluidic 3D cell culture: from tools to tissue models. Curr Opin Biotechnol. 2015;35:118-26.
197. Shin HS, Kim HJ, Min SK, Kim SH, Lee BM, Jeon NL. Compartmental culture of embryonic stem cell-derived neurons in microfluidic devices for use in axonal biology. Biotechnol Lett. 2010;32(8):1063-70.

198. Taylor AM, Dieterich DC, Ito HT, Kim SA, Schuman EM. Microfluidic local perfusion chambers for the visualization and manipulation of synapses. Neuron. 2010;66(1):57-68.
199. Coquinco A, Kojic L, Wen W*, et al.* A microfluidic based in vitro model of synaptic competition. Mol Cell Neurosci. 2014;60:43-52.
200. Taylor AM, Blurton-Jones M, Rhee SW, Cribbs DH, Cotman CW, Jeon NL. A microfluidic culture platform for CNS axonal injury, regeneration and transport. Nature methods. 2005;2(8):599-605.
201. Park J, Koito H, Li J, Han A. Microfluidic compartmentalized co-culture platform for CNS axon myelination research. Biomed Microdevices. 2009;11(6):1145-53.
202. Samson AJ, Robertson G, Zagnoni M, Connolly CN. Neuronal networks provide rapid neuroprotection against spreading toxicity. Scientific reports. 2016;6:33746.
203. Demers CJ, Soundararajan P, Chennampally P*, et al.* Development-on-chip: in vitro neural tube patterning with a microfluidic device. Development. 2016;143(11):1884-92.
204. Park JY, Kim SK, Woo DH, Lee EJ, Kim JH, Lee SH. Differentiation of neural progenitor cells in a microfluidic chip-generated cytokine gradient. Stem Cells. 2009;27(11):2646-54.
205. Uzel SG, Amadi OC, Pearl TM, Lee RT, So PT, Kamm RD. Simultaneous or Sequential Orthogonal Gradient Formation in a 3D Cell Culture Microfluidic Platform. Small. 2016;12(5):612-22.
206. Mauleon G, Fall CP, Eddington DT. Precise spatial and temporal control of oxygen within in vitro brain slices via microfluidic gas channels. PloS one. 2012;7(8):e43309.
207. Oppegard SC, Nam KH, Carr JR, Skaalure SC, Eddington DT. Modulating temporal and spatial oxygenation over adherent cellular cultures. PloS one. 2009;4(9):e6891.
208. Adler M, Polinkovsky M, Gutierrez E, Groisman A. Generation of oxygen gradients with arbitrary shapes in a microfluidic device. Lab Chip. 2010;10(3):388-91.
209. Lo JF, Sinkala E, Eddington DT. Oxygen gradients for open well cellular cultures via microfluidic substrates. Lab Chip. 2010;10(18):2394-401.
210. Liu P, Fu L, Song Z*, et al.* Three dimensionally printed nitrocellulose-based microfluidic platform for investigating the effect of oxygen gradient on cells. Analyst. 2021;146(17):5255-63.
211. Koens R, Tabata Y, Serrano JC*, et al.* Microfluidic platform for three-dimensional cell culture under spatiotemporal heterogeneity of oxygen tension. APL Bioeng. 2020;4(1):016106.
212. Fridman IB, Ugolini GS, VanDelinder V, Cohen S, Konry T. High throughput microfluidic system with multiple oxygen levels for the study of hypoxia in tumor spheroids. Biofabrication. 2021;13(3).
213. Brennan MD, Rexius-Hall ML, Elgass LJ, Eddington DT. Oxygen control with microfluidics. Lab Chip. 2014;14(22):4305-18.

214. Park J, Lee BK, Jeong GS, Hyun JK, Lee CJ, Lee SH. Three-dimensional brain-on-a-chip with an interstitial level of flow and its application as an in vitro model of Alzheimer's disease. Lab Chip. 2015;15(1):141-50.
215. Yin F, Zhu Y, Wang Y, Qin J. Engineering Brain Organoids to Probe Impaired Neurogenesis Induced by Cadmium. ACS Biomater Sci Eng. 2018;4(5):1908-15.
216. Akay M, Hite J, Avci NG*, et al.* Drug Screening of Human GBM Spheroids in Brain Cancer Chip. Scientific reports. 2018;8(1):15423.
217. Wang Y, Wang L, Zhu Y, Qin J. Human brain organoid-on-a-chip to model prenatal nicotine exposure. Lab Chip. 2018;18(6):851-60.
218. Kosodo Y, Suetsugu T, Kobayashi TJ, Matsuzaki F. Systematic time-dependent visualization and quantitation of the neurogenic rate in brain organoids. Biochem Biophys Res Commun. 2017;483(1):94-100.
219. Andjelkovic AV, Stamatovic SM, Keep RF. The protective effects of preconditioning on cerebral endothelial cells in vitro. J Cereb Blood Flow Metab. 2003;23(11):1348-55.
220. Foroutan S, Brillault J, Forbush B, O'Donnell ME. Moderate-to-severe ischemic conditions increase activity and phosphorylation of the cerebral microvascular endothelial cell Na+-K+-Cl- cotransporter. Am J Physiol Cell Physiol. 2005;289(6):C1492-501.
221. Gesuete R, Orsini F, Zanier ER*, et al.* Glial cells drive preconditioning-induced blood-brain barrier protection. Stroke. 2011;42(5):1445-53.
222. Tornabene E, Helms HCC, Pedersen SF, Brodin B. Effects of oxygen-glucose deprivation (OGD) on barrier properties and mRNA transcript levels of selected marker proteins in brain endothelial cells/astrocyte co-cultures. PloS one. 2019;14(8):e0221103.
223. Vemula S, Roder KE, Yang T, Bhat GJ, Thekkumkara TJ, Abbruscato TJ. A functional role for sodium-dependent glucose transport across the blood-brain barrier during oxygen glucose deprivation. J Pharmacol Exp Ther. 2009;328(2):487-95.
224. Wu L, Ye ZM, Pan Y*, et al.* Vascular endothelial growth factor aggravates cerebral ischemia and reperfusion-induced blood-brain-barrier disruption through regulating LOC102640519/HOXC13/ZO-1 signaling. Experimental Cell Research. 2018;369(2):275-83.
225. Cucullo L, Couraud PO, Weksler B*, et al.* Immortalized human brain endothelial cells and flow-based vascular modeling: a marriage of convenience for rational neurovascular studies. J Cereb Blood Flow Metab. 2008;28(2):312-28.
226. Krizanac-Bengez L, Mayberg MR, Cunningham E*, et al.* Loss of shear stress induces leukocyte-mediated cytokine release and blood-brain barrier failure in dynamic in vitro blood-brain barrier model. Journal of cellular physiology. 2006;206(1):68-77.
227. Krizanac-Bengez L, Hossain M, Fazio V, Mayberg M, Janigro D. Loss of flow induces leukocyte-mediated MMP/TIMP imbalance in dynamic in vitro blood-brain barrier model: role of pro-inflammatory cytokines. Am J Physiol Cell Physiol. 2006;291(4):C740-9.

228. Cameron T, Bennet T, Rowe EM, Anwer M, Wellington CL, Cheung KC. Review of Design Considerations for Brain-on-a-Chip Models. Micromachines (Basel). 2021;12(4).
229. Booth R, Kim H. Characterization of a microfluidic in vitro model of the blood-brain barrier (muBBB). Lab Chip. 2012;12(10):1784-92.
230. Griep LM, Wolbers F, de Wagenaar B*, et al.* BBB on chip: microfluidic platform to mechanically and biochemically modulate blood-brain barrier function. Biomed Microdevices. 2013;15(1):145-50.
231. Achyuta AK, Conway AJ, Crouse RB*, et al.* A modular approach to create a neurovascular unit-on-a-chip. Lab Chip. 2013;13(4):542-53.
232. Walter FR, Valkai S, Kincses A*, et al.* Lab-on-a-Chip Tool for Modeling Biological Barriers. J Neuroimmune Pharm. 2016;11:S49-S50.
233. Brown JA, Pensabene V, Markov DA*, et al.* Recreating blood-brain barrier physiology and structure on chip: A novel neurovascular microfluidic bioreactor. Biomicrofluidics. 2015;9(5).
234. Katt ME, Shusta EV. In vitro models of the blood-brain barrier: building in physiological complexity. Curr Opin Chem Eng. 2020;30:42-52.
235. Cho HS, Seo JH, Wong KHK*, et al.* Three-Dimensional Blood-Brain Barrier Model for in vitro Studies of Neurovascular Pathology. Scientific reports. 2015;5.
236. Adriani G, Ma DL, Pavesi A, Kamm RD, Goh ELK. A 3D neurovascular microfluidic model consisting of neurons, astrocytes and cerebral endothelial cells as a blood-brain barrier. Lab on a Chip. 2017;17(3):448-59.
237. Herland A, van der Meer AD, FitzGerald EA, Park TE, Sleeboom JJ, Ingber DE. Distinct Contributions of Astrocytes and Pericytes to Neuroinflammation Identified in a 3D Human Blood-Brain Barrier on a Chip. PloS one. 2016;11(3):e0150360.
238. Partyka PP, Godsey GA, Galie JR*, et al.* Mechanical stress regulates transport in a compliant 3D model of the blood-brain barrier. Biomaterials. 2017;115:30-9.
239. Faley SL, Neal EH, Wang JX*, et al.* iPSC-Derived Brain Endothelium Exhibits Stable, Long-Term Barrier Function in Perfused Hydrogel Scaffolds. Stem cell reports. 2019;12(3):474-87.
240. van Dijk CGM, Brandt MM, Poulis N*, et al.* A new microfluidic model that allows monitoring of complex vascular structures and cell interactions in a 3D biological matrix. Lab Chip. 2020;20(10):1827-44.
241. Bouhrira N, DeOre BJ, Sazer DW, Chiaradia Z, Miller JS, Galie PA. Disturbed flow disrupts the blood-brain barrier in a 3D bifurcation model. Biofabrication. 2020;12(2):025020.
242. Yu F, Kumar NDOS, Foo LC, Ng SH, Hunziker W, Choudhury D. A pump-free tricellular blood-brain barrier on-a-chip model to understand barrier property and evaluate drug response. Biotechnology and Bioengineering. 2020;117(4):1127-36.
243. Nousiainen S. Developing an in vitro stroke model for studying adipose stem cells' paracrine effect on neuronal recovery after ischemia: Tampere Univeristy; 2019.

244. Zou YX, Liu YX, Ruan MH, Zhou Y, Wang JC, Chu ZY. Cordyceps sinensis Oral Liquid Inhibits Damage Induced by Oxygen and Glucose Deprivation in SH-SY5Y Cells. Altern Ther Health Med. 2016;22(2):37-42.
245. Pasca AM, Park JY, Shin HW*, et al.* Human 3D cellular model of hypoxic brain injury of prematurity. Nature medicine. 2019;25(5):784-91.
246. Li H, Durbin R. Fast and accurate long-read alignment with Burrows-Wheeler transform. Bioinformatics. 2010;26(5):589-95.
247. Institute B. Picard toolkit. 2019.
248. Raman L, Dheedene A, De Smet M, Van Dorpe J, Menten B. WisecondorX: improved copy number detection for routine shallow whole-genome sequencing. Nucleic acids research. 2019;47(4):1605-14.
249. Sante T, Vergult S, Volders PJ*, et al.* ViVar: a comprehensive platform for the analysis and visualization of structural genomic variation. PloS one. 2014;9(12):e113800.
250. Ivanov DP, Grabowska AM. Spheroid arrays for high-throughput single-cell analysis of spatial patterns and biomarker expression in 3D. Scientific reports. 2017;7:41160.
251. De Vos WH, Van Neste L, Dieriks B, Joss GH, Van Oostveldt P. High content image cytometry in the context of subnuclear organization. Cytometry A. 2010;77(1):64-75.
252. Houthaeve G, Xiong R, Robijns J*, et al.* Targeted Perturbation of Nuclear Envelope Integrity with Vapor Nanobubble-Mediated Photoporation. ACS Nano. 2018;12(8):7791-802.
253. Zack GW, Rogers WE, Latt SA. Automatic measurement of sister chromatid exchange frequency. J Histochem Cytochem. 1977;25(7):741-53.
254. Geraerts M, Michiels M, Baekelandt V, Debyser Z, Gijsbers R. Upscaling of lentiviral vector production by tangential flow filtration. J Gene Med. 2005;7(10):1299-310.
255. Ibrahimi A, Vande Velde G, Reumers V*, et al.* Highly efficient multicistronic lentiviral vectors with peptide 2A sequences. Human gene therapy. 2009;20(8):845-60.
256. Gottron FJ, Ying HS, Choi DW. Caspase inhibition selectively reduces the apoptotic component of oxygen-glucose deprivation-induced cortical neuronal cell death. Mol Cell Neurosci. 1997;9(3):159-69.
257. Fang Y, Eglen RM. Three-Dimensional Cell Cultures in Drug Discovery and Development. SLAS Discov. 2017;22(5):456-72.
258. Wendt MK, Schiemann WP. Longitudinal Bioluminescent Quantification of Three Dimensional Cell Growth. Bio Protoc. 2013;3(23).
259. Yasunaga M, Fujita Y, Saito R, Oshimura M, Nakajima Y. Continuous long-term cytotoxicity monitoring in 3D spheroids of beetle luciferase-expressing hepatocytes by nondestructive bioluminescence measurement. BMC Biotechnol. 2017;17(1):54.

260. Malik A, Jamasbi RJ, Kondratov RV, Geusz ME. Development of circadian oscillators in neurosphere cultures during adult neurogenesis. PloS one. 2015;10(3):e0122937.
261. Mehta AK, Majumdar SS, Alam P, Gulati N, Brahmachari V. Epigenetic regulation of cytomegalovirus major immediate-early promoter activity in transgenic mice. Gene. 2009;428(1-2):20-4.
262. Prosch S, Stein J, Staak K, Liebenthal C, Volk HD, Kruger DH. Inactivation of the very strong HCMV immediate early promoter by DNA CpG methylation in vitro. Biol Chem Hoppe Seyler. 1996;377(3):195-201.
263. Hsu CC, Li HP, Hung YH*, et al.* Targeted methylation of CMV and E1A viral promoters. Biochem Biophys Res Commun. 2010;402(2):228-34.
264. Hoffmann D, Schott JW, Geis FK*, et al.* Detailed comparison of retroviral vectors and promoter configurations for stable and high transgene expression in human induced pluripotent stem cells. Gene Ther. 2017;24(5):298-307.
265. Song L, Yuan X, Jones Z*, et al.* Functionalization of Brain Region-specific Spheroids with Isogenic Microglia-like Cells. Scientific reports. 2019;9(1):11055.
266. Ormel PR, Vieira de Sa R, van Bodegraven EJ*, et al.* Microglia innately develop within cerebral organoids. Nat Commun. 2018;9(1):4167.
267. Shen XY, Gao ZK, Han Y, Yuan M, Guo YS, Bi X. Activation and Role of Astrocytes in Ischemic Stroke. Front Cell Neurosci. 2021;15:755955.
268. Yakoub AM. Cerebral organoids exhibit mature neurons and astrocytes and recapitulate electrophysiological activity of the human brain. Neural Regeneration Research. 2019;14(5):757-61.
269. Monzel AS, Smits LM, Hemmer K*, et al.* Derivation of Human Midbrain-Specific Organoids from Neuroepithelial Stem Cells. Stem cell reports. 2017;8(5):1144-54.
270. Oberheim NA, Takano T, Han X*, et al.* Uniquely hominid features of adult human astrocytes. The Journal of neuroscience : the official journal of the Society for Neuroscience. 2009;29(10):3276-87.
271. Li J, Pan L, Pembroke WG*, et al.* Conservation and divergence of vulnerability and responses to stressors between human and mouse astrocytes. Nat Commun. 2021;12(1):3958.
272. Zhang Y, Sloan SA, Clarke LE*, et al.* Purification and Characterization of Progenitor and Mature Human Astrocytes Reveals Transcriptional and Functional Differences with Mouse. Neuron. 2016;89(1):37-53.
273. Galatro TF, Holtman IR, Lerario AM*, et al.* Transcriptomic analysis of purified human cortical microglia reveals age-associated changes. Nature neuroscience. 2017;20(8):1162-71.
274. Zhou YY, Song WM, Andhey P*, et al.* Human and mouse single-nucleus transcriptomics reveal TREM2-dependent and -independent cellular responses in Alzhimer's disease. Journal of immunology. 2020;204(1).

275. Ivanov DP, Grabowska AM, Garnett MC. High-Throughput Spheroid Screens Using Volume, Resazurin Reduction, and Acid Phosphatase Activity. Methods in molecular biology. 2017;1601:43-59.
276. Ivanov DP, Parker TL, Walker DA*, et al.* Multiplexing spheroid volume, resazurin and acid phosphatase viability assays for high-throughput screening of tumour spheroids and stem cell neurospheres. PloS one. 2014;9(8):e103817.
277. Riffle S, Hegde RS. Modeling tumor cell adaptations to hypoxia in multicellular tumor spheroids. J Exp Clin Cancer Res. 2017;36(1):102.
278. Chitu V, Gokhan S, Nandi S, Mehler MF, Stanley ER. Emerging Roles for CSF-1 Receptor and its Ligands in the Nervous System. Trends in neurosciences. 2016;39(6):378-93.
279. Calvo CF, Dobbertin A, Gelman M, Glowinski J, Mallat M. Identification of CSF-1 as a brain macrophage migratory activity produced by astrocytes. Glia. 1998;24(2):180-6.
280. Fair SR, Julian D, Hartlaub AM*, et al.* Electrophysiological Maturation of Cerebral Organoids Correlates with Dynamic Morphological and Cellular Development. Stem cell reports. 2020;15(4):855-68.
281. Bodnar B, Zhang Y, Liu J*, et al.* Novel Scalable and Simplified System to Generate Microglia-Containing Cerebral Organoids From Human Induced Pluripotent Stem Cells. Front Cell Neurosci. 2021;15:682272.
282. Sabate-Soler S, Nickels SL, Saraiva C*, et al.* Microglia integration into human midbrain organoids leads to increased neuronal maturation and functionality. Glia. 2022.
283. Brownjohn PW, Smith J, Solanki R*, et al.* Functional Studies of Missense TREM2 Mutations in Human Stem Cell-Derived Microglia. Stem cell reports. 2018;10(4):1294-307.
284. Green AR, Shuaib A. Therapeutic strategies for the treatment of stroke. Drug Discov Today. 2006;11(15-16):681-93.
285. Albers GW, Goldstein LB, Hess DC*, et al.* Stroke Treatment Academic Industry Roundtable (STAIR) recommendations for maximizing the use of intravenous thrombolytics and expanding treatment options with intra-arterial and neuroprotective therapies. Stroke. 2011;42(9):2645-50.
286. Fisher M, Albers GW, Donnan GA*, et al.* Enhancing the development and approval of acute stroke therapies: Stroke Therapy Academic Industry roundtable. Stroke. 2005;36(8):1808-13.
287. Stroke Therapy Academic Industry R. Recommendations for standards regarding preclinical neuroprotective and restorative drug development. Stroke. 1999;30(12):2752-8.
288. Nagotani S, Hayashi T, Sato K*, et al.* Reduction of cerebral infarction in stroke-prone spontaneously hypertensive rats by statins associated with amelioration of oxidative stress. Stroke. 2005;36(3):670-2.

289. Renner H, Grabos M, Becker KJ*, et al.* A fully automated high-throughput workflow for 3D-based chemical screening in human midbrain organoids. eLife. 2020;9.
290. Guo S, Tjarnlund-Wolf A, Deng W*, et al.* Comparative transcriptome of neurons after oxygen-glucose deprivation: Potential differences in neuroprotection versus reperfusion. J Cereb Blood Flow Metab. 2018;38(12):2236-50.
291. Pham MT, Pollock KM, Rose MD*, et al.* Generation of human vascularized brain organoids. Neuroreport. 2018;29(7):588-93.
292. Nashimoto Y, Hayashi T, Kunita I*, et al.* Integrating perfusable vascular networks with a three-dimensional tissue in a microfluidic device. Integr Biol (Camb). 2017;9(6):506-18.
293. Dekkers JF, Alieva M, Wellens LM*, et al.* High-resolution 3D imaging of fixed and cleared organoids. Nature protocols. 2019;14(6):1756-71.
294. Tasnim K, Liu J. Emerging Bioelectronics for Brain Organoid Electrophysiology. J Mol Biol. 2022;434(3):167165.

Curriculum vitae

Personal information	Name	**Elise Van Breedam**
	Nationality	Belgian
	Date of birth	11 November 1994
	Home address	Kloosterstraat 13/2, 2000 Antwerp, Belgium
	Email address	Elise.vanbreedam@uantwerpen.be Elise_vanbreedam@hotmail.com
Education	2015-2017	**Master in Molecular and Cellular Biomedical Sciences**, University of Antwerp, Great distinction
	2017	**Laboratory Animal Science for Scientists (FELASA C certificate)**, University of Antwerp
	2013-2015	**Honours College**, University of Antwerp (incl. internship at VIB (Flanders Institute for Biotechnology), department of Neurodegenerative diseases and Studium Generale lectures cycle)
	2012-2015	**Bachelor in Biomedical Sciences**, University of Antwerp, Great distinction
Work experience	PhD student in Medical Sciences Laboratory of Experimental Hematology, University of Antwerp (2018 – to date) Supervisor: Prof. Dr. Peter Ponsaerts Project: Development, characterization and application of luminescent human iPSC-derived neurospheroids in ischemic stroke research	

Research intern at Laboratory of Cell Biology and Histology, University of Antwerp (Nov. 2016- Jun. 2017)
Master thesis internship: Development and characterization of genome edited model cell lines for laminopathies

Research intern at Center for Cellular Therapy and Regenerative Medicine (CCRG), Laboratory of Ophthalmology, UZA (May 2016 – Jun. 2016)

Research intern at Neurodegenerative Brain Diseases Group, Department of Molecular Genetics, VIB (Jul. 2013 – Jul. 2013)

Honors and awards

Session winner at the 28th European Students' Conference (Genetic Engineering – When chance meets choice) – Charité Berlin (2017)

3rd place scientific contest of the 28th European Students' Conference
(Genetic Engineering – When chance meets choice) – Charité Berlin (2017)

Student guidance

2020-2021 Joyce Hereijgers
Master thesis internship: Comparison of various differentiation media on the viability and the maturation of brain spheroids

2019-2020 Tine Swartenbroekx
Master thesis internship: Neurospheres, derived from human induced pluripotent stem cells, to study neuroinflammation in the context of ischemic stroke

Publication list

Van Breedam E, Ponsaerts P. Promising strategies for the development of advanced *in vitro* models with high predictive power in ischemic stroke research. International Journal of Molecular Sciences. 2022.

Van Broeckhoven J, Erens C, Sommer D, Scheijen E, Sanchez S, Vidal PM, Dooley D, Van Breedam E, et al. Macrophage-based delivery of interleukin-13 improves functional and

histopathological outcomes following spinal cord injury. Journal of neuroinflammation. 2022;19(1):102.

Van Breedam E, Nijak A, Buyle-Huybrecht T, Di Stefano J, Boeren M, Govaerts J, et al. Luminescent Human iPSC-Derived Neurospheroids Enable Modeling of Neurotoxicity After Oxygen-glucose Deprivation. Neurotherapeutics. 2022.

Quarta A, Meese T, Pieters Z, Van Breedam E, Le Blon D, Van Broeckhoven J, et al. Murine induced pluripotent stem cell-derived neuroimmune cell culture models emphasize opposite immune-effector functions of interleukin 13-primed microglia and macrophages in terms of neuroimmune toxicity. Glia. 2021;69(2):326-45.

Quarta A, Le Blon D, D'Aes T, Pieters Z, Hamzei Taj S, Miro-Mur F, Luyckx E, Van Breedam E, et al. Murine iPSC-derived microglia and macrophage cell culture models recapitulate distinct phenotypical and functional properties of classical and alternative neuro-immune polarisation. Brain Behav Immun. 2019;82:406-21.

Poster presentations

Luminescent Human iPSC-Derived Neurospheroids Enable Modeling of Neurotoxicity After Oxygen-glucose Deprivation. EMBL-IBEC Winter Conference – Engineering Multicellular Systems, Barcelona, Spain, 8-10 June 2022.

Talks

Luminescent Human iPSC-Derived Neurospheroids Enable Modeling of Neurotoxicity After Oxygen-glucose Deprivation. 3D Model and Organoid Club Meeting, University College Dublin, Dublin, Ireland, 15 March 2022

Luminescent Human iPSC-Derived Neurospheroids Enable Modeling of Neurotoxicity After Oxygen-glucose Deprivation. Journal club LEH, University of Antwerp, Wilrijk, Belgium, 17 March 2021

Development of 3D human brain organoids for the study and modulation of immune-mediated neurodegeneration in stroke. Organoid session, University of Antwerp, Wilrijk, Belgium, 19 October 2020

Development of next-generation next-generation 3D brain organoids for the study and modulation of immune-mediated neuro-degeneration in stroke. Spearhead Inflammation session, University of Antwerp, Wilrijk, Belgium, 7 February 2020

Additional academic activities

Short research stay at laboratory of Prof. Dr. Tom Vanden Berghe, UGent, Zwijnaarde, Belgium, 6-10 December 2022

Organization of Workshop at Day of Science 2020 – Digital Workshop – 1-2-3 Stem cell!

Organization of Workshop at Day of Science Day of Science 2019 – From Stem cell to organ

6th Annual meeting of the Belgian Society for Stem Cell Research, Brussels, Belgium, 13 September 2019

5th Annual meeting of the Belgian Society for Stem Cell Research – Stem cells: From Fundamental Discoveries to Life Saving Clinical Treatments, Leuven, Belgium, 26 October 2018

Joint RBSM/BSCDB Meeting 2018 – Cell and tissue mechanics in physiology and disease, Antwerp, Belgium, 20-21 September 2018

Spring meeting of the Belgian Society for Cell and Developmental Biology, Liège, Belgium, 8 June 2018

VIB conference on Genome engineering and Synthetic Biology (3rd edition) – Bruges, Belgium, 25-26 January 2018

Acknowledgements

Around four and a half years ago, I started my PhD-journey at the Laboratory of Experimental Hematology. It has been a real adventure, with its necessary ups and downs. Several people helped me making it to the finish line and therefore deserve a special thanks.

First of all, I would like to thank my supervisor, Prof. **Peter** Ponsaerts. The first time I met you, I was still a student Biomedical Sciences. You were teaching 'Medische celbiologie'. It was very obvious how passionate you are about stem cell research and also how proud you were on your former PhD students. Anyway, it is very likely that at that point the seed of my interest for stem cell research had been planted. After my graduation, I started looking for a PhD position in the field of stem cell research and/or gene therapy. I looked up many different stem cell and/or gene therapy labs and institutes inland and abroad. Eventually after thorough research, the number 1 project on my list was the project on PSC-derived brain organoids of your lab at 8km from where I lived. I am very happy you gave me the opportunity to start this challenging project and in fact new research line within your research group. During the PhD, you were always there for all sorts of questions and concerns. I am very grateful for your involvement and for pulling me out of the tunnel vision when I sometimes got lost in the details.

I would like to thank the jury members **Prof. Dr. Samir Kumar-Singh** and **Prof. Dr. Benedicte De Winter**, **Prof. Dr. Ira Mercedes Espuny Camacho** and **Prof. Dr. Tarja Malm** for reading and critically evaluating this thesis.

A special thanks goes to my LEH colleagues and ex-colleagues. Not only for making work far more pleasant, but also for the support over the last years.

Alessandra, you were my desk mate for the longest part of my PhD and, to me, a role model for scientists. I could always turn to you for any sorts of PhD-related questions and concerns. Yes, also for scientific advise, you were the one I could count on. I really appreciated your critical input on scientific matters and your emotional support, every time I needed them. I am also very grateful for introducing me to your friends Daniele, Patrick, Alan, Matilda and my boyfriend Manuel.

Debbie, thank you for being my co-promoter for the first two years of the PhD. It was nice having you as a colleague, and I really enjoyed having the 'day of science'-workshop together with you. Although you moved to building T, I was always happy to run into you in the hallway of T4.

Marlies, in 2018, we were the newbies of the lab. Especially, in the beginning we were working more closely together, culturing the NSCs, and it has been a pleasure. Working next to you in the laminar flow cabinet made even the most boring routine tasks fun. I really enjoyed our conversations, even when it meant putting my multitasking skills to the test at moments I actually needed to focus. I wish you all the best with your following job, with your qualities, I am sure you will do great!

Tamariche, it was a blast working with you. To me, you are a cheerful and easy-to-talk-to person and a real "do-er". Also thank you to always remember EVERYTHING and for the numerous fun conversations and ventilation sessions. Your future colleagues will be blessed having you in their team.

Julia, while you are currently developing an *in vitro* model for multiple sclerosis using mouse cells, I was developing an *in vitro* model for ischemic stroke using human cells. One would think our projects were not much alike, but I don't think anyone could understand better the technical struggles related to developing microglia-containing neurospheroids/organoids than you. Thank you for being in this together with me. I am already excited to see what other results you will obtain in the future. I also appreciated a lot your sense of humor, in the form of funny PhD memes, helping to put things in the right perspective.

Jonas, the male representative of the lab (apart from Peter). I am glad to see that part of my work has already been useful to you. Thank you for joining me to the conference in Barcelona. It was fun and I am happy I got to know you better. You are eager to learn and goal-oriented. I think we can still expect a lot from you. I wish you all the best with your PhD.

Jasmijn, I enjoyed your presence in the lab. Thank you for making the days at the lab even more colourful with your sparkling personality.

Dorien, although we didn't see each other that often, it was always nice to catch up with you each time I came for cryosectioning the neurospheroids or when you came over to our lab for immunostainings.

Evi, although we haven't worked together for that long, I am very happy to have met you during my PhD. Thank you to come up to S6 for a fun chat during the summer holidays, when I was alone at the lab.

Furthermore, I would like to thank the people from CMG for the nice chats while working in the laminar flow cabinet and for keeping me company during cell culture weekends. Also a special thanks to **Ola** for teaching me how to culture iPSCs and providing me the start material for this thesis.

For my project, I have been working in multiple labs and received the help of multiple people. I would like to acknowledge Prof. **Winnok De Vos** for his help with the marker quantification of the neurospheroids, **Isabel Pintelon** and **Sofie Thys** for their help with the Nikon microscope, Axioscan and clearing for the 3D imaging and **Johanna Van den Daele** for providing me hematopoietic progenitor cells for my experiments. I would like to thank Prof. **An Wouters** to make the hypoxia experiments possible, **Jorrit** for solving every issue with the gas bottles of the hypoxic chamber, **Christophe Deben** for his help with measurements on the SparkCyto, and finally **Christophe Hermans** for making the paraffin slices and for the fun talks during the antigen retrieval. I also would like to express my gratitude to Prof. **Erik Fransen** for his help with the statistical analyses. **Hans De Reu**, the flow cytometer king, thank you for your support every time I needed to measure something on one of the flow cytometers. Finally, I am thankful to **Behrouz Hassannia** for his time teaching me how to perform Western blots. I also would like to thank all people working in all these research groups for helping me find my way in the lab and for the nice chats.

I would also like to thank the master students, **Tine** and **Joyce**, for their hard work and generated output during their master theses.

Dan zijn er nog mijn vrienden die ik graag wil bedanken. Mijn 'biomedische' vrienden **Charlotte**, **Melissa**, **Stephanie**, **Laurence** en **Laurijn**. Ik wil jullie bedanken voor jullie emotionele steun, voor jullie geloof in mij en voor jullie begrip als ik bij het vastleggen van datum weeral moet zeggen: 'Ik weet het nog niet zeker. Het kan zijn dat ik dan voor mijn cellen naar het labo moet.' Hetzelfde geldt voor de vrienden van de **Octopus-groep**. Bedankt om met onze etentjes, weekends en andere activiteiten voor de nodige ontspanning te zorgen.

Dit alles was niet mogelijk geweest zonder de vier belangrijkste personen in mijn leven. **Mama**, **papa** en **zus Stephanie**, niemand kent me beter dan jullie. Jullie onvoorwaardelijke steun en geloof in mijn kunnen (zelfs wanneer ik het soms even niet

zie), hebben me gebracht tot waar ik vandaag sta. Jullie stonden altijd klaar met raad, niet alleen tijdens mijn doctoraat, maar voor alles in mijn leven. Een dikke dankjewel hiervoor! **Manuel**, these past few years, you have been my tower of strength. Thank you for enduring all my work-related monologues, with their necessary complains and portion of frustration. Thanks to your endless positivism and positive energy, I was able to counter the difficult times and come back stronger. Also thanks for your patience and to celebrate the little victories with me. With this, I would like to end this chapter, so we can start a new one.